Development of multifunctional ferromagnets based on supramolecular structures and bimetallic oxalate complexes

（超分子構造とシュウ酸金属錯体塩に基づいた
多機能強磁性体の開拓）

北海道大学大学院環境科学院

Wu Jiabing

Table of Contents

Abstract

The molecular-based magnetic networks of $[MnCr(oxalate)_3]^-$ not only exhibit interesting magnetic ordering like ferromagnetism, but also can accommodate other functional cations to design novel multifunctional materials such as ferromagnetic conductors, chiral magnets, optical-active magnets, or multiferroics. The coexistence of more than two ferroic properties (ferroelectricity, ferromagnetism, and ferroelasticity), known as multiferroics, has attracted much attention in the field of novel electronic devices. Especially the coexistence of ferroelectricity and ferromagnetism, the most focusing multiferroics, could be used as magnetoelectric (ME) materials in memory devices to overcome the slow writing problem of ferroelectric memory and the high energy consumption drawback of magnetic random access memory.

In Chapter 2, to realize molecular multiferroic crystals, a series of two-dimensional polar crystals were obtained by introducing supramolecular cations composed of anilinium derivatives and benzo[18]crown-6 into the $[MnCr(oxalate)_3]^-$ system, denoted as (*x*-anilinium$^+$)(benzo[18]crown-6)$[MnCr(oxalate)_3]^-$, where *x* = H, *o*-fluoro, *m*-fluoro, and *p*-fluoro, for **1**, **2**, **3**, and **4**. To obtain the polar space group essential for ferroelectricity, benzo[18]crown-6 with low symmetry was used as a crown ether. All anilinium derivatives gave crystals with polar space groups. Among these crystals, (*o*-fluoroanilinium$^+$)(benzo[18]crown-6)$[MnCr(oxalate)_3]^-$ (**2**) crystallized in the *Cc* space group exhibited a ferroelectric transition at 470 K. In the paraelectric phase of the space group *P*21/*n*, both *o*-fluoroanilinium and benzo[18]crown-6 were observed to be disordered, canceling the dipole moments in the crystal. The molecular motion of (*o*-fluoroanilinium$^+$)(benzo[18]crown-6) supramolecule is the origin of the ferroelectric-paraelectric phase transition. The ferroelectricity is proved by the fact that the sign of the pyroelectric current is inverted by the external electric field. The honeycomb layers of $[MnCr(oxalate)_3]^-$ exhibited ferromagnetic ordering below 5 K. The crystal is the first example of type-I multiferroic based on $[MnCr(oxalate)_3]^-$ layer structure. Flip-flop motion of *m*-fluoroanilinium was observed in crystal **3**. The crystal did not show long-range order of dipole moments, but fluctuations in dipole moments due to rotation of aryl groups were clearly observed as dielectric relaxation, with an activation energy of 34.1 kJ/mol.

In Chapter 3, the supramolecular motions associated with solvent desorption from $[MnCr(oxalate)_3]^-$ crystals were investigated. The majority of the network structure consisting of $[MnCr(oxalate)_3]^-$ readily incorporates crystalline solvents during crystallization. Due to crystal disintegration associated with desolvation, it is often

difficult to evaluate the physical properties of the crystals. A polar crystal (CBA^+)([18]crown-6)[MnCr(oxalate)$_3$]$^-$(CH_3OH) (**5**•CH_3OH) (CBA^+ = 4-carboxybutan-1-aminium) was synthesized. Upon desolvation, crystal **5**•CH_3OH underwent a crystal-to-crystal transformation to form (CBA^+)([18]crown-6)[MnCr(oxalate)$_3$]$^-$(**5**). Both crystals exhibited ferromagnetic ordering at approximately 5 K. The structural transformation was accompanied by a reorganization of hydrogen bonds in the (CBA^+)([18]crown-6) supramolecular assembly. In crystal **5**, a "merry-go-round" motion of [18]crown-6 was observed, with an activation energy of 41.41 kJ/mol. The motion of [18]crown-6 was observed as dielectric relaxation. This crystal-to-crystal structural transformation provides a design strategy for multifunctional hybrid materials that can add new functions based on molecular motion.

[MnCr(oxalate)$_3$]$^-$ gives diverse network structures depending on the valence and shape of the counter cation. Gyroid structure, which is strongly isotropic and induces exotic physical and electronic properties, is one of the most important examples. In Chapter 4, supramolecular cations were used to induce diverse three-dimensional network structures of [MnCr(oxalate)$_3$]$^-$. By using the achiral supramolecular cation (ethanaminium$^+$)(benzo[18]crown-6), a chiral network of [MnCr(oxalate)$_3$]$^-$ was successfully achieved in the crystal (ethanaminium$^+$)(benzo[18]crown-6)[MnCr(oxalate)$_3$]$^-$(1.5CH_3OH) (**6**) crystallized in orthorhombic space group $Pna2_1$. Using chiral cations (1*S*,2*S*)-1,2-diphenylethan-1,2-diaminium (*S*-$DPEDA^{2+}$) and [18]crown-6, another chiral crystal (*S*-$DPEDA^{2+}$)[18]crown-6{[MnCr(oxalate)$_3$]$^-$}$_2$(1.5CH_3OH)(0.5CH_3COCH_3) (**7**) was obtained. In crystals **6**, a homochiral arrangement of the oxalate ligands was observed, similar to the Gyroid network of [MnCr(oxalate)$_3$]$^-$. In crystal **7**, the stereochemistry of the ligands around each transition metal cation exhibits *Λ*-*Λ*-*Δ*-*Δ* combinations, forming an achiral three-dimensional network, but the projected structure of the *bc* and *ac* planes closely resembled a strongly isotropic Gyroid structure. In crystal **7** adjacent four folded screw axes were clockwise or anticlockwise to each other, while in Gyroid all four folded screw axes are the same (either clockwise or anticlockwise). The structure is interesting as a gyroid-like structure from the viewpoint of magnetic properties, and this result demonstrates the usefulness of supramolecular structures to construct novel network structures with interesting physical properties.

List of Schemes

List of Figures

List of Tables

Publications and presentations

Poster presentations:

1. Wu Jiabing, Endo Toru, Takahashi Kiyonori, Kubo Kazuya, Suzuki Yasutaka, Noro Shin-ichiro, Kawamata Jun, and Nakamura Takayoshi, "Ferromagnetic [$Mn^{II}Cr^{III}$(oxalate)$_3$] Salts with Supramolecular Cations based on Benzo[18]crown-6", The International Conference on Science and Technology of Synthetic Metals2018 (ICSM2018), ThP-103, Busan, Korea, July 2018.
2. Wu Jiabing, Endo Toru, Takahashi Kiyonori, Kubo Kazuya, Suzuki Yasutaka, Noro Shin-ichiro, Kawamata Jun, and Nakamura Takayoshi, "Benzo[18]crown-6 Based Supramolecular Cations in Ferromagnetic Salts [MnCr(oxalate)$_3$]", The International Conference on Coordination Chemistry (ICCC2018), S29-P04, Sendai, Japan, August 2018.
3. Wu Jiabing, Endo Toru, Takahashi Kiyonori, Kubo Kazuya, Suzuki Yasutaka, Noro Shin-ichiro, Kawamata Jun, and Nakamura Takayoshi, "2D bimetallic oxalate-based ferromagnets prepared by insertion of benzo[18]crown-6 based supramolecules", 14th IUPAC International Conference on Novel Materials and their Synthesis (NMS-XIV), P29, Guangzhou, China, October 2018.
4. Wu Jiabing, Takahashi Kiyonori, Kubo Kazuya, Suzuki Yasutaka, Noro Shin-ichiro, Kawamata Jun, and Nakamura Takayoshi, "Benzo[18]crown-6 Based Supramolecular Cations in Ferromagnetic Salts of [$Mn^{II}Cr^{III}$(oxalate)$_3$]$^-$", The 19th RIES-HOKUDAI International Symposium 組, P58-B, Sapporo, Japan, December 2018.
5. Wu Jiabing, Endo Toru, Takahashi Kiyonori, Kubo Kazuya, Suzuki Yasutaka, Noro Shin-ichiro, Kawamata Jun, and Nakamura Takayoshi, "Benzo[18]crown-6 Based Supramolecular Cations in Ferromagnetic Salts of [MnCr(oxalate)$_3$]$^-$", 第 7 回錯体化学若手の会 北海道支部勉強会, P-1, Sapporo, Japan, November 2018.

6. Wu Jiabing, Huang Ruikang, Kiyonori Takahashi, and Nakamura Takayoshi, "Solvent Dependence of Molecular Motion in Ferromagnetic [Mn(II)Cr(III)(oxalate)$_3$]$^-$ Sat", International Symposium on Crystalline Organic Metals, Superconductors and Magnets, Le Pouliguen, France, September 2022.

Oral presentations:

7. Wu Jiabing, Takahashi Kiyonori, Hoshino Norihisa, Suzuki Yasutaka, Hisaki Ichiro, Kawamata Jun, Akutagawa Tomoyuki, and Nakamura Takayoshi, "Benzo[18]crown-6 Based Supramolecular Cations in Ferromagnetic Salts of [MnCr(oxalate)$_3$]$^-$", 化学系学協会北海道支部 2018 年冬季研究発表会, 1C-18, Sapporo, Japan, January 2019.
8. Wu Jiabing, Takahashi Kiyonori, Hoshino Norihisa, Suzuki Yasutaka, Hisaki Ichiro, Kawamata Jun, Akutagawa Tomoyuki, and Nakamura Takayoshi, "Crystal Structure, Dielectric and Magnetic properties of Oxalate-Bridged MnCr Complex with Supramolecular Cation of (Anilinium Derivatives)(Benzo[18]crown-6)", 日本化学会第 99 春季年会, 4D3-10, Kobe, Japan, March 2019.
9. Wu Jiabing, Takahashi Kiyonori, Fujibayashi Masaru, Huang Ruikang, Xue Chen, Kokado Kenta, Suzuki Yasutaka, Kawamata Jun, Nishihara Sadafumi, Hisaki Ichiro, Akutagawa Tomoyuki, and Nakamura Takayoshi, "Ferroelectricity based on Supramolecular Structure in Ferromagnetic [$Mn^{II}Cr^{III}$(oxalate)$_3$]$^-$ Crystal", the 15th Annual Meeting of Japan Society for Molecular Science 2021, 3D10, online, September 2021.
10. Jiabing Wu, Kiyonori Takahashi, Norihisa Hoshino, Yasutaka Suzuki, Ryo Tsunashima, Sadafumi Nishihara, Ichiro Hisaki, Jun Kawamata, Tomoyuki Akutagawa, and Takayoshi Nakamura, "Molecular Multiferroics Design Through Combining Bimetallic Oxalate Complex and Supramolecular Structure", Pacifichem 2021, online, December 2021.
11. Jiabing Wu, Kiyonori Takahashi, Yasutaka Suzuki, Sadafumu Nishihara, Ryo Tsunashima, Jun Kawamata, Tomoyuki Akutagawa, and Takayoshi Nakamura, "Oxalate-Bridged Bimetallic Ferromagnetic Hybrid Complexes: Crystal

Structures, Magnetism, Molecular Rotation, and Ferroelectricity", ICSM 2022, Glasgow, Britain, July 2022.

Acknowledgements

First and foremost, I am extremely grateful to my supervisor, Prof. T. Nakamura for his invaluable advice, continuous support, and patience during my research life. His immense knowledge and plentiful experience have encouraged me all the time in my academic research and daily life. I would also like to thank Dr. K. Takahashi, Dr. Rui-kang Huang, and Dr. Chen Xue for their technical support in my study and for the friendship built through daily life. I would like to thank all the members of the Nakamura Laboratory. It is their kind help and support that have made my study and life in Japan a wonderful time.

I am grateful to the research assistants from Prof. T. Akutagawa, Prof. S. Nishihara, Prof. R. Tsunasima, Dr. M. Fujibayashi, Mr. Tsuchiya, Mr. Kurihara.

I would like to thank and acknowledge my dearest family who have supported and inspired me so much; my father who encouraged me to face every challenge, and my mother who taught me to be patient and kind to myself and others. Thank you also to my friends who are like family, Bo-long Wu, Quan Gong, Yixiu Chen, Liujun Hu, and Kai Pi in China – I am forever grateful for your support, care, and invaluable friendship.

Chapter 1. Introduction

1-1. Multifunctionality in $[M^{II}M^{III}(oxalate)_3]^-$ system (M = transition metals)

This work focuses on bimetallic oxalate-bridged $[MnCr(oxalate)_3]^-$ system-based hybrid crystals, which are expected to be multifunctional molecular materials via incorporating functional cations.

1-1-1. Structural features and magnetic properties of $[M^{II}M^{III}(oxalate)_3]^-$ networks

In the structure of $[M^{II}M^{III}(oxalate)_3]^-$, two transition metal ions were generally bridged by organic ligand $(C2O_4)^{2-}$ to form the bis-bidentate chelate form. The topology and dimensionality and the magnetic exchange interaction in this can be regulated by the templating cations and the transition metal types, which allowed for the preparation of a large variety of magnetic networks, such as ferro-, ferri-, or canted antiferromagnets.[1, 2] For example, Okawa has reported a family of ferromagnetic salt of $[XR_4][M^{II}Cr(oxalate)_3]$ ($XR_4^+ = NBu^{4+}$; M^{II} = Mn, Fe, Co, Ni, Cu, Zn), where the different transition metal M^{II} gave rise of different ferromagnetic ordering temperature range from 6 to 12 K.[1] By using D_3 symmetric templating complexes, the network of $[M^{II}M^{III}(oxalate)_3]^-$ was found that being forced to form three-dimensional structure with all the central metals exhibited a homochiral configuration (ΔΔ or ΛΛ). The 3D networks attributed to ferro- and ferrimagnetic ordering with lower critical temperature compared to 2D networks due to their weak magnetic exchange in 3D networks.[3-6]

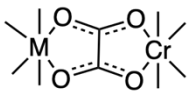

M = Mn, Fe, Co, Ni, Cu, Zn

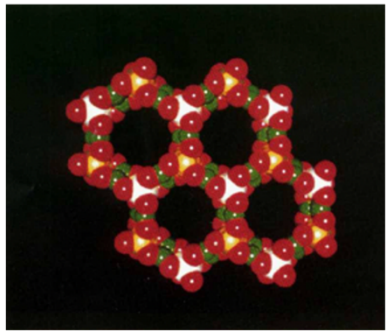

Figure 1-1. A bis-bidentate chelate form of $[MCr(oxalate)_3]^-$ (left). Schematic structure of a two-dimensional structure of $[MCr(oxalate)_3]^-$ in $[XR_4][M^{II}Cr(oxalate)_3]$ complexes.[1]

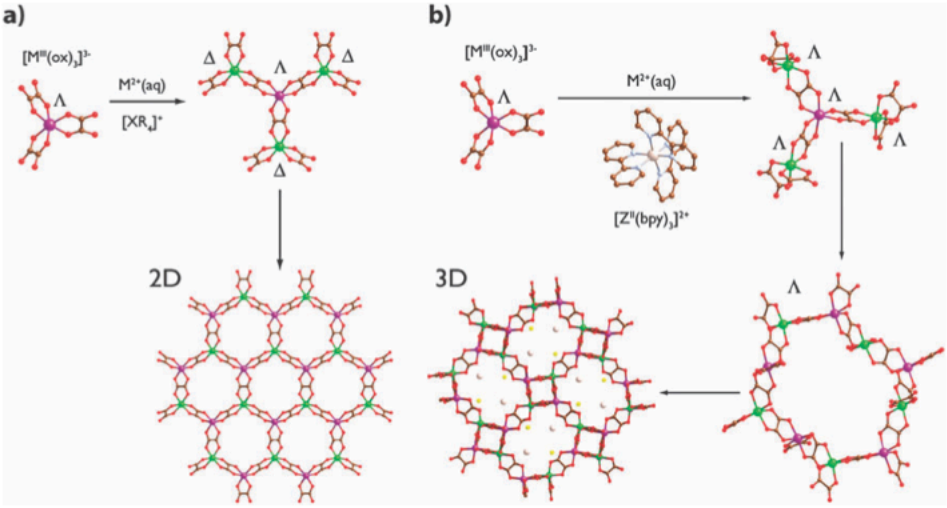

Figure 1-2. Diagram illustrating the formation of 2D heterochiral (a) and 3D homochiral (b) oxalate-based architectures depending on the nature of the templating cation.[7]

1-1-2. Examples of multifunctionality in $[M^{II}M^{III}(oxalate)_3]^-$ systems

Thanks to the negatively charged feature of $[M^{II}M^{III}(oxalate)_3]^-$ network, it possibly incorporates many functional molecular cations for constructing hybrid molecular materials which exhibit a second property besides magnetic ordering arising from the anionic network of $[M^{II}M^{III}(oxalate)_3]^-$. Some remarkable works were summarized:

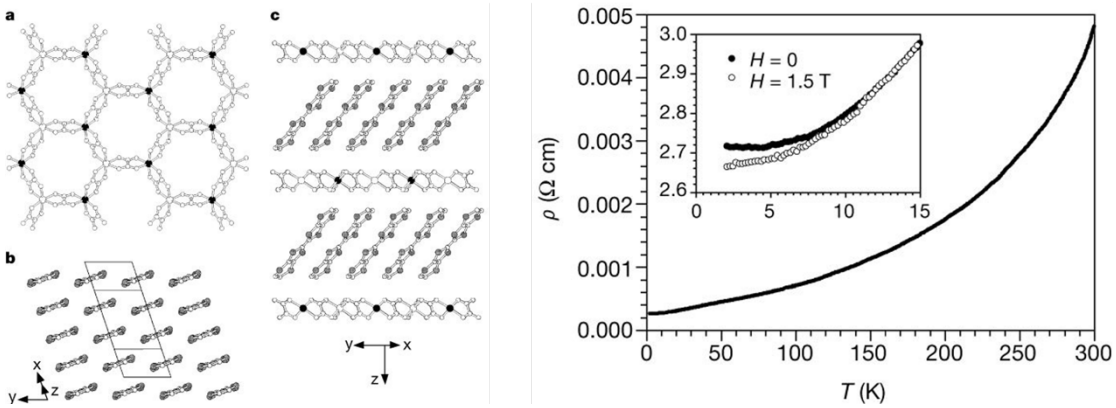

Figure 1-3. Left: Layered structure of $(BEDT\text{-}TTF)_3[MnCr(oxalate)_3]$. Right: Metallic conductivity in hybrid crystal. Insert: the low-temperature magnetoresistance with a magnetic field applied perpendicular to the layers.[8]

Ferromagnetic conductors. E. Coronado et al. reported a ferromagnetic conductor, $(BEDT\text{-}TTF)_3[MnCr(oxalate)_3]$ (BETT-TTF: bis(ethylenedithio)tetrathiafulvalene), based on an alternate layered structure of organic cation radical assembly and $[MnCr(oxalate)_3]$ anion.[8] The $(BEDT\text{-}TTF)_3^-$ anion radical assembly sandwiched by ferromagnetic layer showed metallic conduction with negative magnetoresistance at low temperature (Figure 1-3).

Optical active ferromagnets. A series of $A[M^{II}Cr^{III}(oxalate)_3]\bullet n$ solvent (A = cationic chromophores, M^{II} = Mn, Fe, Co, Ni, Cu) has been reported as second-order optical nonlinear active ferromagnets.[9] The cationic chromophores layers are alternately stacked with a magnetic layer of $[M^{II}Cr^{III}(oxalate)_3]$. The layer of $[M^{II}Cr^{III}(oxalate)_3]$ accountefor d the hybrid crystals' ferromagnetic ordering from 6 to 13 K. The proper assembly of chromophores gave rise to structural dipoles, resulting in their second-order optical nonlinear activity (Figure 1-4).

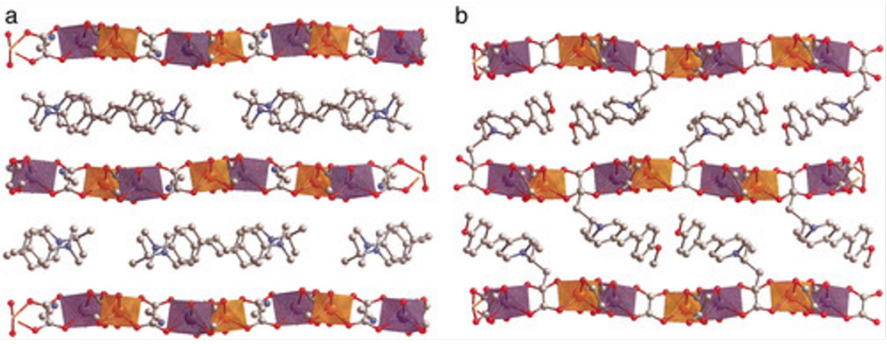

	DAZOP	DAMS	DAES	DAPS	MIPS	MHS	CINDAMS
$[MnCr(ox)_3]$	100	100	0	0	0	30	40
$[FeCr(ox)_3]$	19	17	5	19	4	21	10
$[CoCr(ox)_3]$	100	10	0	7	6	0	21
$[NiCr(ox)_3]$	25	25	0	0	0	0	1
$[CuCr(ox)_3]$	32	10	0	1	0	0	8

Figure 1-4. Anionic-cationic layered structure of optical active hybrid crystals (up). The SHG signals relative to Urea (below).[9]

Chiral ferromagnets. Magneto-chiral dichroism (MChD) is a theoretically predicted phenomenon that spatial asymmetry and magnetization should give rise to an optical anomaly. This phenomenon combines chirality and magnetization in a single

compound. By using resolved chiral cations [N(CH$_3$)(*n*-C$_3$H$_7$)$_2$((*S*, or *R*)-*s*-C$_4$H$_9$)], the enantioselective formation of the [MnCr(oxalate)$_3$] network was realized by C. Train group, presented as [N(CH$_3$)(*n*-C$_3$H$_7$)$_2$((*S*)-*s*-C$_4$H$_9$)][(*Λ*)-Mn(*Δ*)-Cr(ox)$_3$], and [N(CH$_3$)(*n*-C$_3$H$_7$)$_2$((*R*)-*s*-C$_4$H$_9$)][(*Δ*)-Mn(*Λ*)-Cr(ox)$_3$].[10] These two compounds showed equivalent ferromagnetic properties which was determined by the identical structures of [Mn^{II}Cr^{III}(oxalate)$_3$] but with different configurations. The MChD effect in a chiral magnetic system was first revealed through this research.

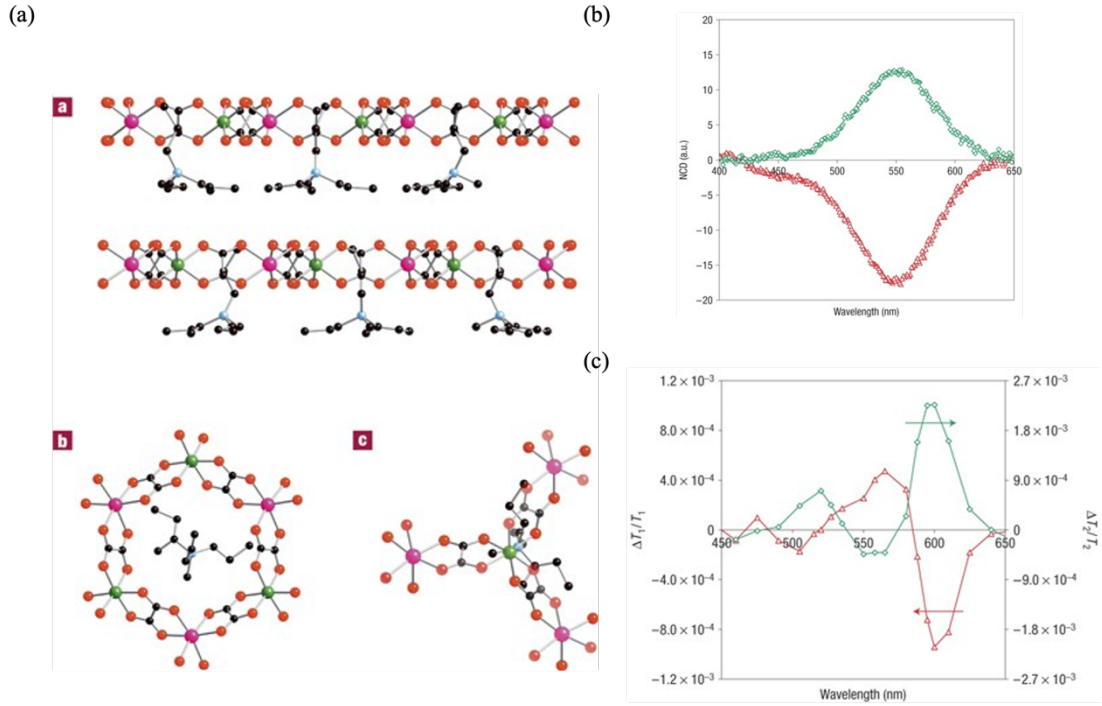

Figure 1-5. (a) Crystal structure of [N(CH$_3$)(*n*-C$_3$H$_7$)$_2$((*S*)-*s*-C$_4$H$_9$)][(*Λ*)-Mn(*Δ*)-Cr(ox)$_3$]. (b) NCD signals of two chiral hybrid crystals. (c) Magneto-chiral dichroism measured in ferromagnetic ordering at 4 K.[10]

Multiferroics. Although demonstrating [M^{II}M^{III}(oxalate)$_3$]$^-$ networks for the construction of molecular multiferroics, where ferroelectric and ferromagnetic order coexist, has not yet made much progress, [7] there are some examples of attempts to synthesize multiferroics by using other coordination polymers, like Rb$_{0.82}$Mn[Fe(CN)$_6$]$_{0.94}$•H$_2$O and [Mn$_3$(HCOO)$_6$](C$_2$H$_5$OH).[11,12] In Rb$_{0.82}$Mn[Fe(CN)$_6$]$_{0.94}$•H$_2$O, the ordering of valence-delocalized Mn^{2+} and Mn^{3+} ions in the hybrid crystal gave the ferromagnetic magnetization with a Curie temperature of 11 K. The author explained a local electric dipole moment created by Fe vacancy, and

Jahn-Teller distortion of Mn^{III} may result in a ferroelectric transition, though a nice polarization hysteresis was not observed in this coordination polymer.

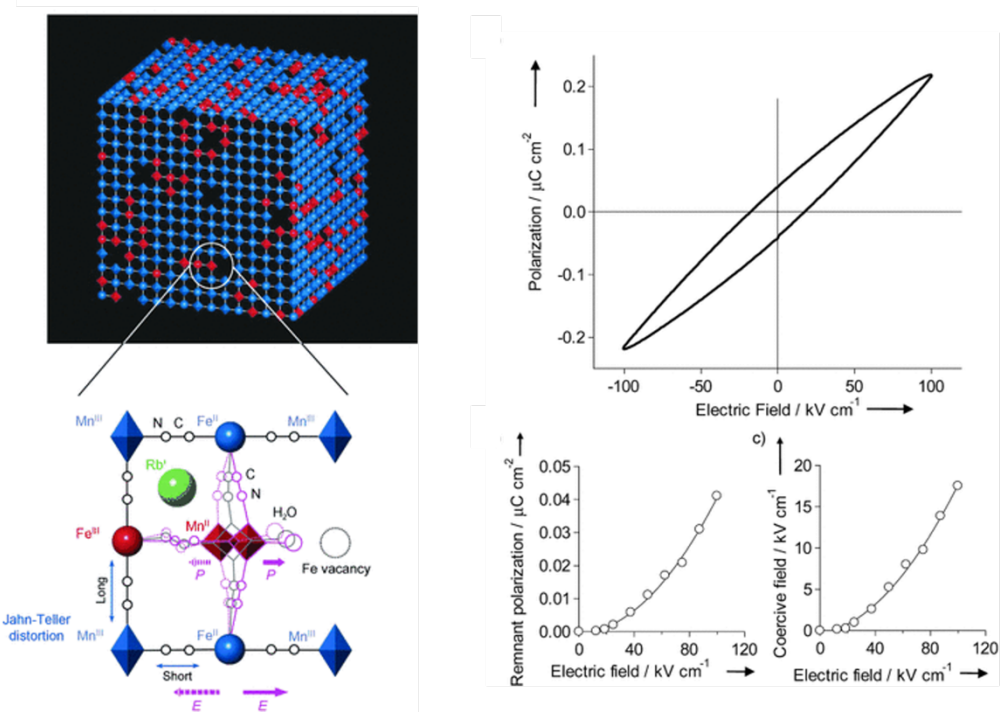

Figure 1-6. Left: Scheme illustration to explain the mechanism of ferroelectricity in $Rb_{0.82}Mn[Fe(CN)_6]_{0.94}\bullet H_2O$. Right: *P*-*E* curve and remnant polarization.

1-2. Molecular multiferroics

Multiferroics are materials that have more than one ferric polarization, including spontaneous magnetization (ferromagnetism), spontaneous electric polarization (ferroelectricity), and spontaneous strain (ferroelasticity).[13-15] Multiferroics are generally divided into two subgroups. One of the subgroups is multiferroic heterostructures and composites,[16, 17] where the coexistence between ferroic orders is realized by combining two independent layers with different ferroic orders into a composite structure. Another type of multiferroics is called molecular multiferroics.[18-20] In molecular multiferroics, two or three ferroic orders coexist in a single compound. The hybrid molecular materials are ideal candidates for molecular multiferroics.[21, 22]

This study only focused on molecular multiferroics with ferromagnetism and ferroelectricity.

1-2-1. Ferromagnetism

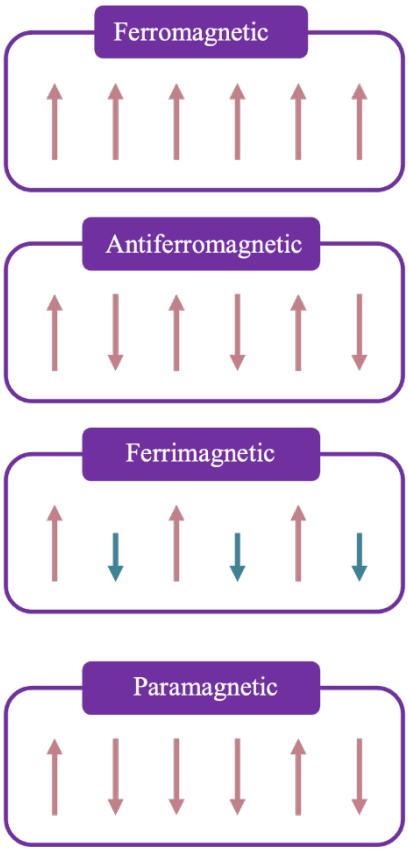

Figure 1-7. Schematic figures of magnetic orders.

Ferromagnetism is a physical phenomenon in which certain electrically neutered materials strongly attract each other.[23-25] The magnetic moments in ferromagnetic ordering parallel aligned, arising large net magnetization. Hence, spontaneous magnetization can be observed in ferromagnetic materials even without an applied magnetic field, and in strong magnetic fields, the magnetization approaches a limit saturate value depending on the nature of magnetic materials. When a field is applied and then removed, the magnetization does not return to its original value–this phenomenon is referred to as hysteresis. Even though ferromagnetic exchange forces in ferromagnets are large, thermal energy eventually overcomes the exchange so that the order of ferromagnetism cannot keep. This critical temperature is called the Curie temperature (Tc). Below Tc, the ferromagnet is ordered and above it, disordered.

In antiferromagnetic materials, magnetic moments in a sublattice are exactly equal but opposite, the net moment is zero. Another type of magnetic ordering is called

ferrimagnetism. The magnetic structure is like antiferromagnetic order, but the magnetic moments with opposite alignment are not equal and result in a net magnetic moment. The behavior of ferrimagnetism is therefore similar to ferromagnetism, exhibiting spontaneous magnetization, Curie temperatures, hysteresis, and remanence. The paramagnetic materials have a net magnetic moment due to unpaired electrons in partially filled orbitals, but between the individual magnetic moments, they do not interact with each other, resulting in zero magnetization when the magnetic field is removed. Under a magnetic field, a partial alignment of the magnetic moments in the direction of the field induces a net positive magnetization.[26-28]

1-2-2. Ferroelectricity

Ferroelectricity is a physical property observed in nonconducting solid materials, or dielectrics, that exhibit spontaneous electric polarization, and the polarization can be reversed in direction by applying an external electric field.[29]

Ferroelectric materials exhibit a hysteresis loop like ferromagnetic materials. A typical ferroelectric hysteresis loop is shown in Figure 1-8, at low electric fields and very high electric fields, a ferroelectric material behaves like an ordinary dielectric with a high dielectric constant, but when increasing the electric field to a coercive field (E_c), a reversal signal of polarization will be observed. The maximum amount of polarization that ferroelectric materials can induce at a high electric field is called saturation polarization (P_s). When reducing the electric field to zero fields (E_0), the electric displacement within a single domain has two values ($-P_R$ and $+P_R$), representing the opposite orientation of the spontaneous polarization. Because the ferroelectric crystals have multiple domains, the measured value of P_r is smaller than the real remanent polarization.[30, 31]

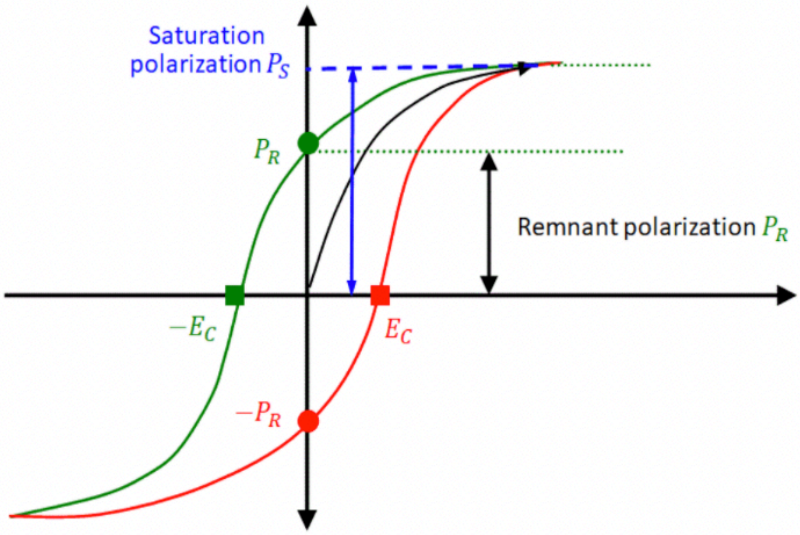

Figure 1-8. Ferroelectric hysteresis loop.[32]

The feature of reversible polarization controlled by the electric field in ferroelectric materials allows potential applications for use in electronics, ranging from tunable nonlinear components to energy generation.[33-35]

1-2-3. Molecular multiferroics

Molecular multiferroic materials should possess ferromagnetic and ferroelectric orders in a single-phase.[13-15] Magnetoelectric (ME) coupling effect may arise in multiferroic materials, indicating coupling between the magnetic and the electric properties in a single material. Through magnetoelectric coupling, the polarization related to ferroelectric order can be controlled by the magnetic field, and the magnetization related to magnetic order is correlated with applying an electric field.[15] [36] [37] ME coupling effect allows the applications in memory devise to overcome the slow writing problem of ferroelectric memory and high energy consumption drawback of magnetic random access memory due to the energy efficiency of the magnetic field.[38] [39]

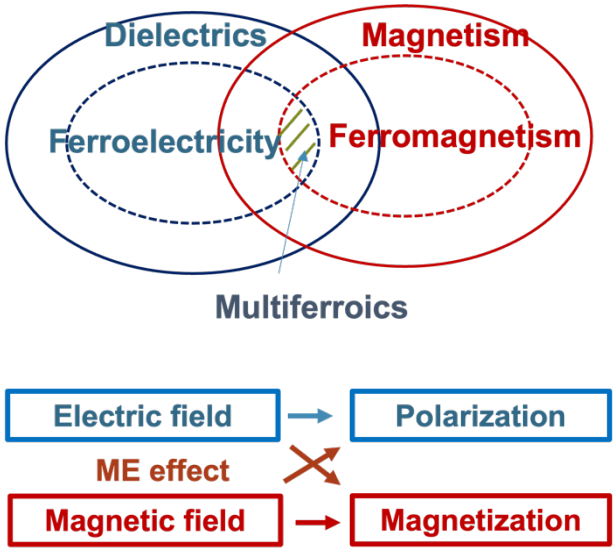

Figure 1-9. The relationship between ferroelectric and ferromagnetic orders.

Molecular multiferroics are divided into two subgroups, type-I, and type-II multiferroics according to the origin of ferroic orders.[21]

Type-I multiferroics. The first group is type-I multiferroics, where the ferroelectric and ferromagnetic orders originated from two different structural units and appear largely independently of one another. The most common type-I multiferroics are inorganic oxides like $BiFeO_3$. In the perovskite structure of $BiFeO_3$, the cation of Bi^{3+} resulted in ferroelectricity due to the ordering of lone pairs on Bi^{3+}, and the ferrite ions on FeO_3^{3-} sites gave rise to magnetism. [40] N. A Spaldin discussed that two independent orders of ferroelectricity and ferromagnetism are hard to coexist, and only a moderate ME effect could be observed due to the weak spin-lattice interaction in multiferroics.[41]

Type-II multiferroics. The second type of molecular multiferroics is type-II multiferroics, where ferroelectricity is induced by magnetization. Because the sources of ferroelectric and ferromagnetic are the same, they always show strong ME effects. The most famous type-II multiferroic material is the manganite perovskite $TbMnO_3$,[42] in which the behavior of spin frustration directedly induced a ferroelectric order, and therefore the ME effect was giant. Thereafter, another magnetic-induced ferroelectricity was reported in $TbMn_2O_5$.[43] Though the ME effect in these type-II multiferroics, their magnetic-induced polarization tends to be small, which limits future applications.[44]

1-3. Point to be addressed for multiferroics design in [MnCr(oxalate)$_3$] network

Apart from the inorganic oxide-based multiferroics, a few metal-organic frameworks (MOFs) were used for constructing type-I multiferroics. Generally, the metallic coordinated frameworks bring about magnetic ordering, and the alignments of guest cations afford ferroelectricity in these hybrid MOFs. However, the reported examples of multiferroics are still rare, and most of them are formate-base MOFs.[21]

1-3-1. Strict symmetric limitation for ferroelectricity

As one of the necessary orders in multiferroics, ferroelectric materials are inseparable from symmetry breaking. According to the summarized works,[45] the point group of ferroelectric materials must belong to the 10 polar point groups (Table 1-1).

Table 1-1. 68 ferroelectric space groups belonging to the 10 polar point groups. [45]

Point group	Space group
C_1	$P1$
C_2	$P2$, $P2_1$, $C2$
C_{1h}	Pm, Pc, Cm, Cc
C_{2v}	$Pmm2$, $Pmc2_1$, $Pcc2$, $Pma2$, $Pca2_1$, $Pnc2$, $Pmn2_1$, $Pba2$, $Pna2_1$, $Pnn2$, $Cmm2$, $Cmc2_1$, $Ccc2$, $Amm2$, $Abm2$, $Ama2$, $Aba2$, $Fmm2$, $Fdd2$, $Imm2$, $Iba2$, $Ima2$
C_4	$P4$, $P4_1$, $P4_2$, $P4_3$, $I4$, $I4_1$
C_{4v}	$P4mm$, $P4bm$, $P42cm$, $P4_2nm$, $P4cc$, $P4nc$, $P4_2mc$, $P4_2bc$, $I4mm$, $I4cm$, $I4_1md$, $I4_1cd$
C_3	$P3$, $P3_1$, $P3_2$, $R3$
C_{3v}	$P3m1$, $P31m$, $P3c1$, $P31c$, $R3m$, $R3c$
C_6	$P6$, $P6_1$, $P6_5$, $P6_2$, $P6_4$, $P6_3$
C_{6v}	$P6mm$, $P6cc$, $P6_3cm$, $P6_3mc$

T. Nakamura group has reported a ferroelectric rotor of (*m*-fluoroanilinium)dibenzo[18]crown-6 in $[Ni(dmit)_2]^-$ (dmit: 2-thioxo-1,3-dithiole-4,5-dithiolate) salt.[46] As shown in Figure 1-10, the cation (*m*-fluoroanilinium) underwent a 180° flip-flop motion with dipole moments changed along the *a*-axis direction. Such rotation can be controlled by the external electric field, and it is a good candidate for constructing hybrid multiferroics due to its ferroelectric property and positively charged structure.

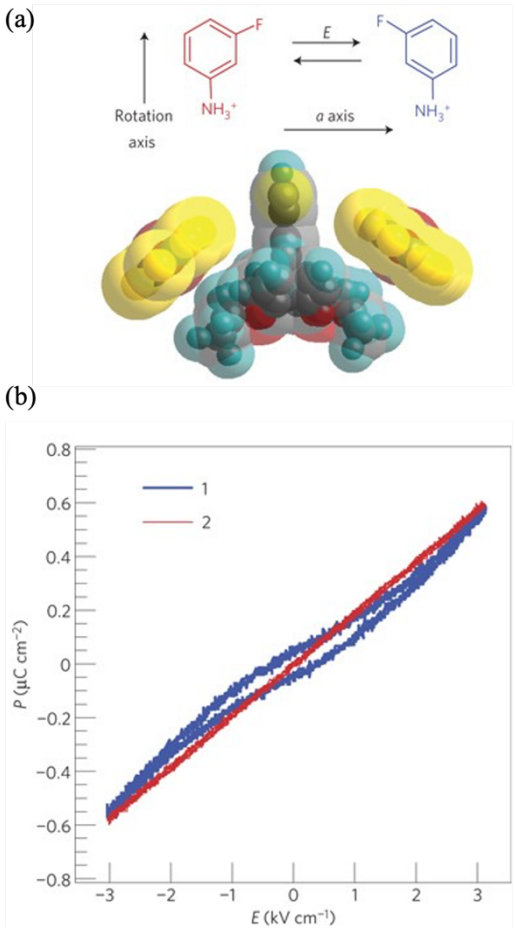

Figure 1-10. (a) Flip-flop motion of (*m*-fluoroanilinium) with reversal polarization. (b) The *P*-*E* curve (blue) for ferroelectric (*m*-$FAni^+$)(DB[18]crown-6)$[Ni(dmit)_2]^-$.

In previous work, we have attempted using supramolecular rotor (*m*-fluoroanilinium)dibenzo[18]crown-6 to induce ferroelectricity in $[MnCr(oxalate)_3]^-$ network.[47] As a result, a hybrid crystal (*m*-fluoroanilinium)dibenzo[18]crown-6$[MnCr(oxalate)_3]^-$ $(CH_3OH)(CH_3CN)$ was obtained, exhibiting alternating layers of a two-dimensional honeycomb layer of $[MnCr(oxalate)_3]^-$ and (*m*-

fluoroanilinium)dibenzo[18]crown-6 supramolecular cation. This hybrid salt showed ferromagnetic ordering at 5.5 K. However, due to the space hindrance, the flip-flop motion of (*m*-fluoroanilinium) did not realize in this hybrid crystal, crystallized in unpolar space group $P2_1/c$, which did not belong to the required space group for ferroelectricity.

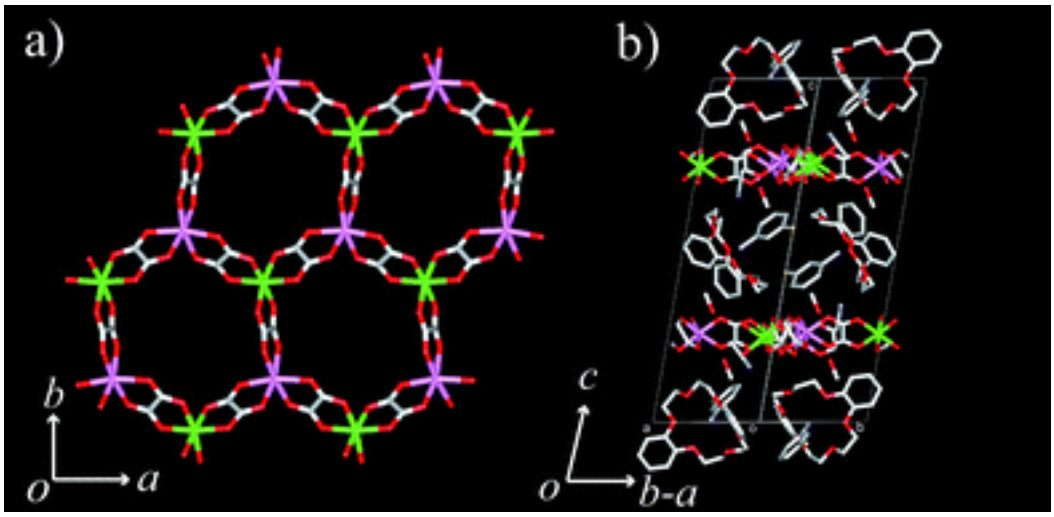

Figure 1-11. Crystal structure of (*m*-fluoroanilinium)dibenzo[18]crown-6[$MnCr(oxalate)_3$]$^-$ (CH_3OH)(CH_3CN). Space group: $P2_1/c$.

1-3-2. Negative effects from guest solvents

As the first example of molecular multiferroics based on MOFs, $[Mn_3(HCOO)_6](C_2H_5OH)$, the disordered behavior of guest solvents C_2H_5OH in $[Mn_3(HCOO)_6]$ channels afforded a ferroelectric transition at 163 K, the alignment of Mn^{2+} bridged by $HCOO^-$ ligands gave rise to a ferrimagnetic transition at 8.5 K.[11] The ferroelectric property in this multiferroic crystal exhibited strongly dependent on the existence of guest molecular C_2H_5OH. A gradual weight loss was observed from 300 K to 373 K. The desolvated structure of these multiferroic materials did not show any ferroelectric order anymore due to the loss of ferroelectric source C_2H_5OH. The volatility of the solvent makes this multiferroic unstable at room temperature, limiting its application as a ferroelectric material.

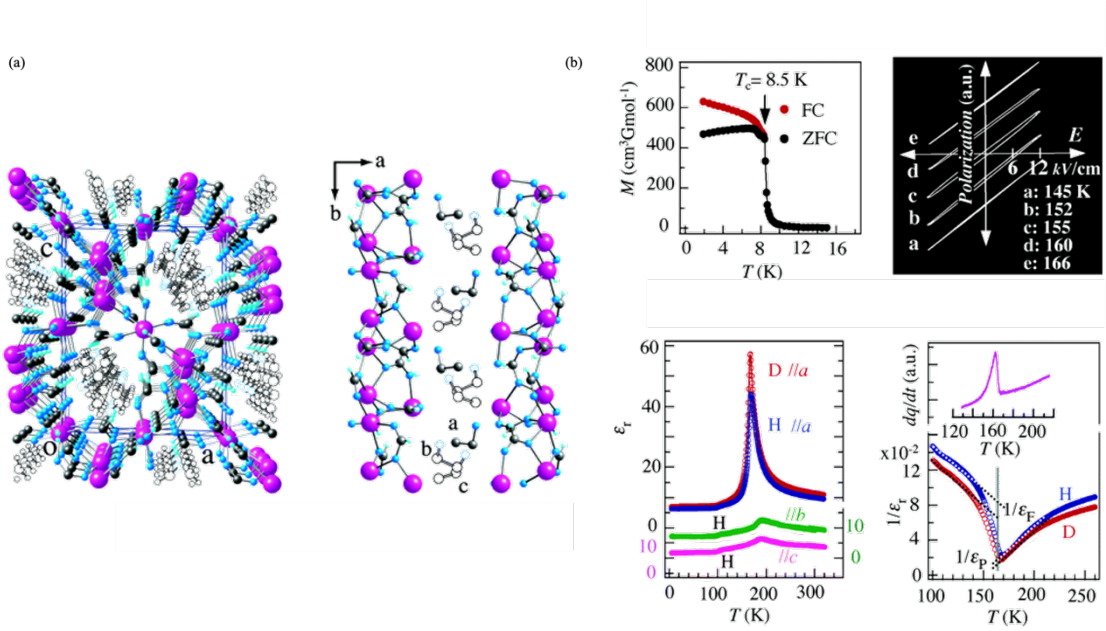

Figure 1-12. (a) Crystal structure of $[Mn_3(HCOO)_6](C_2H_5OH)$. (b) Multiferroics properties.

The guest solvents, which play the role of ferroelectric source in multiferroics not only make the ferroelectric properties disappear upon desolvation, but in some solvent-contained crystals, the desolvation of the solvents causes the crystals to crack, making it difficult to test the physical properties, as well as multiferroic properties.

In $[MnCr(oxalate)_3]^-$ system, it can be a good candidate for molecular multiferroics due to the feature of ferromagnetic ordering and incorporation of functional cations. We did several attempts in this study field, although the $[MnCr(oxalate)_3]^-$ exhibited

various dimensionalities in the crystals, such as 3D cage structures[48] and typical 2D layers,[47 49, 50] however, they readily crystallize with solvent molecules, especially in the cavities of the honeycomb layers. The solvent molecules incorporated in the crystal often make it difficult to determine the physical properties of the crystals, especially above room temperature. This is because the crystals become unstable and collapse owing to desolvation. In addition, due to the presence of solvent between supramolecules and $[MnCr(oxalate)_3]^-$, the spatial hindrance increases and inhibits the rotation of the supramolecular rotor, so it is difficult to obtain ferroelectrics.[47]

1-4. Gyroid structure

The gyroid is a type of 3D periodic structure with highly symmetric structures. Due to its strong isotropic feature, the gyroid structure shows huge potential in mechanical strength and exotic photonic and electronic properties. By designing a proper templating cation, $[MnCr(oxalate)_3]^-$ can form a gyroid structure. Due to the unique properties of the gyroid as mentioned, the bimetallic oxalate-bridged network exhibiting the gyroid structure will provide a new idea for the study of multifunctional magnetic materials.

1-4-1. Gyroid structure

The concept of gyroid was from an infinitely connected triply-periodic minimal surface discovered by Shoen,[51] represented by an equation $\sin x \cos y + \sin y \cos z + \sin z \cos x = 0$. There was no distinction between the front and back sides of gyroid surface. A gyroid surface separates a three-dimensional space into a pair of enantiomeric channels, and these channels are called single gyroids. When two single gyroids with different chirality are paired in a 3D space, this structure is called a double-gyroid. (Figure 1-13) The single gyroid with a chirality belongs to the cubic space group of $I4_132$, including 3-fold axes and 4-fold screw axes (4_1 or 4_3).

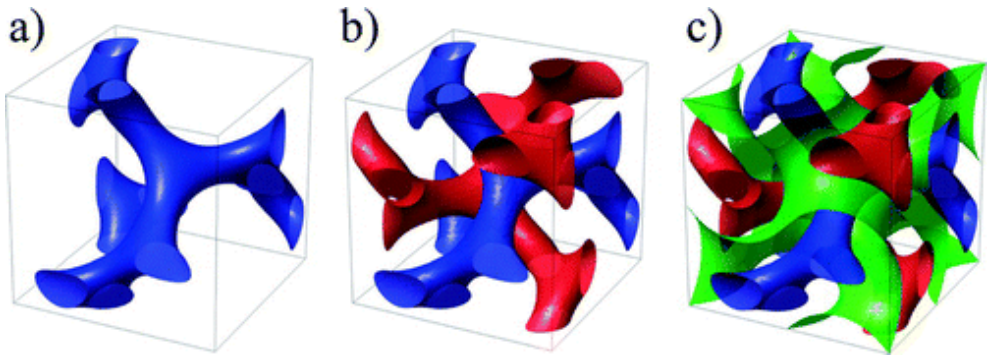

Figure 1-13. Single gyroid (a), double gyroid (b), and gyroid surface (green) between the single gyroids.[52, 53]

1-4-2. Unique physical properties in gyroid structure

The carbon with the gyroid lattice was theoretically discussed. It was found that the carbon with gyroid structure exhibited a metallic ground state and the existence of Dirac cones through band calculation,[54, 55] which contrasts with the insulating property of diamond. The researchers mentioned the spin cross-over (SCO) occurred in the band structure of carbon gyroid, resulting in the splitting of the $S = 1$ Dirac point into the $S = 3/2$ and $S = 1/2$ Weyl points.[56] The unique band structure in carbon gyroid was thought to be the result of the maximal symmetry and a strong isotropic property.

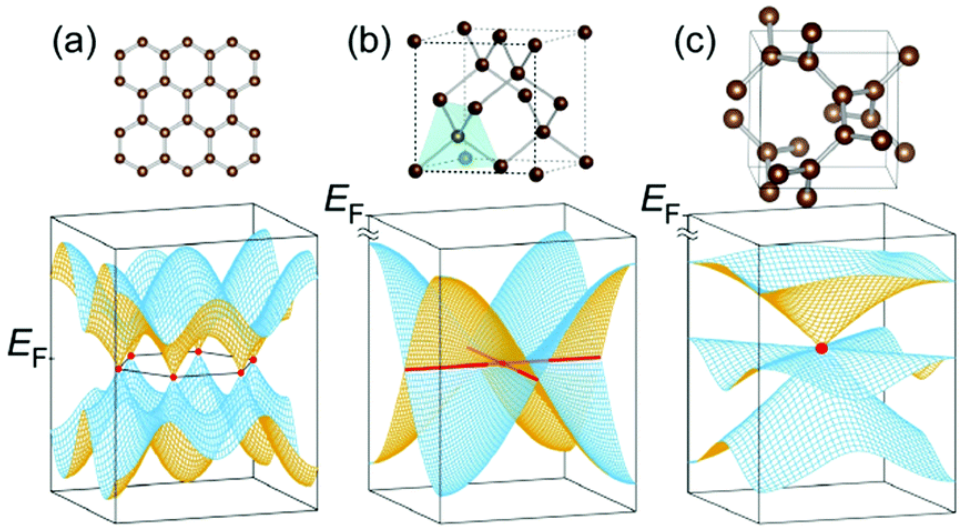

Figure 1-14. Electronic band structure of (a) graphene with Dirac cones, (b) diamond with Dirac nodal lines, and (c) gyroid carbon with $S = 1$ Dirac cones.[57]

Besides gyroid carbon, K. Awaga group has successfully synthesized the gyroid structure by using organic naphthalene diimide (NDI)- Δ. An antiferromagnetic intermolecular interaction with the Weiss constant of θ = -10 K was confirmed in this radical anion salt. The band structure calculation revealed a metallic ground state, Dirac cones, and flat bands.[58] In an extended work, the same group also reported the gyroid $(TBA)_{1.5}$[(–)-(NDI)-Δ] (TBA = tetrabutylammonium) showed spin-liquid state and the possibility of 3D spin frustration.[59]

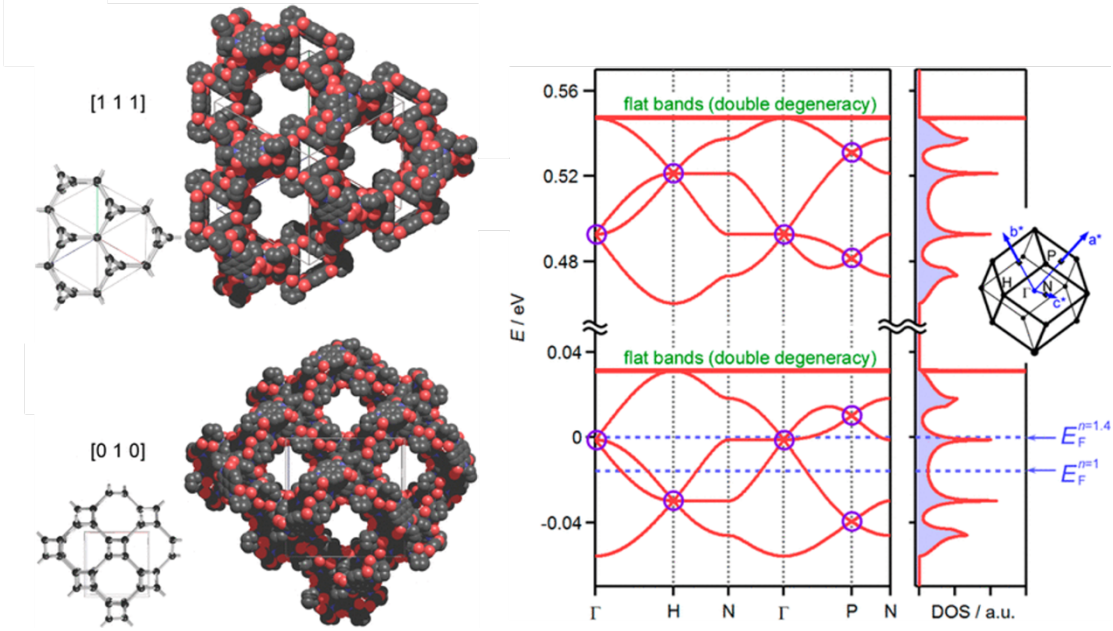

Figure 1-15. Left: The crystal structures of gyroid carbon and (–)-(NDI)-Δ gyroid structure. Right: band structure and density of state (DOS). The purple area in DOS indicated Dirac cones.

1-4-3. Gyroid structure based on oxalate complexes

The gyroid structure can also be constructed by metallic oxalate-bridged structures. Because metallic oxalate-bridged structure shows structural variation, the key factor for gyroid of 3-fold symmetry and chirality can be designed in oxalate complexes. To data, some examples of oxalate gyroid structures were reported by using a chiral metallic complex to template the whole structure be gyroid, such as $[Fe(II)(bpy)_3][(FeII)_2(oxalate)_3]$ (bpy = 2,2'-bipyridine) (Figure 1-16).[5]

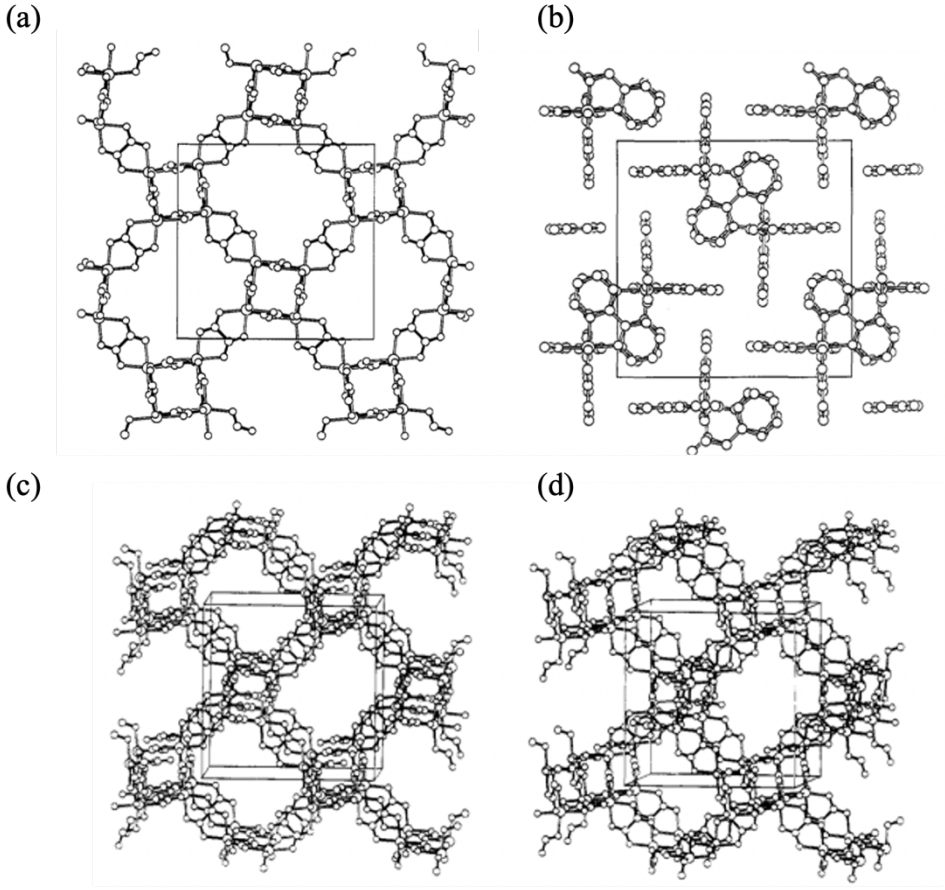

Figure 1-16. Projection of gyroid structure of $[(FeII)_2(oxalate)_3]^-$ (a) (c) (d), and chiral cation $[Fe(II)(bpy)_3]^+$ (b).

So far, there are only a few oxalate gyroid structures formed by using achiral c cations such as $\{(Me_2NH_2)_3(SO_4)\}^+$. As shown in Figure 1-17, D_3 symmetric supramolecular cation $\{(Me_2NH_2)_3(SO_4)\}^+$ adopted the network of $[(M^{II})_2(oxalate)_3]^-$ (M = Fe, Co, Ni) be a homochiral 3D structure. The oxalate network showed strongly isotropic properties viewed from the projection structure along the *a*, *b*, and *c*-axis.[60]

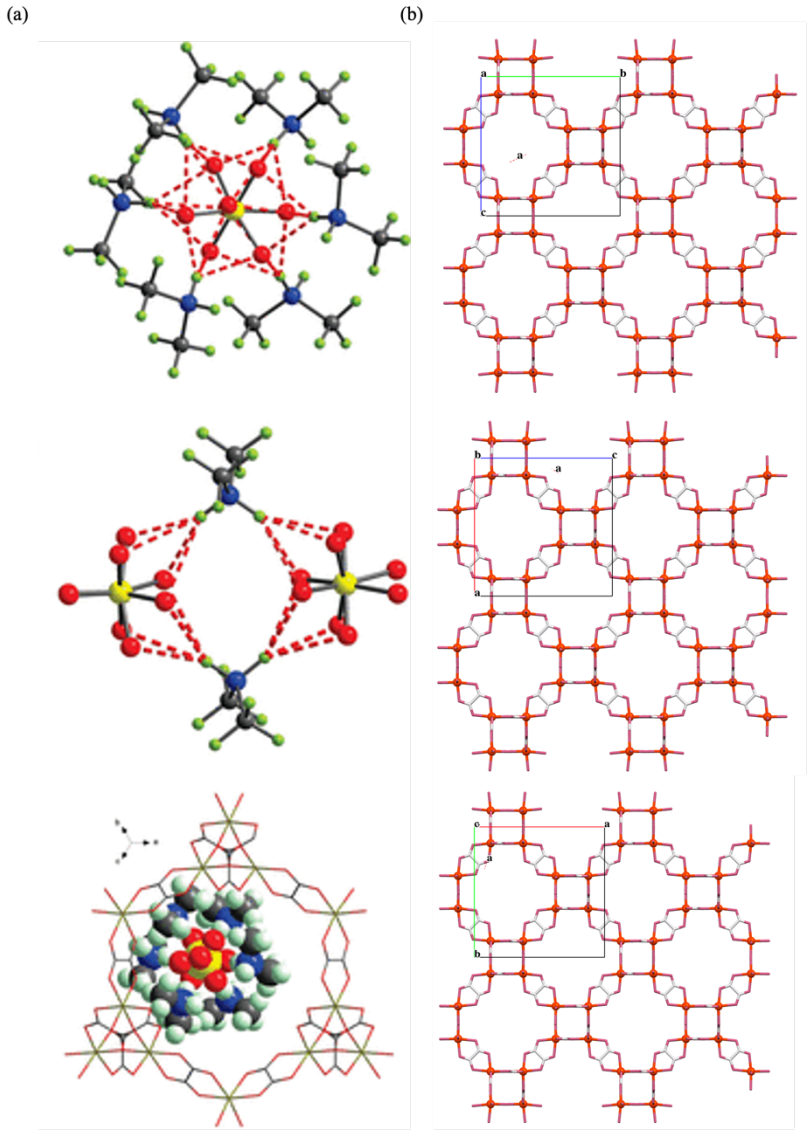

Figure 1-17. (a) D_3 symmetric supramolecular $\{(Me_2NH_2)_3(SO_4)\}^+$ (b) Projection of $[Fe_2(oxalate)_3]^-$, viewed along *a*, *b*, and *c*-axis.

In these oxalate gyroid structures, though their magnetic spin was formed in the 3D gyroid structure of localized spins, there were no unique magnetic properties so far to the exotic structural aspects of gyroids, such as chirality, minimal surface, and porosity. More details about oxalate gyroid should be reclaimed.

1-5. Research objectives

The major focus of my research project is multifunctionality in hybrid crystals based on the $[MnCr(oxalate)_3]^-$ system. Among multifunctional materials, molecular multiferroics, where ferroelectric and ferromagnetic orders coexist, have attracted much attention due to the potential applications of their magnetoelectric coupling effect for novel memory devices.

The anionic $[MnCr(oxalate)_3]^-$ the system can exhibit ferromagnetic ordering at low temperatures. However, the ferroelectric order generally shows mutually exclusive with ferromagnetic order in a single compound. The first issue is to design proper hybrid crystal structures which can meet the requirement of symmetry for ferroelectric materials. From the reported $[MnCr(oxalate)_3]^-$ based hybrid crystals, we already know that the structure of cation essentially rules the dimensionality and the second functional property in ferromagnetic $[MnCr(oxalate)_3]^-$. We aim to introduce supramolecular cations, like supramolecular rotor (*m*-fluoroanilinium)dibenzo[18]crown-6, into the $[MnCr(oxalate)_3]^-$ network to realize the coexistence between ferroelectricity and ferromagnetism. To evaluate the multifunctional properties of target crystals, this thesis includes the synthesis of single crystals, and crystal structure determination via single-crystal X-ray diffraction, dielectric, and magnetic measurements.

The research background is summarized in chapter **1**, among many functional materials based on $[MnCr(oxalate)_3]^-$, I focus on constructing multiferroic materials. I strive to discover the first example of $[MnCr(oxalate)_3]^-$ based multiferroic crystal. This section mentioned two challenging points: the strict symmetric condition in ferroelectrics, and the guest solvent-induced structure cracking. At the end of this section, I try to touch on an interesting three-dimensional periodic structure–gyroid structure and believe that gyroid oxalate with strong isotropic feature and chirality could lead to new research on multifunctional oxalate bridged complexes.

In Chapter **2**, through adjusting dibenzo[18]crown-6 in supramolecular rotor of (*m*-fluoroanilinium)dibenzo[18]crown with less symmetric benzo[18]crown-6, a series of non-solvent contained, polar crystals were synthesized, consist of supramolecular (*x*-

anilinium)benzo[18]crown-6 and anionic $[MnCr(oxalate)_3]^-$ (x = H, *o*-fluoro, *m*-fluoro, and *p*-fluoro). Among them, the first example of a molecular multiferroic crystal based on $[MnCr(oxalate)_3]^-$ was obtained. This result demonstrates that the supramolecular structure of (*o*-fluoroanilinium)benzo[18]crown-6 in $[MnCr(oxalate)_3]^-$ is capable of inducing ferroelectric transition, and the advantage of the structural flexibility of supramolecular structure in the construction of multiferroic materials is proved.

In Chapter **3**, I focus on addressing the issue of guest solvents in the development of multifunctional materials. Hydrogen bond active supramolecular cation of (carboxybutan-1-aminium$^+$) was designed for combining with $[MnCr(oxalate)_3]^-$ network. A hybrid polar crystal (carboxybutan-1-aminium$^+$)[18]crown-6$[MnCr(oxalate)_3](CH_3OH)$ were synthesized, crystalized in *Cc* space group. The polar structure of the crystal was retained after CH_3OH desolvation. And the "merry-go-round" motion of [18]crown-6 was intrigued by this desolvation. The crystal-to-crystal structural transition provides an ideal for designing multifunctional hybrid materials, where. The second function arises from molecular motion.

I have made a preliminary attempt at the research matter that constructing gyroid oxalate via organic supramolecular structures in Chapter **4**. At this stage, achiral, less symmetric supramolecular (ethanaminium$^+$)benzo[18]crown-6 and chiral supramolecular {(1*S*, 2*S*)-1,2-diphenylethan-1,2-diaminium}[18]crown-6 were used in synthesis of three-dimensional structure of $[MnCr(oxalate)_3]^-$. These crystals both show chirality, however, the gyroid structure is not realized.

The conclusions and experimental methods of this thesis are summarized in Chapter **5** and Chapter **6** respectively.

Reference

1. H. Tamaki, Z. J. Zhong, N. Matsumoto, S. Kida, M. Koikawa, N. Achiwa, Y. Hashimoto and H. Okawa, *J. Am. Chem. Soc.*, 1992, **114**, 6974-6979.
2. C. Mathoniere, C. J. Nuttall, S. G. Carling and P. Day, *Inorg. Chem.*, 1996, **35**, 1201-1206.
3. M. Clemente-Leon, E. Coronado, C. J. Gomez-Garcia and A. Soriano-Portillo, *Inorg. Chem.*, 2006, **45**, 5653-5660.
4. E. Coronado, J. R. Galan-Mascaros, C. J. Gomez-Garcia and J. M. Martinez-Agudo, *Inorg. Chem.*, 2001, **40**, 113-120.
5. S. Decurtins, H. W. Schmalle, P. Schneuwly and H. R. Oswald, *Inorg. Chem.*, 1993, **32**, 1888-1892.
6. F. Pointillart, C. Train, M. Gruselle, F. Villain, H. W. Schmalle, D. Talbot, P. Gredin, S. Decurtins and M. Verdaguer, *Chem. Mater.*, 2004, **16**, 832-841.
7. M. Clemente-Leon, E. Coronado, C. Marti-Gastaldo and F. M. Romero, *Chem. Soc. Rev.*, 2011, **40**, 473-497.
8. E. Coronado, J. R. Galan-Mascaros, C. J. Gomez-Garcia and V. Laukhin, *Nature*, 2000, **408**, 447-449.
9. S. Benard, P. Yu, J. P. Audiere, E. Riviere, R. Clement, J. Guilhem, L. Tchertanov and K. Nakatani, *J. Am. Chem. Soc.*, 2000, **122**, 9444-9454.
10. C. Train, R. Gheorghe, V. Krstic, L. M. Chamoreau, N. S. Ovanesyan, G. L. J. A. Rikken, M. Gruselle and M. Verdaguer, *Nat. Mater.*, 2008, **7**, 729-734.
11. H. B. Cui, Z. M. Wang, K. Takahashi, Y. Okano, H. Kobayashi and A. Kobayashi, *J. Am. Chem. Soc.*, 2006, **128**, 15074-15075.
12. S. Ohkoshi, H. Tokoro, T. Matsuda, H. Takahashi, H. Irie and K. Hashimoto, *Angew. Chem. Int. Ed.*, 2007, **46**, 3238-3241.
13. M. Fiebig, T. Lottermoser, D. Meier and M. Trassin, *Nat Rev Mater*, 2016, **1**.
14. N. A. Spaldin and M. Fiebig, *Science*, 2005, **309**, 391-392.
15. N. A. Spaldin and R. Ramesh, *Nat. Mater.*, 2019, **18**, 203-212.

16. L. Martin, S. P. Crane, Y. H. Chu, M. B. Holcomb, M. Gajek, M. Huijben, C. H. Yang, N. Balke and R. Ramesh, *J Phys-Condens Mat*, 2008, **20**.
17. R. Ramesh and N. A. Spaldin, *Nat. Mater.*, 2007, **6**, 21-29.
18. Y. Hu, S. Broderick, Z. P. Guo, A. T. N'Diaye, J. S. Bola, H. Malissa, C. Li, Q. Zhang, Y. L. Huang, Q. X. Jia, C. Boehme, Z. V. Vardeny, C. Zhou and S. Q. Ren, *Nat. Commun.*, 2021, **12**.
19. E. Pardo, C. Train, H. B. Liu, L. M. Chamoreau, B. Dkhil, K. Boubekeur, F. Lloret, K. Nakatani, H. Tokoro, S. Ohkoshi and M. Verdaguer, *Angew. Chem. Int. Ed.*, 2012, **51**, 8356-8360.
20. Q. Song, C. A. Occhialini, E. Ergecen, B. Ilyas, D. Amoroso, P. Barone, J. Kapeghian, K. Watanabe, T. Taniguchi, A. S. Botana, S. Picozzi, N. Gedik and R. Comin, *Nature*, 2022, **602**, 601-+.
21. X. L. Liu, D. Li, H. X. Zhao, X. W. Dong, L. S. Long and L. S. Zheng, *Adv. Mater.*, 2021, **33**.
22. G. Rogez, N. Viart and M. Drillon, *Angew. Chem. Int. Ed.*, 2010, **49**, 1921-1923.
23. D. C. Jiles and D. L. Atherton, *J. Magn. Magn. Mater.*, 1986, **61**, 48-60.
24. C. Kittel, *Rev Mod Phys*, 1949, **21**, 541-583.
25. C. Kittel, *J Geophys Res-Sol Ea*, 1998, **103**, 30533-30536.
26. F. Keffer and C. Kittel, *Phys Rev*, 1952, **85**, 329-337.
27. N. Roques, V. Mugnaini and J. Veciana, *Functional Metal-Organic Frameworks: Gas Storage, Separation and Catalysis*, 2010, **293**, 207-258.
28. C. J. M. D, *Cambridge university press*, 2010.
29. R. G. Kepler and R. A. Anderson, *Adv Phys*, 1992, **41**, 1-57.
30. T. Hang, W. Zhang, H. Y. Ye and R. G. Xiong, *Chem. Soc. Rev.*, 2011, **40**, 3577-3598.
31. H. Y. Liu, H. Y. Zhang, X. G. Chen and R. G. Xiong, *J. Am. Chem. Soc.*, 2020, **142**, 15205-15218.
32. J. Valasek, *Phys Rev*, 1921, **17**, 475-481.
33. T. Y. Kim, S. K. Kim and S. W. Kim, *Nano Converg*, 2018, **5**.
34. J. D. Childress, *J. Appl. Phys.*, 1962, **33**, 1793-+.

35. Z. Liu, L. J. Deng and B. Peng, *Nano Res*, 2021, **14**, 1802-1813.
36. M. Fiebig, *J Phys D Appl Phys*, 2005, **38**, R123-R152.
37. W. Eerenstein, N. D. Mathur and J. F. Scott, *Nature*, 2006, **442**, 759-765.
38. M. Bibes and A. Barthelemy, *Nat. Mater.*, 2008, **7**, 425-426.
39. T. Wu, A. Bur, K. Wong, P. Zhao, C. S. Lynch, P. K. Amiri, K. L. Wang and G. P. Carman, *Appl. Phys. Lett.*, 2011, **98**.
40. J. Wang, J. B. Neaton, H. Zheng, V. Nagarajan, S. B. Ogale, B. Liu, D. Viehland, V. Vaithyanathan, D. G. Schlom, U. V. Waghmare, N. A. Spaldin, K. M. Rabe, M. Wuttig and R. Ramesh, *Science*, 2003, **299**, 1719-1722.
41. N. A. Hill, *J. Phys. Chem. B*, 2000, **104**, 6694-6709.
42. T. Kimura, T. Goto, H. Shintani, K. Ishizaka, T. Arima and Y. Tokura, *Nature*, 2003, **426**, 55-58.
43. N. Hur, S. Park, P. A. Sharma, J. S. Ahn, S. Guha and S. W. Cheong, *Nature*, 2004, **429**, 392-395.
44. W. Kleemann, P. Borisov, S. Bedanta and V. V. Shvartsman, *Ieee T Ultrason Ferr*, 2010, **57**, 2228-2232.
45. P. P. Shi, Y. Y. Tang, P. F. Li, W. Q. Liao, Z. X. Wang, Q. Ye and R. G. Xiong, *Chem. Soc. Rev.*, 2016, **45**, 3811-3827.
46. T. Akutagawa, H. Koshinaka, D. Sato, S. Takeda, S. I. Noro, H. Takahashi, R. Kumai, Y. Tokura and T. Nakamura, *Nat. Mater.*, 2009, **8**, 342-347.
47. T. Endo, T. Akutagawa, S. Noro and T. Nakamura, *Dalton Trans.*, 2011, **40**, 1491-1496.
48. T. Endo, K. Kubo, M. Yoshitake, S. Noro, N. Hoshino, T. Akutagawa and T. Nakamura, *Cryst. Growth Des.*, 2015, **15**, 1186-1193.
49. T. Endo, K. Kubo, M. Yoshitake, S. Noro, T. Akutagawa and T. Nakamura, *Chem. Lett.*, 2013, **42**, 137-139.
50. M. Yoshitake, K. Kubo, T. Endo, S. Noro, T. Akutagawa and T. Nakamura, *Bull. Chem. Soc. Jpn.*, 2016, **89**, 354-360.
51. A. H. Schoen, *National Aeronautics and Space Administration*, 1970, **5541**.

52. J. A. Dolan, B. D. Wilts, S. Vignolini, J. J. Baumberg, U. Steiner and T. D. Wilkinson, *Adv Opt Mater*, 2015, **3**, 12-32.
53. A. Mizuno, Y. Shuku and K. Awaga, *Bull. Chem. Soc. Jpn.*, 2019, **92**, 1068-1093.
54. J. L. Manes, *Phys Rev B*, 2012, **85**.
55. M. Okeeffe, G. B. Adams and O. F. Sankey, *Phys. Rev. Lett.*, 1992, **68**, 2325-2328.
56. M. Tsuchiizu, *Phys Rev B*, 2016, **94**.
57. Y. Shuku, A. Mizuno, R. Ushiroguchi, C. S. Hyun, Y. J. Ryu, B. K. An, J. E. Kwon, S. Y. Park, M. Tsuchiizu and K. Awaga, *Chem. Commun.*, 2018, **54**, 3815-3818.
58. A. Mizuno, Y. Shuku, P. Suizu, M. M. Matsushita, M. Tsuchiizu, D. R. Maneru, F. Illas, V. Robert and K. Awaga, *J. Am. Chem. Soc.*, 2015, **137**, 7612-7615.
59. A. Mizuno, Y. Shuku, M. M. Matsushita, M. Tsuchiizu, Y. Hara, N. Wada, Y. Shimizu and K. Awaga, *Phys. Rev. Lett.*, 2017, **119**.
60. C. R. Li, S. L. Li and X. M. Zhang, *Cryst. Growth Des.*, 2009, **9**, 1702-1707.

Chapter 2: Two-dimensional layered molecular multiferroics with magnetoelectric correlation

2-1. Introduction

The molecular materials with two or more distinct functions are highly desirable for novel technical applications. For example, the coexistence of metallic or super-conductivity with ferromagnetism in a solid material could attribute to novel molecular electronics.[1] The coexistence of more than two ferroic properties (ferroelectricity, ferromagnetism, and ferroelasticity), known as multiferroic, has attracted much attention in the field of novel electronic devices.[2, 3] Especially the coexistence of ferroelectricity and ferromagnetism, the most focusing multiferroics, could be used as magnetoelectric (ME) materials in memory devices to overcome the slow writing problem of ferroelectric memory and high energy consumption drawback of magnetic random access memory.[4, 5]

Molecular multiferroics showing ME coupling effects are divided generally into two groups. The first group, known as type-I multiferroics, includes those materials where ferroelectricity and magnetism originated from different sources and appear largely independently of one another. An example is perovskite $BiFeO_3$. In $BiFeO_3$, the ordering of lone pairs on Bi^{3+} sites resulted in ferroelectric order, and the ferrite ions on FeO_3^{3-} sites gave rise to magnetism.[6] The theoretical work presented by N.A Spaldin et al. proved that due to strong independence of the electric and magnetic orders, ME coupling effect between these two sources is hardly realized,[7] and only a moderate ME effect could be observed due to the weak spin-lattice interaction in multiferroics. The second group of multiferroics is called type-II multiferroics. In type-II multiferroics, the magnetic orders can cause ferroelectricity, which implies the correlation between magnetic and ferroelectric orders are strong. For example, the manganite perovskite $TbMnO_3$ was found as type-II multiferroics, in which the effect of spin frustration directly induced ferroelectricity, and thus the ME effect was giant.[4] Thereafter, another magnetic-induced ferroelectricity was reported in $TbMn_2O_5$.[8] The discovery of those type-II multiferroics with significant ME coupling, though the polarization tends to be small, indicate the possible development of magnetically recorded ferroelectric memory.

It is also worth noticing that, by combining two separate ferroelectric and ferromagnetic oxides into the multilayered structure, strong ME coupling above room temperature could be obtained, although they are not molecular multiferroics.[9]

In addition to the inorganic oxides, a few metal-organic frameworks (MOFs) are demonstrated as molecular multiferroics.[10] Generally, the coordination frameworks in MOFs give rise to magnetic ordering, and the ordered guest cations determine their electric properties (type-I multiferroics). However, the reported examples of ME coupling effects in multiferroic MOFs are extremely rare, and most of them are formate-base MOFs.[11]

Compared with those multiferroics with perovskite structure or multiferroic composites, the fruitful molecular materials as the candidate for multiferroics are uncultivated even if they can incorporate a huge number of structural combinations.[12, 13] The development of two-dimensional (2D) metal-halogen perovskite materials as 2D multiferroics opens up a novel strategy to found a candidate for multiferroics.[14, 15] Similarly, 2D metal-oxalate hybrid system with a honeycomb layer structure, maybe another candidate for molecular multiferroics. Studies have demonstrated that in $[MnCr(oxalate)_3]^-$ hybrid system, the structure of counter cation not only templates the whole structure to be 2D, but the structural characteristics of cations can regulate the spin texture of center metals Mn^{2+} and Cr^{3+} in $[MnCr(oxalate)_3]^-$ layers and moderate the distance between stacked $[MnCr(oxalate)_3]^-$ layers.[16,17] Therefore, the 2D ferromagnetic $[MnCr(oxalate)_3]^-$ system has been investigated as the potential multifunctional materials by accommodating diverse kinds of the functional cation.[1, 17, 18] We already found a supramolecular rotator (*m*-fluoroanilinium$^+$)DB[18]crown-6 in $[Ni(dmit)_2]^-$ salt, which shows ferroelectric transition at 348 K,[19] and successfully introduced this supramolecular cation into $[MnCr(oxalate)_3]^-$ system to obtain a hybrid molecular salt.[19] As a result, the correlation between cationic structure and the spin state was observed in these two seemingly independent layers. Based on these results, we believe that the ferromagnetic orders of $[MnCr(oxalate)_3]^-$ could also be affected by the alternate cationic layer showing ferroelectric ordering, which means that considerable ME effects are likely to be present in this molecular system.

In this chapter, I have successfully constructed the 2D parallel-stacked layered polar crystals (*x*-anilinium^{+})(benzo[18]crown-6)[MnCr(oxalate)$_3$]$^{-}$, where *x* = H, *o*-fluoro, *m*-fluoro, and *p*-fluoro (**1**, **2**, **3** and **4**). The anionic layers of [MnCr(oxalate)$_3$]$^{-}$ formed the 2D honeycomb layered structures in crystals **1**-**4**, exhibiting ferromagnetic ordering at around 5 K. The polar layer is composed of the (*x*-anilinium^{+})(benzo[18]crown-6) supramolecular adduct between the anionic layers of [MnCr(oxalate)$_3$]$^{-}$, forming a 2D layered structure. In the specific crystal (*o*-fluoroanilinium^{+})(benzo[18]crown-6)[MnCr(oxalate)$_3$]$^{-}$ (**2**), the supramolecular motion afforded a ferroelectric ordering up to 460 K. Notably, the magnetization of crystal **2** at 2K was found regulated by electric poling.

2-2. Polar crystal design

In the previous work, introducing ferroelectric supramolecular rotator (*m*-FAni$^+$)DB18C6 (*m*-FAni$^+$ = *m*-fluoroanilinium$^+$, DB18C6 = dibenzo[18]crown-6) in [MnCr(oxalate)$_3$]$^-$ network could only template the nonpolar crystal with centrosymmetric space group $P2_1/c$.[1] To realize ferroelectricity, the development of crystals with polar space groups belonging to one of 10 polar point groups is necessary.[2] We already found that flexible and less symmetrical supramolecular cations induce polar crystal structure even combined with spherical anions such as Keggins.[3] Therefore, we employed less symmetric crown ether of benzo[18]crown-6 combining with anilinium derivatives to form supramolecular structures.

By introducing anilinium derivatives supramolecular cations between [MnCr(oxalate$_3$)]$^-$ layers, polar crystals of (*x*-anilinium$^+$)(benzo[18]crown-6)[MnCr(oxalate)$_3$]$^-$ were obtained, where *x* = H, *o*-fluoro, *m*-fluoro, and *p*-fluoro, for **1**, **2**, **3**, and **4**, respectively. They crystallized in polar space groups $P2_1$, *Cc*, $P2_1$, and $Pna2_1$, for **1**, **2**, **3**, and **4**, respectively (Table 2-1).

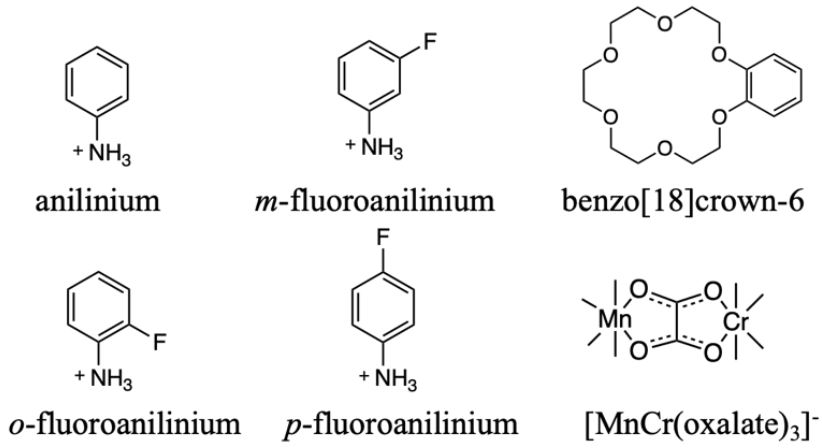

Scheme 2-1. Chemical structures used in Chapter **2**.

Table 2-1. Crystallographic data for **1**-**4**.

	1	**2**	**3**	**4**
Cation	Ani^+	*o*-$FAni^+$	*m*-$FAni^+$	*p*-$FAni^+$
Temperature / K	273	223	293	293
Formula weight	777.48	795.47	795.47	795.47
Space group	$P2_1$	*Cc*	$P2_1$	$Pna2_1$
a, Å	8.7994(6)	23.694(10)	8.8266(6)	17.9439(9)
b, Å	23.3733(12)	16.990(5)	23.4177(11)	16.7899(7)
c, Å	9.4320(6)	8.803(5)	9.4649(5)	23.3525(9)
β, deg	115.541(8)	108.949(15)	115.847(7)	90
V, $Å^3$	1750.31(19)	3352(3)	1760.3(2)	7035.6(5)
Z	2	4	2	8
D_{calc}, $g \cdot cm^{-3}$	1.475	1.570	1.501	1.502
μ, mm^{-1}	0.748	6.541	0.750	0.750
R_{int}	0.0466	0.1771	0.0243	0.0412
R_1 [a]	0.0784	0.0772	0.0537	0.0531
$R_w(F^2)$ [a]	0.2371	0.2006	0.1216	0.1400
GOF	1.061	0.902	1.052	1.023

[a] $R_1 = \Sigma||F_o| - |F_c|| / \Sigma|F_o|$ and $R_w = (\Sigma\omega(|F_o| - |F_c|)^2 / \Sigma\omega F_o^2)^{1/2}$.

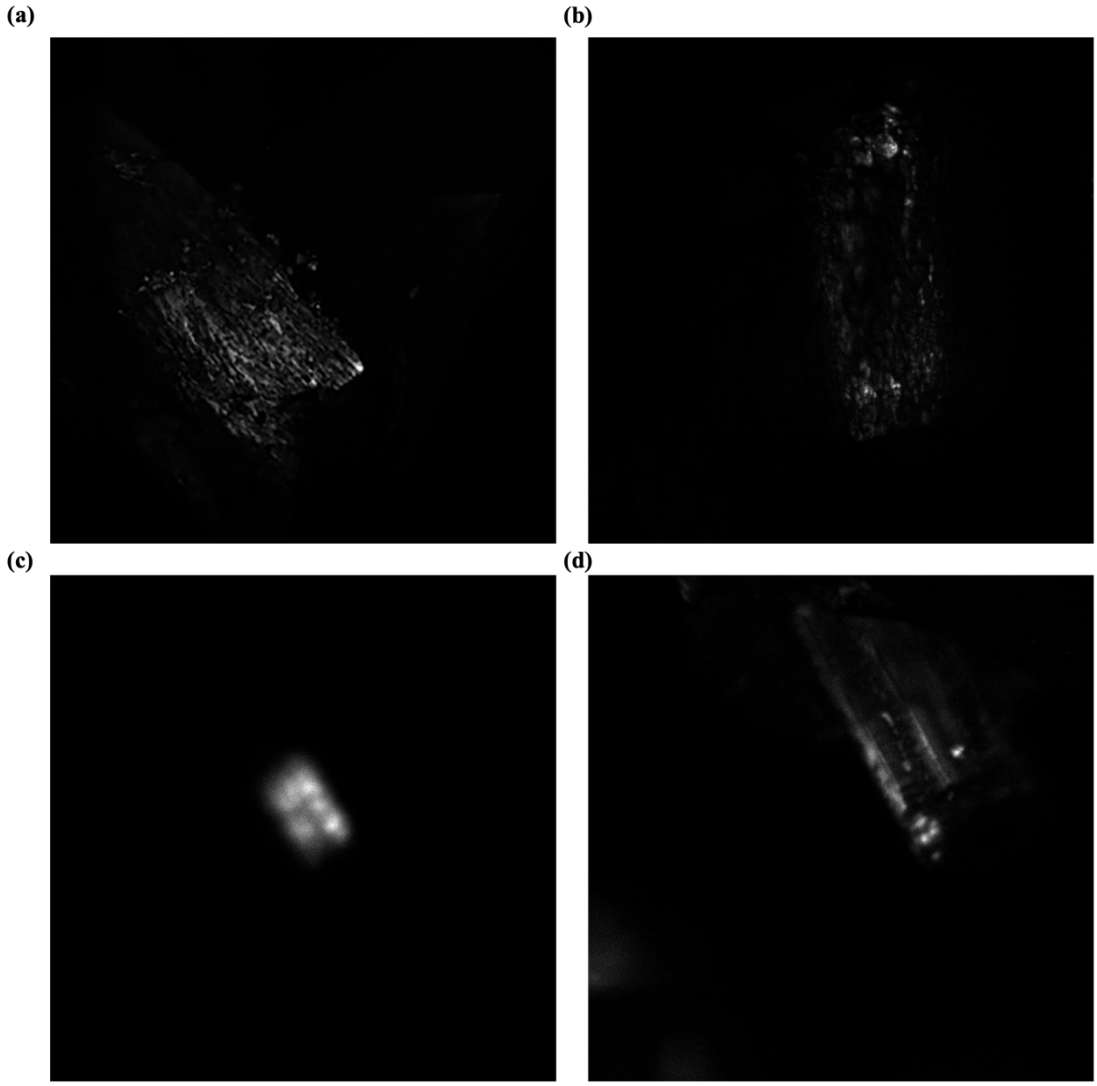

Figure 2-1. Photographs of **1** (a), **2** (b), **3** (c), and **4** (d), exposed by the laser light source at the wavelength of 1030 nm at 300 K. The output signal of bright color indicated the wavelength of incident light halved to the visible light wavelength range 515 nm.

The structural polarity of **1**–**4** was confirmed by optical second-harmonic generation measurements. The single crystals were respectively exposed by the laser light source at the wavelength of 1030 nm at 300 K. As shown in Figure 2-1, The signal of bright light from the light reflection was observed, which indicated the crystal was polar so that can twice the incident frequency. The SHG intensity related to that of caster sugar of **1**-**4** is 1.408, 0.694, 0.862, and 1.847, respectively.

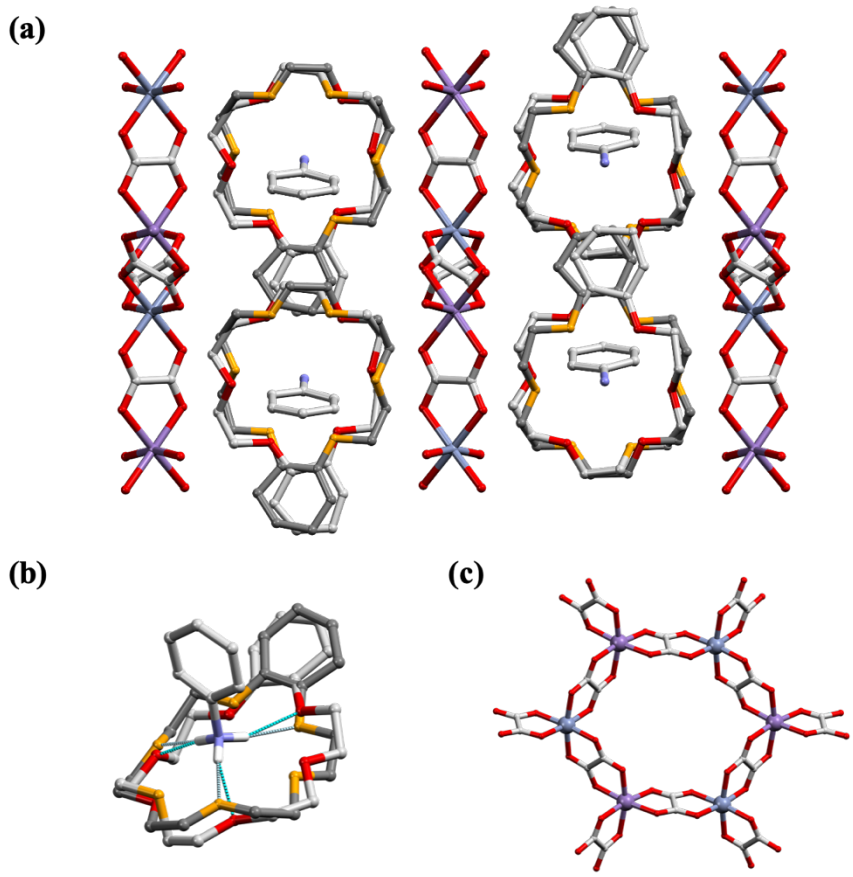

Figure 2-2. The crystal structure of **1** at 273 K. (a) Top view along *a*-axis. The disorder of benzo[18]crown-6 was divided by light grey (part1) and dark grey (part2) colors and an equal occupancy ratio of 1:1. (b) Supramolecular structure of (ani^{+})benzo[18]crown-6. The blue dotted lines show hydrogen bonds. (c) A honeycomb-like layer of [MnCr(oxalate)$_3$]$^{-}$. Purple for manganese, light blue for chromium, red for oxygen, grey for carbon, and blue for nitrogen.

All the crystal **1**–**4** shares a similar hybrid 2D structure with alternately stacking cationic supramolecular layer and anionic layer [MnCr(oxalate)$_3$]$^{-}$. Take crystal **1** as an example (Figure 2-2), in the [MnCr(oxalate)$_3$]$^{-}$ layer, center metal ions Mn^{2+} and Cr^{3+} were octahedrally coordinated by three oxalate ligands and formed a honeycomb-like layer. The supramolecular layer packed paralleling to the metal-oxalate layer by the cationic (ani^{+})benzo[18]crown-6 (ani^{+} = anilinium^{+}), which the ani^{+} connected with benzo[18]crown-6 through N-H•••O hydrogen bonds.

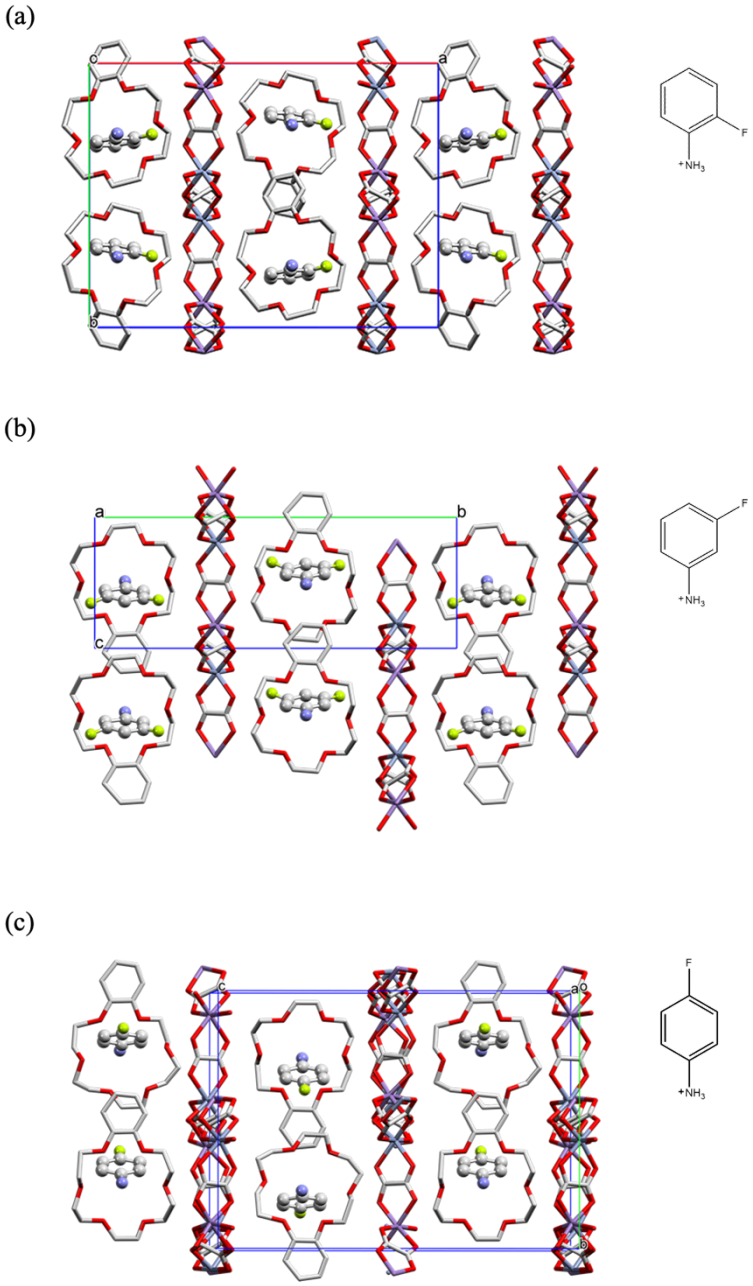

Figure 2-3. The stacking layered structure of (a) **2**, (b) **3**, and (c) **4**, which was crystallized in space group groups *Cc*, $P2_1$, and $Pna2_1$, respectively.

In this analogous stacking structure of **1**–**4** (Figure 2-3), the cationic supramolecular layers, however, were distinctive. Figure 2-4 showed the arrangement of anilinium derivatives in a supramolecular layer **1**–**4**. The ammonium groups ($–NH_3$) of ani$^+$, *o*-FAni$^+$ (*o*-fluoroanilinium$^+$), *m*-FAni$^+$ (*m*-fluoroanilinium$^+$), and *p*-FAni$^+$ (*p*-fluoroanilinium$^+$) in **1**–**4** point in the same direction within the 2D layer. Since the

aminium groups in the next layer point in the opposite direction compensating dipole moments originated from aminium groups in whole crystals except for crystal **2**. In crystal **4**, even the presence of fluorine groups in *p*-$FAni^+$ could not attribute any electric dipoles because the dipole moments from fluorine substituents in the whole crystal were zero due to the cancelation between or within layers. The polarity source in **1** and **4** was the displacement structure of benzo[18]crown-6 resulting from the tilt motion (Figure 2-5).

In crystal **3** crystallized in $P2_1$, the arrangement of *m*-$FAni^+$ was no different from that of Ani^+ in **1** except that the fluorine substituent at the *m*- site showed disorder with uneven probability, devoting structural polarity. The fluorine group at *m*- site induced the dipole moment perpendicular to the possible molecular rotational axis along with the C-N bond between carbon atoms of the benzene ring and aminium nitrogen in *m*-$FAni^+$ cation, which can be an origin of the ferroelectric response of the crystal as in the case of (*m*-fluoroanilinium$^+$)DB[18]crown-6[$Ni(dmit)_2$]$^-$. Among others, crystal **2** belonging to space group *Cc* showed a peculiar molecular arrangement of *o*-$FAni^+$. As shown in Figure 2-4 b, all the aminium groups are directed in the same direction in different layers. Fluorine groups at the *o*- position pointed to +*a* direction suggesting strong polarization of the crystal in **2**.

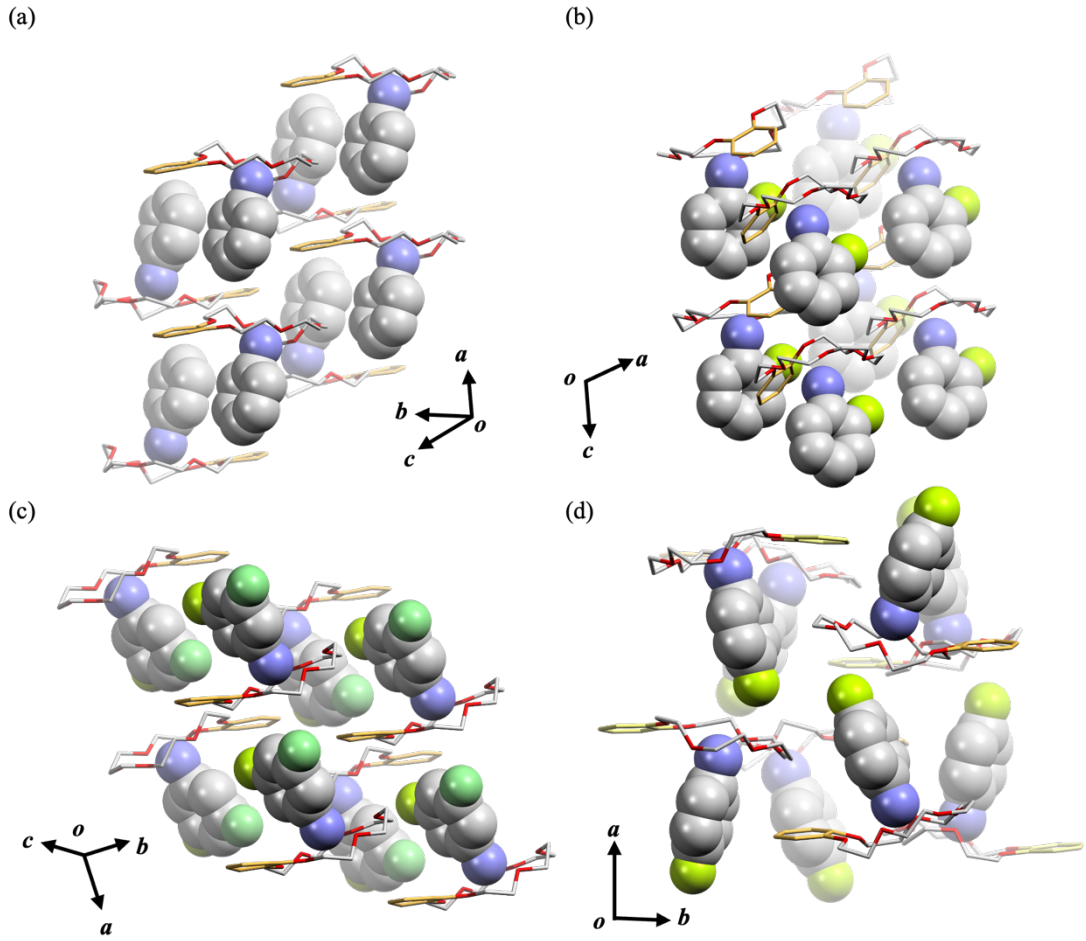

Figure 2-4. Supramolecular arrangement in **1**-**4**. The adjacent two supramolecular layers were only presented.

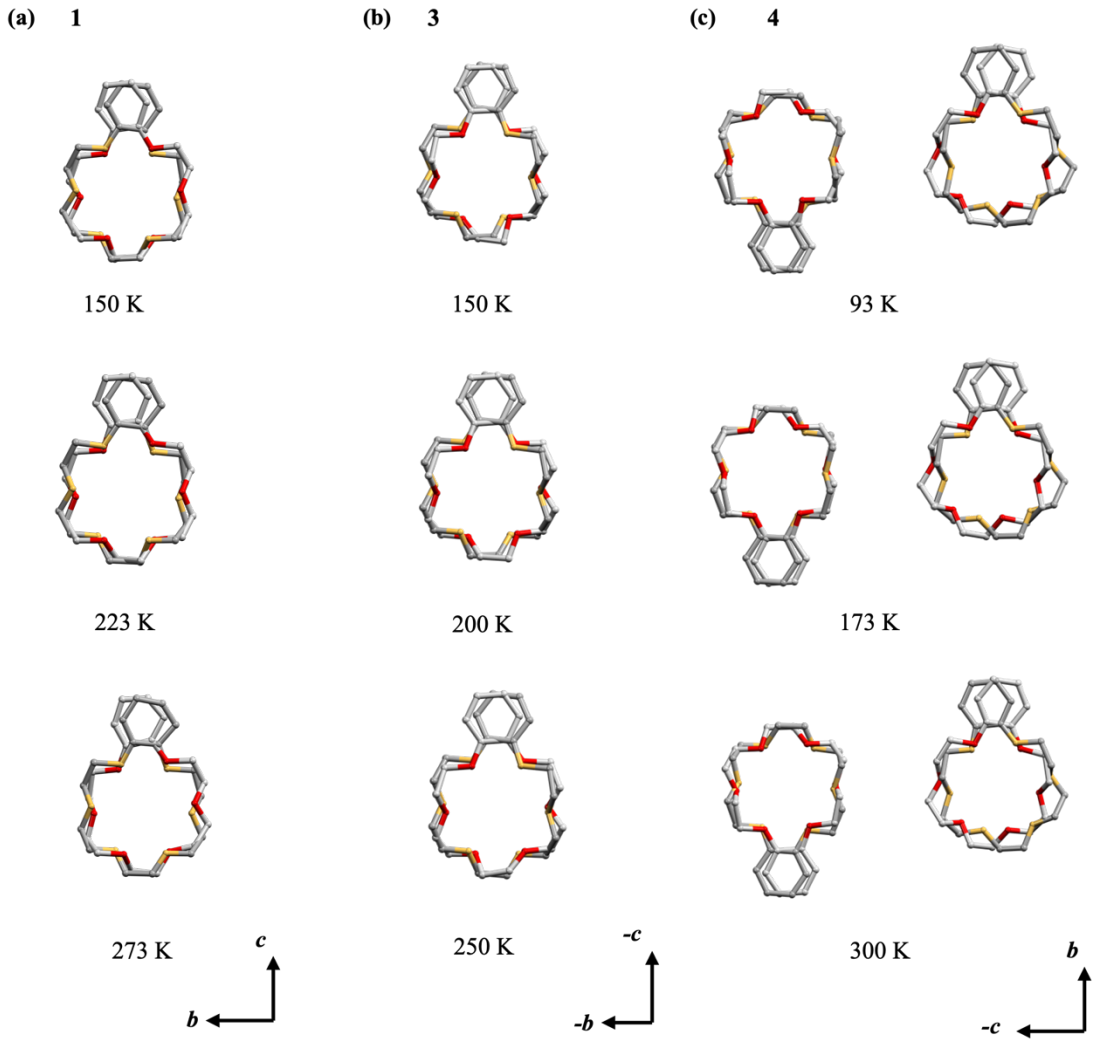

Figure 2-5. [a] The displacement structure of benzo[18]crown-6.

[a] The structure of benzo[18]crown-6 showed disorder, presented as grayish for part 1, gay for part 2. Occupancy at different temperature: (a) in **1**, part 1: 0.29, part 2: 0.71 at 150 K; part 1: 0.44, part 2: 0.56 at 223 K; part 1: 0.43, part 2: 0.57 at 273 K. (b) In **3**, part 1: 0.29, part 2: 0.71 at 150 K; part 1: 0.44, part 2: 0.56 at 200 K; part 1: 0.43, part 2: 0.57 at 250 K; (c) in **4**, two independent molecules of B18C6 were observed in asymmetric unit. Left: molecule 1, part 1: 0.51, part 2: 0.49 at 93 K; part 1: 0.49, part 2: 0.51 at 173 K; part 1: 0.52, part 2: 0.48 at 300 K. Right: molecule 2, part 1: 0.48, part 2: 0.52 at 93 K; part 1: 0.48, part 2: 0.53 at 173 K; part 1: 0.52, part 2: 0.48 at 300 K.

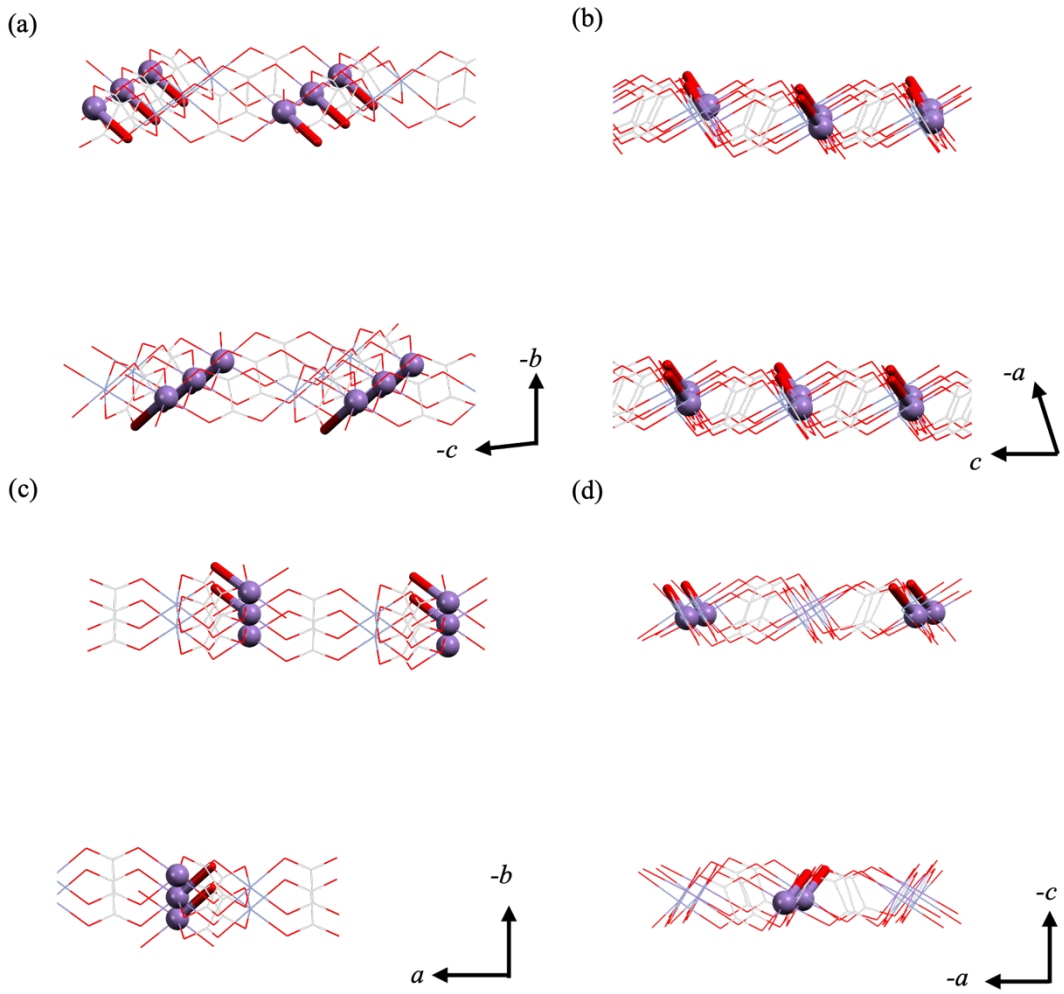

Figure 2-6. The elongated band of Mn-O results in the asymmetric distortion in the $[MnCr(oxalate)_3]^-$ layer in crystals **1** (a), **2** (b), **3** (c), and **4** (d). The elongated bond was shown as a bold stick.

The distorted structure in $[MnCr(oxalate)_3]^-$ layer was observed in crystals **1**-**4**. The elongated bonds of Mn-O in **1**–**4** was summarized in Figure 2-6 and in Table 2-2. For example, in hexagonal coordinated Mn-O structure in **1**, the bond length between O17 and Mn1 is 2.1278 Å, which was much longer than the other Mn-O bonds (Table 2-2). The bonds of O17-Mn elongated along *b*-axis, made the whole structure be asymmetric.

Table 2-2. The bond length between Mn/Cr and O in $[MnCr(oxalate)_3]^-$ layer for **1-4**.

1, 273 K						
Bond type	Mn1-O7	Mn1-O9	Mn1-O12	Mn1-O14	Mn1-O15	Mn1-O17
Bond length / Å	2.092	2.098	2.091	2.090	2.093	2.127
Bond type	Cr1-O8	Cr1-O10	Cr1-O11	Cr1-O13	Cr1-O16	Cr1-O18
Bond length /Å	2.044	2.054	2.032	2.049	2.026	2.046

2, 223 K						
Bond type	Mn2A-O7X	Mn2A-O8X	Mn2A-O9X	Mn2A-O10X	Mn2A-O11X	Mn2A-O12X
Bond length / Å	1.982	2.058	2.111	2.054	2.110	2.042
Bond type	Cr1A-O1X	Cr1A-O2X	Cr1A-O3X	Cr1A-O4X	Cr1A-O5X	Cr1A-O6X
Bond length /Å	2.056	2.085	2.146	2.063	2.059	2.148

3, 300 K						
Bond type	Mn1-O00D	Mn1-O00C	Mn1-O00T	Mn1-O004	Mn1-O005	Mn1-O006
Bond length / Å	2.119	2.099	2.128	2.114	2.089	2.114
Bond type	Cr2-O00I	Cr2-O00H	Cr2-O00E	Cr2-O003	Cr2-O008	Cr2-O009
Bond length / Å	2.034	2.064	2.045	2.013	2.038	2.018

4, 300 K						
Bond type	Mn1-O13	Mn1-O14	Mn1-O15	Mn1-O16	Mn1-O19	Mn1-O20
Bond length / Å	2.086	2.034	2.083	2.129	2.058	2.089
Bond type	Mn2-O17	Mn2-O18	Mn2-O25	Mn2-O26	Mn2-O27	Mn2-O28
Bond length / Å	2.020	2.048	2.109	2.040	2.039	2.100
Bond type	Cr1-O9	Cr1-O10	Cr1-O11	Cr1-O12	Cr1-O29	Cr1-O30
Bond length /Å	2.076	2.051	2.072	2.047	2.065	2.108
Bond type	Cr2-O7	Cr2-O8	Cr2-O21	Cr2-O22	Cr2-O23	Cr2-O24
Bond length /Å	2.064	2.077	2.074	2.063	2.074	2.060

2-3. Supramolecular motion

2-3-1. Tilting motion of benzo[18]crown-6

To investigate the dynamic features, the temperature-dependent single-crystal X-ray diffusion (VT-SXRD) of **1**-**4** was measured (Table 2-3). The structures of benzo[18]crown-6 in **1** were solved at 150, 223, and 273 K. As shown in Figure 2-5 and Figure 2-7, benzo[18]crown-6 showed drastic disorder, presented as part1 (grayish) and part2 (gray), indicating a dynamic state of benzo[18]crown-6. As the temperature rises, the occupancy (occ) ratio of part1 and par2 changes from 0.29:0.71 at 150 K to 0.44:0.56 at 223 K, and 0.43:0.57 at 273 K. we consider this structural disorder of benzo[18]crown-6 as the in-plane molecular motion, benzo[18]crown-6 tilted between the two positions solved as part1 and part2. Similar disorder behaviors of benzo[18]crown-6 were also observed in *m*-FAni$^+$, and *p*-FAni$^+$ salts (Figure 2-5, Figure 2-7). Through measuring the temperature- and frequency-dependent dielectric constants of **1** and **2**, in the curves of the dielectric loss, both showed dielectric relaxation, indicating the molecular motion of benzo[18]crown-6. The activation energy of the dielectric relaxation in 200–300 K in crystal **1** was 31.8 kJ/mol, and the activation energy of the dielectric relaxation around 180–250 K in crystal **4** was 36.4 kJ/mol, calculated by the Arrhenius equation.

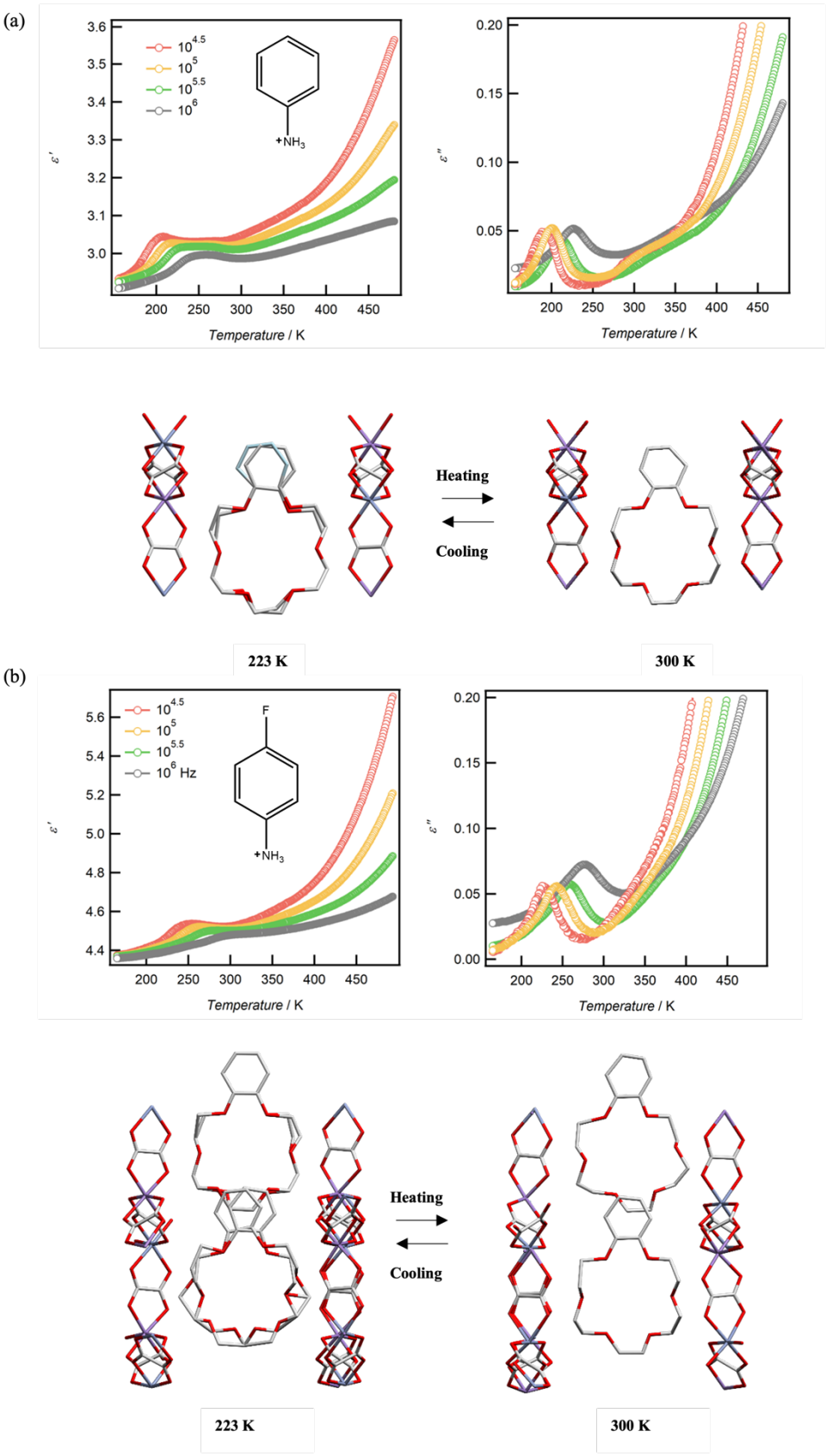

Figure 2-7. The molecular motion of benzo[18]crown-6 in crystal **1** (a) and **4** (b). The peaks occurred in ε'' versus temperature gave the evidence of molecular motion.

Table 2-3. Temperature-dependent single crystal X-ray diffraction results of **1**–**4**.

1			
Cation	Ani^+		
Temperature / K	150	223	273
Chemical formula	$C_{28}H_{32}CrMnO_{18}N$		
Formula weight	777.48		
Space group	$P2_1$		
a, Å	8.7581(7)	8.7849(4)	8.7994(6)
b, Å	23.2124(15)	23.3248(8)	23.3733(12)
c, Å	9.4283(7)	9.4416(4)	9.4320(6)
β, deg	115.324(10)	115.443(6)	115.541(8)
V, Å^3	1732.5(2)	1747.01(15)	1750.31(19)
Z	2		
D_{calc}, g·cm^{-3}	1.490	1.478	1.475
μ, mm^{-1}	0.756	0.749	0.748
Reflections measured	21849	22583	22150
Independent reflections	8541	8657	8736
R_{int}	0.0670	0.0317	0.0466
R_{sigma}	0.0630	0.0370	0.0501
R_1 [a]	0.0709	0.0479	0.0485
$R_w(F^2)$ [a]	0.1786	0.1114	0.1199
GOF	1.080	1.067	1.061
Flack Parameter	0.39(6)	0.42(5)	0.46(5)

[a] $R_1 = \Sigma||F_o| - |F_c|| / \Sigma|F_o|$ and $R_w = (\Sigma\omega(|F_o| - |F_c|)^2 / \Sigma\omega F_o^2)^{1/2}$.

	2	
Cation	*o*-FAni$^+$	
Temperature / K	223	460
Chemical formula	$C_{28}H_{31}CrFMnNO_{18}$	
Formula weight	795.48	
Space group	*Cc*	$P2_1/c$
a, Å	23.694(10)	11.9046(6)
b, Å	16.990(5)	16.6594(6)
c, Å	8.803(5)	9.0382(5)
β, deg	108.949(15)	94.417(4)
V, Å^3	3352(3)	1787.16(15)
Z	4	2
D_{calc}, g·cm^{-3}	1.570	1.474
μ, mm^{-1}	6.541	1.065
Reflections measured	22697	11607
Independent reflections	6349	3149
R_{int}	0.1771	0.0322
R_{sigma}	0.1421	0.0558
R_1 [a]	0.0772	0.0322
$R_w(F^2)$ [a]	0.2006	0.0558
GOF	0.902	1.001
Flack Parameter	-0.004(11)	-

[a] $R_1 = \Sigma||F_o| - |F_c|| / \Sigma|F_o|$ and $R_w = (\Sigma\omega(|F_o| - |F_c|)^2 / \Sigma\omega F_o^2)^{1/2}$.

	3			
Cation		*m*-FAni$^+$		
Temperature / K	93	150	200	250
Chemical formula		$C_{28}H_{31}CrFMnNO_{18}$		
Formula weight		795.48		
Space group		$P2_1$		
a, Å	8.7453(9)	8.7564(6)	8.7804(7)	8.8007(6)
b, Å	23.1038(16)	23.1857(10)	23.2171(13)	23.2985(11)
c, Å	9.4716(9)	9.4654(6)	9.4445(6)	9.4428(6)
β, deg	115.647(12)	115.664(8)	115.624	115.733(8)
V, Å^3	1725.2(3)	1732.1(2)	1736.0(2)	1744.2(2)
Z	2	2	2	2
D_{calc}, g·cm^{-3}	1.531	1.525	1.522	1.515
μ, mm^{-1}	0.765	0.762	0.760	0.757
Reflections measured	13950	26404	15272	18911
Independent reflections	6467	8627	7612	8244
R_{int}	0.0656	0.0685	0.0816	0.0361
R_{sigma}	0.0699	0.0603	0.0890	0.0489
R_1 [a]	0.1034	0.0847	0.0836	0.0490
$R_w(F^2)$ [a]	0.2715	0.2276	0.2315	0.1129
GOF	1.036	1.051	1.064	1.053
Flack Parameter	0.43(8)	0.41(6)	0.45(6)	0.39(5)

Continued from previous Table:

	3		
Cation		*m*-FAni$^+$	
Temperature / K	300	350	400
Chemical formula		$C_{28}H_{31}CrFMnO_{18}N$	
Formula weight		795.48	
Space group		$P2_1$	
a, Å	8.8266(6)	8.8543(6)	8.8798(7)
b, Å	23.4177(11)	23.4804(14)	23.5310(14)
c, Å	9.4649(5)	9.4526(6)	9.4495(6)
β, deg	115.874(7)	116.030(8)	116.167(8)
V, Å^3	1760.3(2)	1765.9(2)	1772.1(2)
Z		2	
D_{calc}, g·cm^{-3}	1.501	1.496	1.491
μ, mm^{-1}	0.750	0.747	0.745
Reflections measured	10255	10144	10188
Independent reflections	7025	7044	7067
R_{int}	0.0243	0.0275	0.0322
R_{sigma}	0.0545	0.0586	0.0668
R_1 [a]	0.0537	0.0555	0.0550
$R_w(F^2)$ [a]	0.1216	0.1328	0.1391
GOF	1.052	1.058	1.032
Flack Parameter	0.55(6)	0.48(7)	0.51(7)

[a] $R_1 = \Sigma||F_o| - |F_c|| / \Sigma|F_o|$ and $R_w = (\Sigma\omega(|F_o| - |F_c|)^2 / \Sigma\omega F_o^2)^{1/2}$.

	4		
Cation		*p*-FAni$^+$	
Temperature / K	93	173	300
Chemical formula		$C_{28}H_{31}CrFMnO_{18}N$	
Formula weight		795.48	
Space group		$Pna2_1$	
a, Å	17.8297(6)	17.8771(8)	17.9439(9)
b, Å	16.8058(6)	16.8033(8)	16.7899(7)
c, Å	23.1047(7)	23.2460(9)	23.3535(9)
β, deg	90	90	90
V, Å^3	6923.1(4)	6983.0(5)	7035.6(5)
Z		8	
D_{calc}, g·cm^{-3}	1.526	1.513	1.502
μ, mm^{-1}	0.762	0.756	0.750
Reflections measured	55860	64510	52398
Independent reflections	16745	17291	13703
R_{int}	0.0453	0.0500	0.0412
R_{sigma}	0.0534	0.0536	0.0405
R_1 [a]	0.0618	0.0584	0.0531
$R_w(F^2)$ [a]	0.1447	0.1544	0.1400
GOF	1.030	1.032	1.023
Flack Parameter	0.54(5)	0.54(5)	0.47(6)

[a] $R_1 = \Sigma||F_o| - |F_c|| / \Sigma|F_o|$ and $R_w = (\Sigma\omega(|F_o| - |F_c|)^2 / \Sigma\omega F_o^2)^{1/2}$.

2-3-2. Rotation of *m*-FAni$^+$

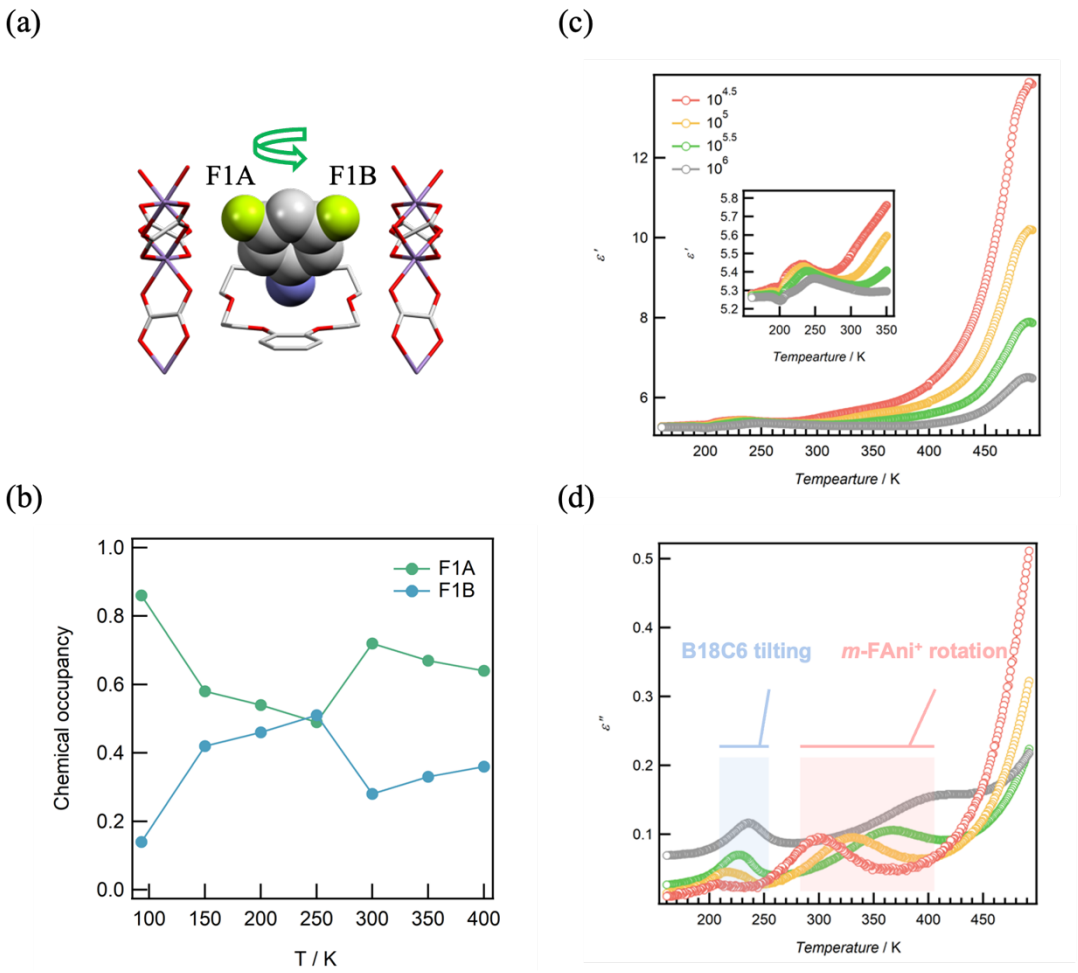

Figure 2-8. (a) The supramolecular motion of *m*-FAni$^+$ in crystal **3**. (b) Temperature-dependent chemical occupancy of disorder fluorine substituent based on the data of temperature-dependent single-crystal X-ray diffraction. (c)(d) Temperature- and frequency-dependent dielectric constants (ε′ and ε′′) of **3** using compacted sample.

In addition to benzo[18]crown-6 motion, the rotational motion of cations with dipole moment inversion was observed for crystals **2** and **3**. The structure of **3** was determined in non-centrosymmetric space group $P2_1$ at 93, 150, 200, 250, 300, 350, and 400 K (Table 2-3). At 93 K, the fluorine substituent was disorder-fixed to two sites F1A and F2B with the occupancy ratio of F1A: F1B = 0.86:0.14, directing parallel to the -*b* axis. Heating **3** to 150 K, the fluorine substituent disordered over two opposite sites with the occupancy ratio between F1A: F1B = 0.57:0.43. On increasing the

temperature to 200, 250, 300, 350, and 400 K, the fluorine substituent was disordered with the occ ratio F1A:F1B = 0.54:0.46 at 200 K, 0.51:0.49 at 250 K, 0.72:0.28 at 300 K, 0.67:0.33 at 350 K, and 0.64:0.36 at 400 K, respectively. The VT-SXRD results evidenced that the supramolecular rotator *m*-FAni$^+$ was dynamically rotating from 93 to 400 K (Figure 2-8).

The rotation of *m*-FAni$^+$ in **3** was confirmed by dielectric relaxation in the 250-400 K region at the frequency of $10^{4.5}$-10^6 Hz (Figure 2-8 (d)). Another type of dielectric relaxation was observed in lower temperature regions between 200-250 K, which was attributed to the tilting motion of benzo[18]crown-6. Since the dielectric response of the lower temperature region was also observed for **1** and **4** (Figure 2-7), which cannot be exhibit a dielectric response originating from fluorine substituent inversion, therefore the response in the lower temperature region was supposed to the tilting motion of benzo[18]crown-6, which was like the responses occurred in **1** and **4**. The dielectric relaxation in higher temperature regions 250-400 K should be due to the flip-flop motion of *m*-FAni$^+$ cation in **3**. The activation energies belonging to the two types of dielectric relaxations were calculated by an Arrhenius analysis (Figure 2-9). The activation energy Ea_1 at the lower temperature region was 51.2 kJ/mol, and the activation energy at the higher temperature region Ea_2 was 34.1 kJ/mol.

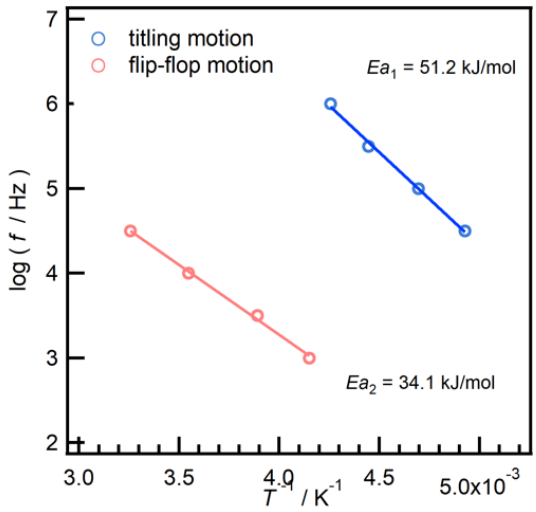

Figure 2- 9. Arrhenius plots of log(*f*) *vs.* T^{-1}. The results were calculated based on the dielectric relaxation peaks in Figure 2-8 (d).

To further investigate the dynamic property of the solid-state molecular rotator (*m*-FAni)$^{+}$benzo[18]crown-6, a plate of **3** was poled under ±20 kV/cm, respectively, and the pyroelectric currents were monitored at 100-395 K after applying reverse electric fields. The pyroelectric current was almost zero up to 120 K. A sharply increased signal of pyroelectric current was observed after 120 K, reaching the maximum value of 1.98 pA at 157 K. Then the pyroelectric current started to drop gradually until it was close to zero at around 200 K. By applying opposite electric fields, the signal of pyroelectric current was reversed, which indicates that the flip-flop motion of (*m*-FAni)$^{+}$ accompanied by dipoles inversion gave rise the ferroelectric response for **3**.

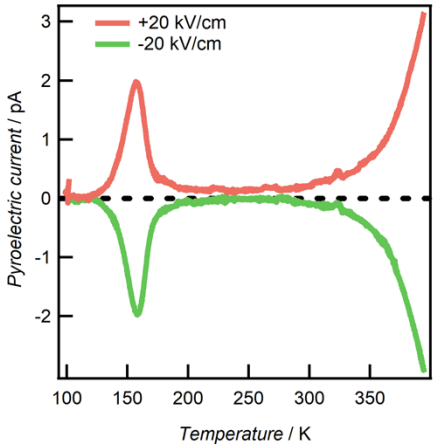

Figure 2-10. The pyroelectric currents for crystal **3**, were collected after the electric poling under ± 20 kV/ cm electric fields by using the compact plate.

2-4. Multiferroic properties for crystal 2

2-4-1. Phase transition

Crystal **2** clearly showed reversible first-order phase transition with ca. 28 K thermal hysteresis indicated by DSC measurements. As shown in Figure 2-11 (a), exso and endo thermic behavior at 430 and 458 K, respectively, were observed upon cooling and heating, respectively, between 400-490 K. The crystal **2** had good thermal stability up to 545 K (Figure 2-11(b)).

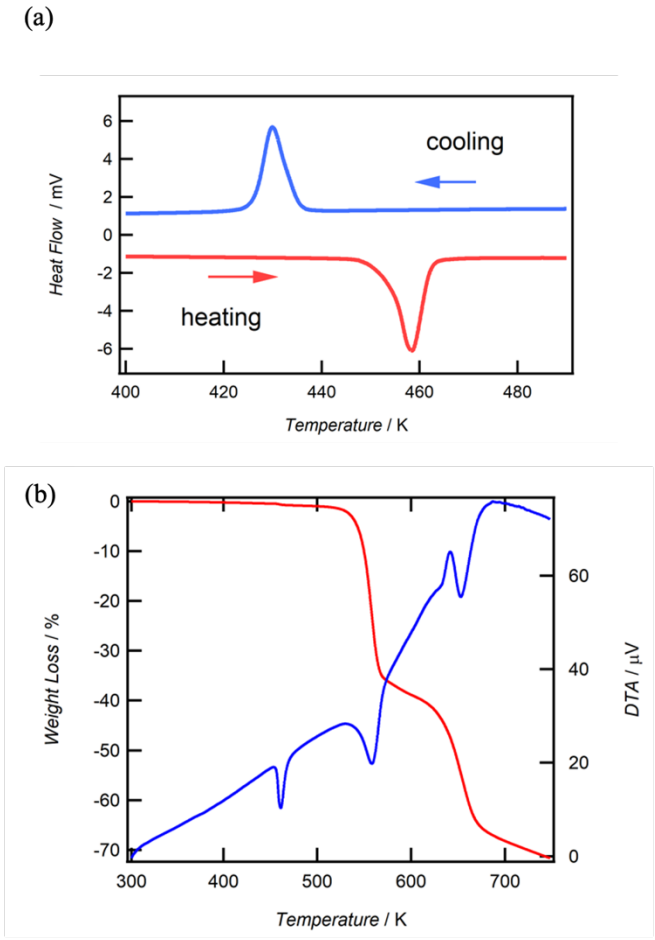

Figure 2-11. Thermal properties of crystal **2**. (a) The DSC curves upon heating and cooling of polycrystals **2**. (b) TG-DTA curves.

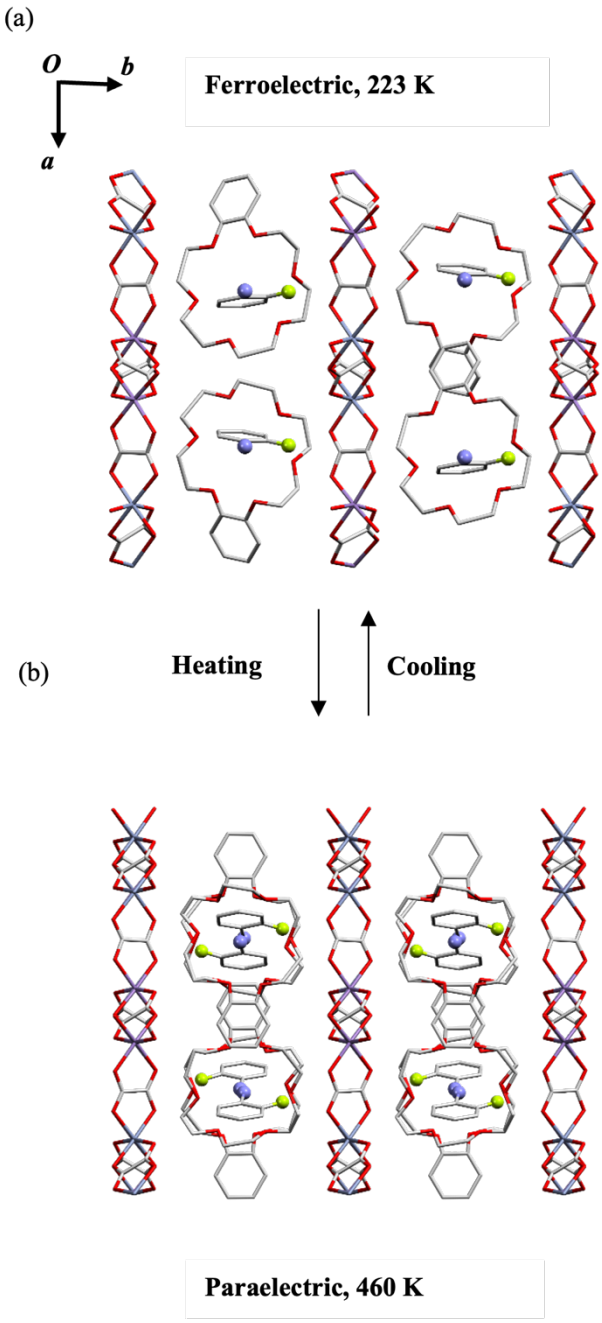

Figure 2- 12. The crystal structure was determined at (a) 223 K, ferroelectric phase, and (b) 460 K, paraelectric phase.

To further investigate the phase transition, the crystal structures at 460 K in the paraelectric phase were determined by using synchrotron radiation (Table 2-3). Crystal **2** crystallized in the polar space group of *Cc* at 223 K in the ferroelectric phase in which the fluorine substituents in *o*-FAni$^+$ cations were directed in the same direction along the *b* axis. Upon heating above the phase transition point 460 K, crystal **2** belonged to

the centrosymmetric space group of $P2_1/c$ with an inverse center to cancel the polarity in **2**, which is in good agreement with the paraelectric state of the crystal. The electric dipoles of fluorine substituents thus are zero at 460 K. The flip-flop motion of *o*-$FAni^+$ cations upon phase transition resulted in polarization disappearance.

2-4-2. Ferroelectric properties

(a)

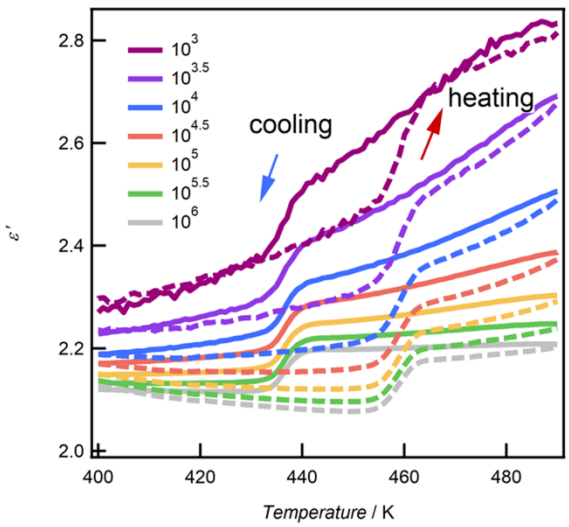

(b)

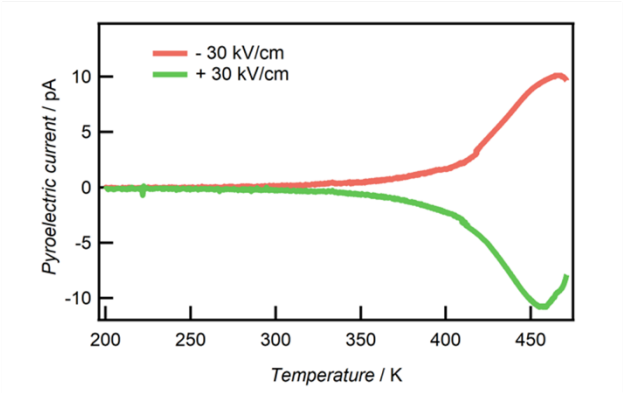

Figure 2-13. (a) The dielectric constant ε′ *vs.* temperature is 1 kHz to 1 MHz. (b) The pyroelectric currents signal for crystal **2**.

As shown in Figure 2-13 (a), a large hysteresis was also observed for dielectric constant ε′ upon heating and cooling. The dielectric constant ε′ indicated a sharp increase with increasing temperature at 455 K upon heating, and a sharp decrease upon cooling was observed at 432 K without frequency dependence. The hysteresis loop in the temperature-dependent dielectric constant curve along with ca. 23 K was corresponding to the thermal hysteresis in Figure 2-11 (a). Since the crystal has a space

group of *Cc*, the phase transition should be associated with the ferroelectric-paraelectric transition. Indeed, the inversion of pyroelectric current under the opposite applied electric field was observed indicating that crystal **2** is ferroelectric.

2-4-3. Magnetic properties

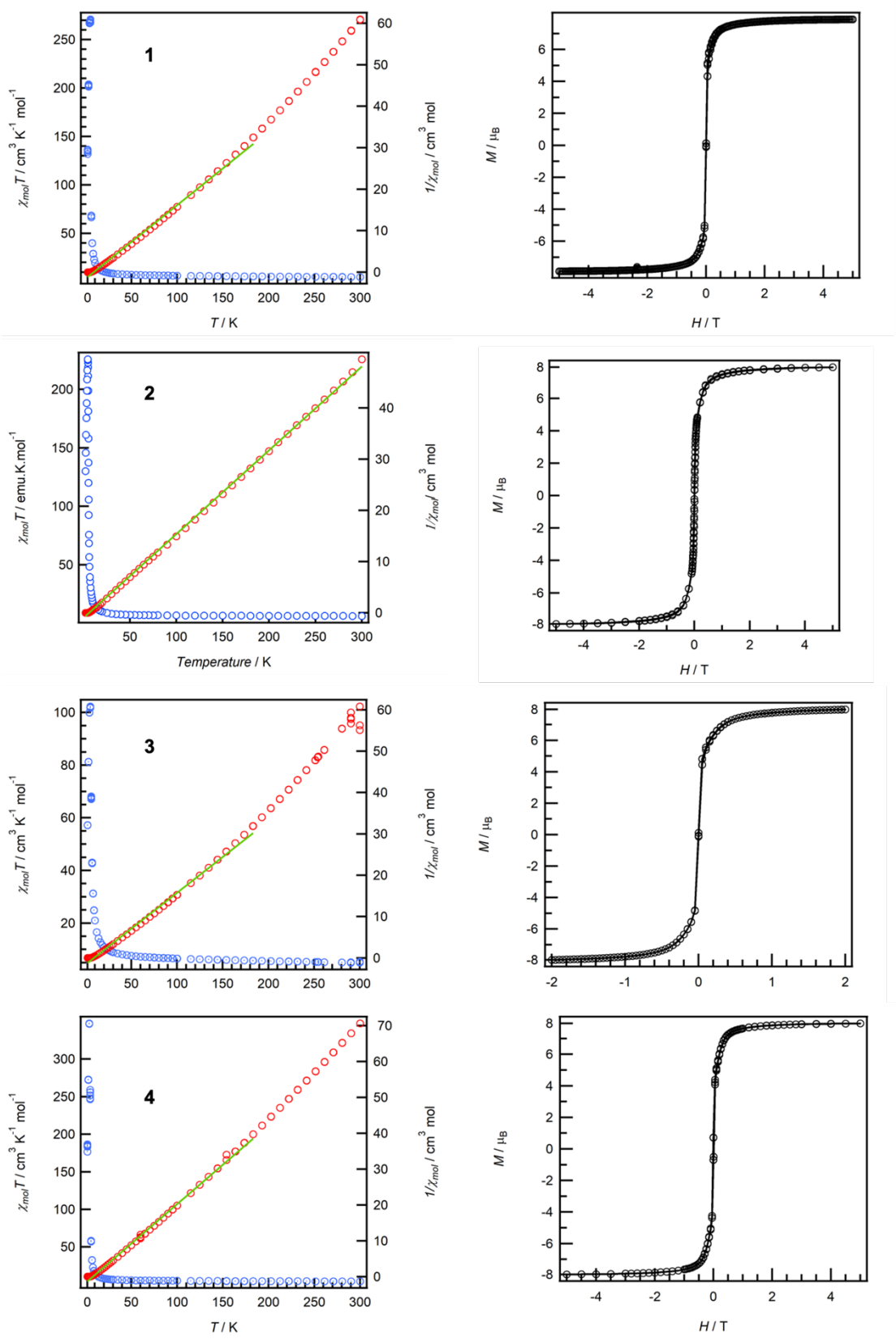

Figure 2-14. The magnetic properties of **1**-**4**. Left: *M*-*T*, right: *M*-*H*.

Like other 2D $[MnCr(oxalate)_3]^-$ complexes, the series of (*x*-anilinium$^+$)benzo[18]crown-6$[MnCr(oxalate)_3]^-$ exhibited ferromagnetic ordering at low temperature due to the exchange interaction between Mn^{2+} and Cr^{3+} ions bridged by oxalate ligands. The ferromagnetic properties of **1**-**4** were summarized in Figure 2-14. (Salt **1**: Curie-Weiss fitting in 2-183 K, the curie constant C = 5.64 emu K mol^{-1}, the Weiss temperature θ = 8.55 K. Salt **2**: Curie-Weiss fitting in 2-300 K, the curie constant C = 6.11 emu K mol^{-1}, the Weiss temperature θ = 5.95 K. Salt **3**: Curie-Weiss fitting in 2-183 K, the curie constant C = 5.77 emu K mol^{-1}, the Weiss temperature θ = 8.85 K. Salt **4**: Curie-Weiss fitting in 2-183 K, the Curie constant C = 4.55 emu K mol^{-1}, the Weiss temperature θ = 7.94 K. From *M*-*H* curves, the salts **1**-**4** reached the saturated magnetization value of 7.76, 7.92, 7.97, and 7.83 μ_B at 2 T, respectively. All the samples showed saturation behavior in magnetization (M) of magnetic field (H) dependence corresponding to the high spin state of Mn^{2+} (S = 5/2) and Cr^{3+} (S = 3/2) with small hysteresis.

Since the ferroelectric-paraelectric phase transition was observed, the correlation between ferroelectric and ferromagnetic orders in multiferroic **2** was inspected. We polarized the polycrystalline sample at 450 K and measured *M*-*H* dependence at 2 K. Then the sample was depolarized by heating to 460 K and the *M*-*H* curve was measured in the same conditions by using the annealed sample. The comparison of the *M*-*H* curves is shown in Figure 2-15. The saturated value of magnetization of the depolarized sample was enhanced by 1.5% compared with that of the polarized sample indicating that the polarization of the sample significantly affected the magnetic order. It is the first observation of the magnetoelectric effect in type-I multiferroic composed of the molecularly hybrid two-dimensional system without perovskite structure. We assumed such magnetoelectric coupling effect was attributed to the distortion of $[MnCr(oxalate)_3]^-$ upon phase transition.

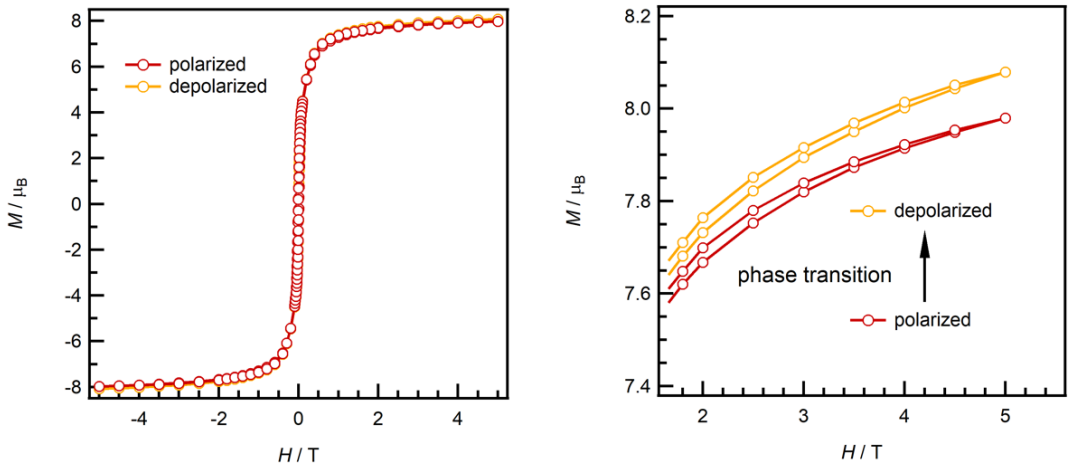

Figure 2-15. *M*-*H* curves of polarized and depolarized crystal **2**.

2-5. Conclusion

In this work, four polar crystals (*x*-anilinium^{+})(benzo[18]crown-6)[MnCr(oxalate)$_3$]$^{-}$, where *x* = H, *o*-fluoro, *m*-fluoro, and *p*-fluoro, for **1**, **2**, **3**, and **4**,were obtained. The supramolecular layer is alternatively stacked with [MnCr(oxalate)$_3$]$^{-}$ layer. The alignment of Mn^{2+} and Cr^{3+} leads to a ferromagnetic transition in these crystals, with Weiss temperature from 5.95 K to 8.85 K. In crystals **1**, **2**, and **4**, the tilting motion of benzo[18]crown-6 was observed from the results of temperature varied single-crystal X-ray diffraction. These molecular motions resulted in dielectric relaxation, with the activation energy of 31.8 kJ/mol for **1**, 51.2 kJ/mol for **3**, and 36.4 kJ/mol for **4**. In addition to the tilting motion of the benzo[18]crown, molecular rotation of (*m*-fluoroanilinium) was also observed in crystal **3**, giving rise to another dielectric relaxation at a higher temperature region with activation energy 34.1 kJ/mol. A ferroelectric to paraelectric phase transition occurred at 470 K in crystal **2**. Upon phase transition, supramolecular (*o*-fluoroanilinium)benzo[18]crown-6 underwent an in-plane 180° rotation, making the dipole moments become net zero in the paraelectric phase. The inversion of pyroelectric signals under opposite electric fields indicated its ferroelectric feature. Crystal **3** is the first example of multiferroic materials based on [MnCr(oxalate)$_3$]$^{-}$. The magnetoelectric coupling was investigated by comparing the saturated magnetization between polarized and depolarized samples. The result showed a 1.5% difference between the saturated magnetization values.

Reference

1. E. Coronado, J. R. Galan-Mascaros, C. J. Gomez-Garcia and V. Laukhin, *Nature*, 2000, **408**, 447-449.
2. W. Eerenstein, N. D. Mathur and J. F. Scott, *Nature*, 2006, **442**, 759-765.
3. M. Bibes and A. Barthelemy, *Nat. Mater.*, 2008, **7**, 425-426.
4. T. Kimura, T. Goto, H. Shintani, K. Ishizaka, T. Arima and Y. Tokura, *Nature*, 2003, **426**, 55-58.
5. M. Fiebig, *J Phys D Appl Phys*, 2005, **38**, R123-R152.
6. J. Wang, J. B. Neaton, H. Zheng, V. Nagarajan, S. B. Ogale, B. Liu, D. Viehland, V. Vaithyanathan, D. G. Schlom, U. V. Waghmare, N. A. Spaldin, K. M. Rabe, M. Wuttig and R. Ramesh, *Science*, 2003, **299**, 1719-1722.
7. N. A. Hill, *J. Phys. Chem. B*, 2000, **104**, 6694-6709.
8. N. Hur, S. Park, P. A. Sharma, J. S. Ahn, S. Guha and S. W. Cheong, *Nature*, 2004, **429**, 392-395.
9. L. Martin, S. P. Crane, Y. H. Chu, M. B. Holcomb, M. Gajek, M. Huijben, C. H. Yang, N. Balke and R. Ramesh, *J Phys-Condens Mat*, 2008, **20**.
10. X. L. Liu, D. Li, H. X. Zhao, X. W. Dong, L. S. Long and L. S. Zheng, *Adv. Mater.*, 2021, **33**.
11. H. B. Cui, Z. M. Wang, K. Takahashi, Y. Okano, H. Kobayashi and A. Kobayashi, *J. Am. Chem. Soc.*, 2006, **128**, 15074-15075.
12. Y. M. You, W. Q. Liao, D. W. Zhao, H. Y. Ye, Y. Zhang, Q. H. Zhou, X. H. Niu, J. L. Wang, P. F. Li, D. W. Fu, Z. M. Wang, S. Gao, K. L. Yang, J. M. Liu, J. Y. Li, Y. F. Yan and R. G. Xiong, *Science*, 2017, **357**, 306-309.
13. M. Clemente-Leon, E. Coronado, C. Marti-Gastaldo and F. M. Romero, *Chem. Soc. Rev.*, 2011, **40**, 473-497.
14. C. Shi, L. Ye, Z. X. Gong, J. J. Ma, Q. W. Wang, J. Y. Jiang, M. M. Hua, C. F. Wang, H. Yu, Y. Zhang and H. Y. Ye, *J. Am. Chem. Soc.*, 2020, **142**, 545-551.
15. C. Han, J. A. McNulty, A. J. Bradford, A. M. Z. Slawin, F. D. Morrison, S. L. Lee and P. Lightfoot, *Inorg. Chem.*, 2022, **61**, 3230-3239.

16. F. Pointillart, C. Train, M. Gruselle, F. Villain, H. W. Schmalle, D. Talbot, P. Gredin, S. Decurtins and M. Verdaguer, *Chem. Mater.*, 2004, **16**, 832-841.
17. C. Train, R. Gheorghe, V. Krstic, L. M. Chamoreau, N. S. Ovanesyan, G. L. J. A. Rikken, M. Gruselle and M. Verdaguer, *Nat. Mater.*, 2008, **7**, 729-734.
18. S. Benard, P. Yu, J. P. Audiere, E. Riviere, R. Clement, J. Guilhem, L. Tchertanov and K. Nakatani, *J. Am. Chem. Soc.*, 2000, **122**, 9444-9454.
19. T. Akutagawa, H. Koshinaka, D. Sato, S. Takeda, S. I. Noro, H. Takahashi, R. Kumai, Y. Tokura and T. Nakamura, *Nat. Mater.*, 2009, **8**, 342-347.

Chapter 3: Solvent dependence of crystal structure and dielectric relaxation in ferromagnetic $[MnCr(oxalate)_3]$ salt

3-1 Introduction

Oxalate-bridged transition-metal complexes have attracted much attention due to their diverse network structures, as well as a variety of magnetic properties that depend on the metal centers. Two-dimensional (2D) honeycomb structures that exhibit ferromagnetic order have been studied extensively.[1-4]

Their ability to accommodate a variety of functional cations between the two-dimensional layers has resulted in interesting multifunctional hybrid magnets. For example, E. Coronado *et al.* reported a ferromagnetic conductor, (BEDT-TTF)$_3$[MnCr(oxalate)$_3$] (BEDT-TTF = bis(ethylenedithio)tetrathiafulvalene), based on the alternate-layered structure of an organic cation radical assembly and a [MnCr(oxalate)$_3$]$^-$ anion.[2] This (BEDT-TTF)$_3^+$ cation radical assembly, which was sandwiched by ferromagnetic layers, showed metallic conduction with negative magnetoresistance at low temperatures. Train *et al*. synthesized an enantiopure chiral ferromagnet by inserting a chiral quaternary ammonium cation between the ferromagnetic layers of [MnCr(oxalate)$_3$]$^-$.[3] The chiral cation regulated the absolute configurations of the metal centers in the [MnCr(oxalate)$_3$]$^-$ layers. As a result, the crystals exhibited strong magnetochiral dichroism. Furthermore, the coexistence of spin-crossover (SCO) and ferromagnetic ordering was also realized by incorporating [Fe^{III}(sal$_2$-trien)]$^+$ into [MnCr(oxalate)$_3$]$^-$ 2D layers.[5-6]

Ferromagnetic honeycomb oxalate-bridged complexes afford a variety of multifunctional materials by incorporating functional cationic units between the layers. However, they readily crystallize with solvent molecules, especially in the cavities of the honeycomb layers. The solvent molecules incorporated in the crystal often make it difficult to determine the physical properties of the crystals, especially above room temperature. This is because the crystals become unstable and collapse owing to desolvation.[7-10]

We have focused on introducing supramolecular rotors into 2D honeycomb oxalate-bridged complexes to develop novel multifunctional materials, especially multiferroics.[11-12] We carefully designed supramolecular structures composed of crown

ether derivatives and organic ammonium cations so that supramolecular cation assemblies between the $[MnCr(oxalate)_3]^-$ layers formed, leaving no space for solvent molecules. For example, when *trans-syn-trans*-dicyclohexano[18]crown-6 exhibited a flat conformation, the cyclohexane incorporated into the crystal honeycomb holes prevented solvent incorporation.[13-14]

In this study, we report on the polar crystal $(CBA^+)([18]crown-6)[MnCr(oxalate)_3](CH_3OH)$ (CBA^+ = 4-carboxybutan-1-aminium) (**5**•CH_3OH) of space group *Cc*. The crystals remain in a single-crystal state even when the solvent is removed by heating. The solvent-free crystal $(CBA^+)([18]crown-6)[MnCr(oxalate)_3]^-$ (**1**) has the space group *C*2 retaining the polarity of the crystal. It is noteworthy that crystal **5** after desolvation showed a clear dielectric relaxation in the temperature range from 100 K to 300 K with a disorder of [18]-crown-6. The crystal structure, dielectric, and magnetic properties of the crystals before and after desolvation will be discussed in detail.

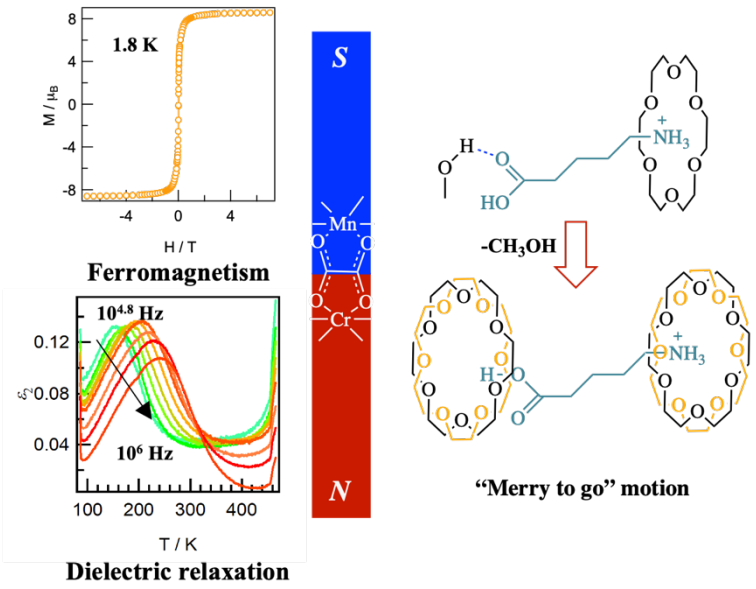

Scheme 3-1. Structural phase transition induced by solvent desolvation in ferromagnetic $[MnCr(oxalate)_3]^-$ salt.

3-2 Thermal analysis of $(CBA^{+})18C6[MnCr(oxalate)_3]^{-}\bullet CH_3OH$

The desorption of methanol in crystal **5**•CH_3OH was verified by TG measurement. Polycrystals of **1**•CH_3OH isolated from the mother solution were left to stand at room temperature for 15 minutes before the first cycle of TG measurement. As shown in Figure 3-1, curve 1 indicated the weight loss behavior of **5**•CH_3OH in the temperature region 300-500 K. The slight weight loss of the sample was observed from the start point of 300 K. From around 340 K, the weight sharped decreased, reducing 4.10% at 380 K. After this drastic weight change, the weight of the sample began to become stable until the decomposition temperature of around 510 K. The value of 4.10% of weight loss between 340 K and 380 K was in good agreement with the weight ratio of one molecule of methanol in **5**•CH_3OH, calculated as 4.08%. This result indicated that one molecule of methanol was desolvated from **5**•CH_3OH at 380 K, and kept thermal stable up to 510 K. The polycrystals of **5**•CH_3OH were heated at 400 K for 15 minutes under a nitrogen gas flow environment to desolvate the contained solvent methanol. After this pretreatment, the samples were used for TG measurement, and the result was shown as curve 2 in Figure 3-1. The compound showed good thermal stability up to 510 K without significant weight change.

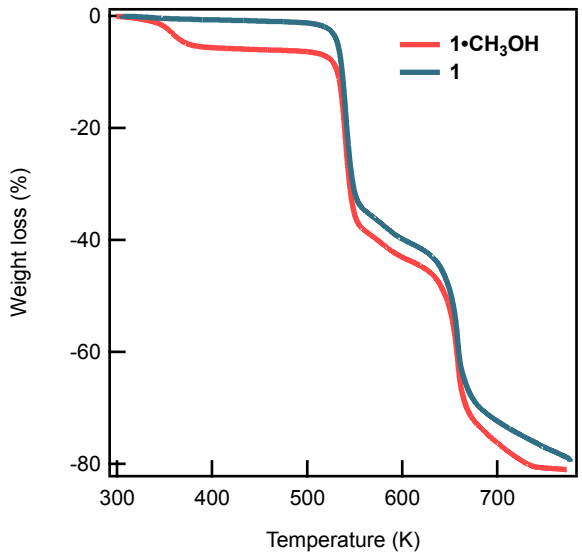

Figure 3- 1. TG-DTA curve of polycrystals **5**•CH_3OH. Red: polycrystals of **5**•CH_3OH. Blue: annealed polycrystals **5**•CH_3OH after heating at 400 K for 15 min.

3-3 Crystal structure analysis

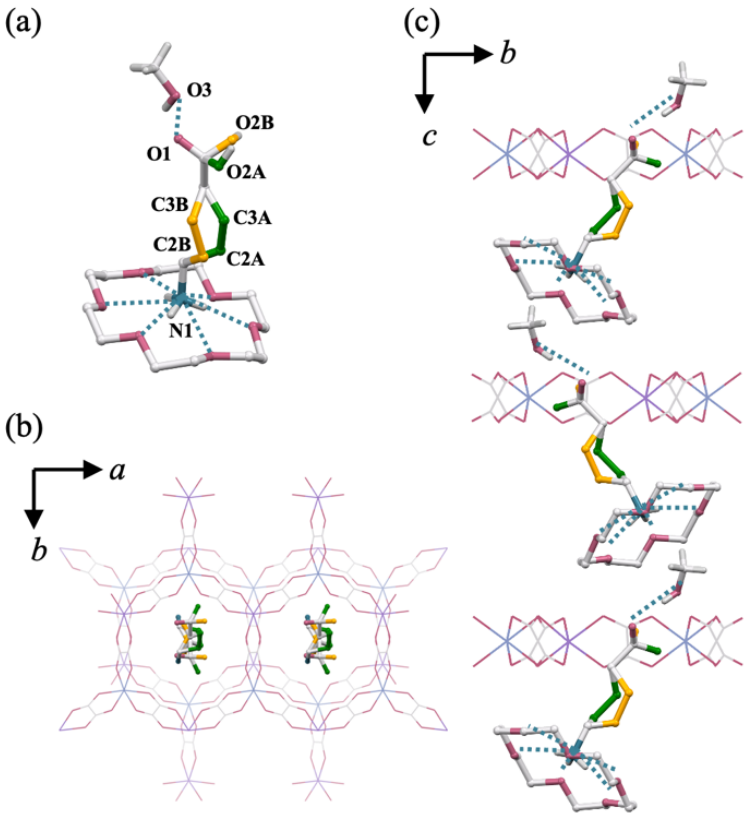

Figure 3-2. Crystal structures of **5**•CH_3OH. (a) The supramolecular cation CBA^+ was fixed by guest molecule CH_3OH and crown ether via hydrogen bonding, respectively. (b) The honeycomb structure of $[MnCr(oxalate)_3]$ layers, projected in the *ab* plane. For clarity, crown ether and solvents were omitted. (c) Crystal structure viewed along the *a*-axis. CBA^+ cation penetrated the honeycomb. The supramolecular cation CBA^+ was fixed by crown ether via hydrogen bonding.

The crystal structure of **5**•CH_3OH was revealed by single-crystal X-ray diffraction at 273 K. The crystallographically independent unit was composed of one molecule of $[MnCr(oxalate)_3]^-$ anion, one molecule of supramolecular (CBA^+)([18]crown-6), and one molecule of methanol used as a solvent. The $[MnCr(oxalate)_3]^-$ formed the 2D honeycomb layer template by supramolecular cation (CBA^+)([18]crown-6). (CBA^+)([18]crown-6) formed a supramolecular layer, which was stacked alternately with $[MnCr(oxalate)_3]^-$ honeycomb layer along the *c*-axis. In the CBA^+ cation, C2 and

C3 carbon atoms of the alkyl chain, as well as O2 oxygen of the carbonyl group, are disordered at the two positions with an occupancy ratio of 1:1, which are shown in green and yellow in Figure 2-2. All of the carbonyl groups of CBA^+ insert into the void of the 2D honeycomb layer. The solvent of methanol occupied the space between these two layers. CH_3OH formed a hydrogen bond with ordered carbonyl oxygen (O1) of CBA^+. The ammonium group on the other side of CBA^+ was fixed by the crown ether via N–H···O hydrogen bonding. Due to the unidirectional insertion of CBA^+ cations along the *c*-axis, the crystal **5**•CH_3OH showed structural polarity and crystallized with the polar space group *Cc*.

3-4 Desolvation-induced structural phase transition

Table 3-1. Crystallographic data of $(CBA^{+})18C6[MnCr(oxalate)_3]^{-}\bullet CH_3OH$ and solvent-free structure.

	5•CH_3OH	**5**
Solvent	CH_3OH	*none*
Temperature / K	273	93
Chemical formula	$C_{24}H_{39}CrMnO_{21}N$	$C_{23}H_{35}CrMnO_{20}N$
Formula weight	784.49	752.45
Space group	*Cc*	*C*2
a, Å	9.2411(3)	8.9417 (6)
b, Å	16.5508 (4)	17.0164 (8)
c, Å	22.7081 (8)	10.4599 (9)
β, deg	94.612 (3)	98.318 (7)
V, $Å^3$	3461.92 (17)	1574.79 (19)
Z	4	2
D_{calc}, $g\cdot cm^{-3}$	1.353	1.580
μ, mm^{-1}	0.870	0.888
Reflections measured	25801	10250
Independent reflections	7458	3915
R_{int}	0.0451	0.0453
R_{sigma}	0.0407	0.0556
R_1 [a]	0.0671	0.1038
$R_w(F^2)$ [a]	0.1440	0.2131
GOF	1.061	1.035
Flack Parameter	0.103(13)	0.52(6)

[a] $R_1 = \Sigma||F_o| - |F_c|| / \Sigma|F_o|$ and $R_w = (\Sigma\omega(|F_o| - |F_c|)^2 / \Sigma\omega F_o^2)^{1/2}$.

The TG measurement revealed that **5**•CH_3OH desorbs one molecule of methanol at 380 K and is thermally stable up to 510 K. The guest solvent-free structure of crystal **5** was obtained after the heating procedure at 380 K for 30 minutes and its structure was determined at 93 K. After desolvating methanol, the space group of the crystal transit to *C*2 with halved *c*-axis length of 10.4599 Å (Table 3-1).

As shown in Figure 3-3, in crystal **5**, the carboxylic group of CBA^+ cation slid from the honeycomb cavity to the interlamination of $[MnCr(oxalate)_3]^-$ layers due to the disappearance of the hydrogen bond between CH_3OH and CBA^+. The carboxylic group in CBA^+ cation, instead, formed hydrogen bonds with ether oxygen of [18]crown-6 with the bond length between O2···O3 and O2···O8 of 3.097 Å and 3.184 Å, respectively (Figure 3-3 (b)). On the other side of CBA^+, the $-NH_3$ group formed hydrogen bonds with [18]crown-6. The CBA^+ and [18]crown-6 alternately stacked forming a column structure along the *a*-axis between $[MnCr(oxalate)_3]^-$ layers.

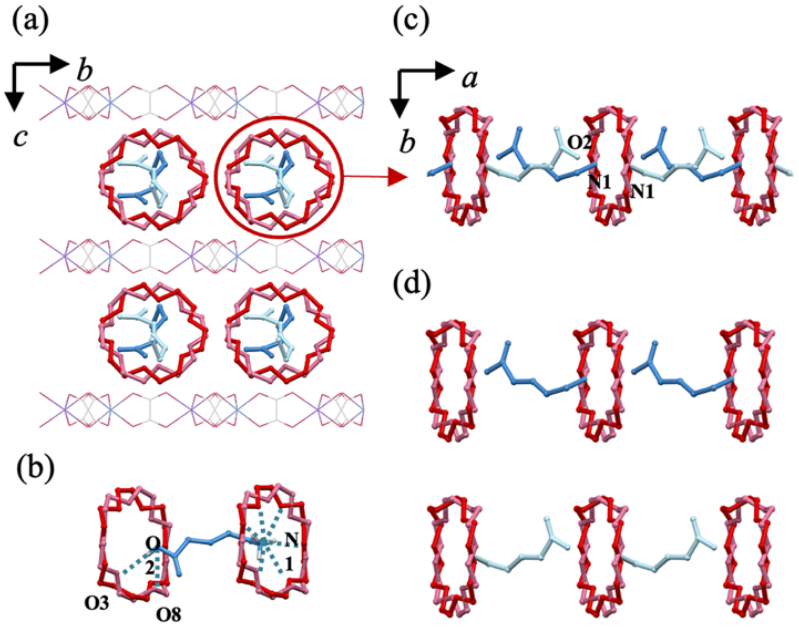

Figure 3-3. (a) Crystal structure of **5** viewed along the *a*-axis. (b) Hydrogen bond structure between CBA^+ and [18]crown-6. (c) Supramolecular column of (CBA^+)([18]crown-6), viewed along the *c*-axis. The CBA^+ shows statical disorder with each occupancy of 0.5 indicated by blue and light blue. The [18]crown-6 showed dynamic disorder due to Merry-go-round motion. The occupancy ratio of two molecules indicated by red and pink is 1:1. (d) Head-to-tail supramolecular cationic assembly composed of each static disorder of CBA^+.

Both CBA^+ and [18]crown-6 were disordered in crystal **5** as shown in Figure 3-3 (c). The CBA^+ cations showed a positional disorder at two sites indicated by blue and light blue in Figure 3-3 (c) with equal occupancy of 0.5. Within the supramolecular column, the distances between $–NH_3$ groups and those between $–NH_3$ and carboxyl –OH group between adjacent CBA^+ were 2.066 Å and 3.429 Å, respectively, showing no direct interaction less than the sum of van der Waals radii between CBA^+ cations. However, considering electrostatic interactions between ammonium and carboxyl groups, a head-to-tail cationic assembly composed of only one of the positionally disordered CBA^+ should be a reasonable structure for each one-dimensional supramolecular column (Figure 3-3(d)).

3-5 Dynamic properties

The [18]crown-6 also showed a disorder at two sites with an occupancy ratio of 1:1 independent from a positional disorder of CBA^+. The disorder should originate from the rotation of [18]crown-6 known as the "merry-go-round" motion. We already reported the [18]crown-6 rotation in (anilinium)([18]crown-6)Ni(dmit)$_2$ ($dmit^{2-}$ = 2-thioxo-1,3-dithiole-4,5-dithiolate) in addition to flip-flop motion of phenyl ring in the crystal.[15] In the case of Cs_2([18]crown-6)$_3$[Ni(dmit)$_2$]$_2$, [18]crown-6 rotation in Cs_2([18]crown-6)$_3$ triple-decker structure affected the magnetism arising from Ni(dmit)$_2$ dimer largely.[16] The "Merry-go-round" motion of [18]crown-6 in the crystal was detected as dielectric relaxation behavior in the temperature dependence of dielectric measurements.

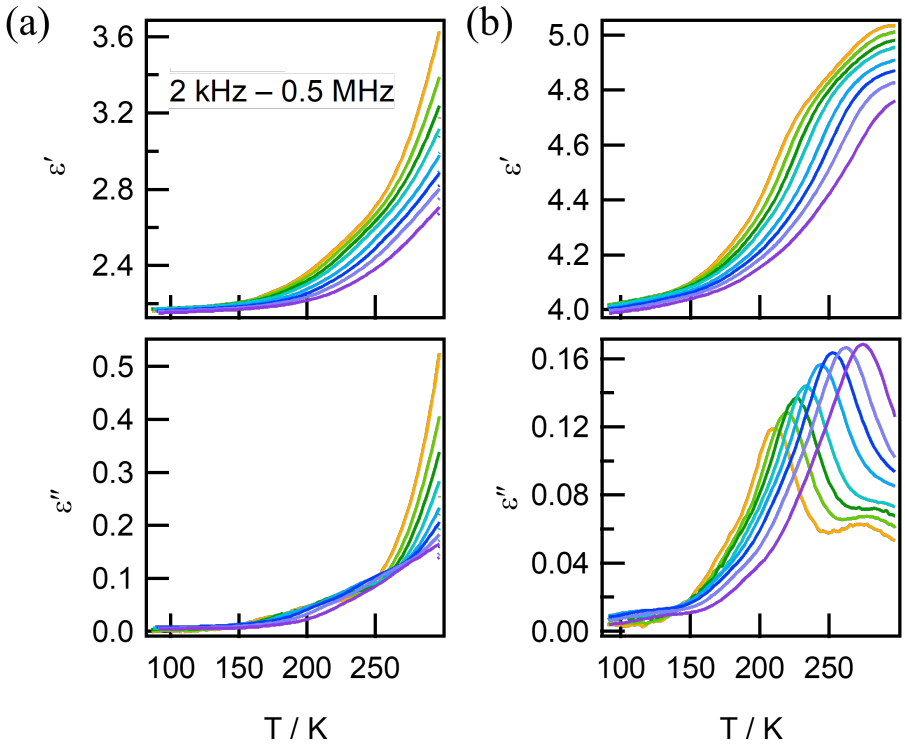

Figure 3- 4. Temperature- and frequency-dependent dielectric constants were measured on pellet samples of **5**•CH_3OH (a) and **5** (b).

To investigate the dynamic feature of disorders observed in the crystals, the frequency- and temperature-dependent dielectric constants were measured on compacted pellets of **5**•CH_3OH and **5**.

The sample was held at 400 K for 30 min for removing solvents. The second cycle of dielectric measurement was conducted by using the heated sample, whose PXRD pattern was in good agreement with the calculated pattern of **5** (Figure 3-5). The peaks of the imaginary part of the dielectric constant (ε_2) were observed. The clear frequency dependence indicates that dielectric relaxation behavior originated from molecular motion within the crystal. The activation energy for the motion was calculated as 41.41 kJ/mol (Figure 3-6). The relaxation behavior should be originated from [18]crown-6 rotation within the crystal. The activation energy for the "merry-go-round" motion of [18]crown-6 reported for malononitrile complex crystal was 41.41 kJ/mol measured by 2H-NMR.[17] The similar activation energy observed for crystal **5** indicates the proper spatial environment for [18]crown-6 rotation in the crystalline state.

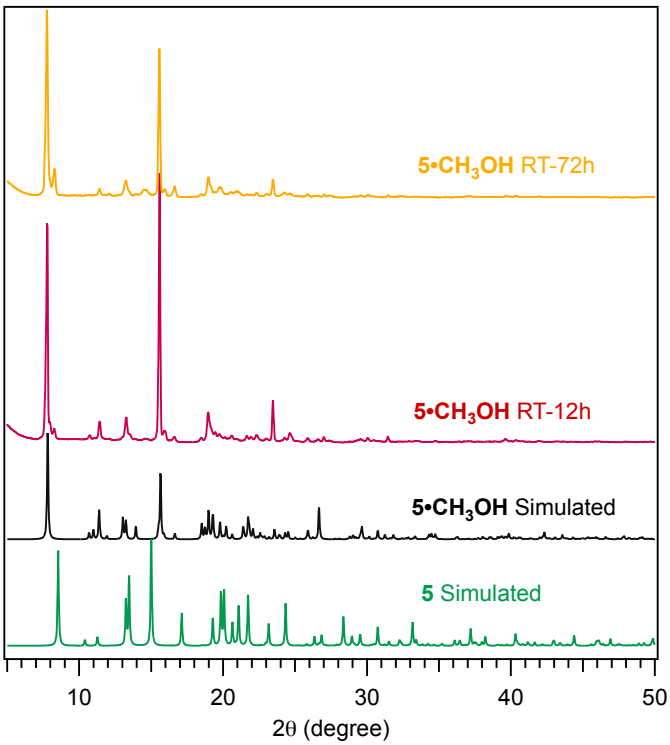

Figure 3-5. Experimental and simulated PXRD patterns of solvent contained **5**•CH_3OH samples and solvent-free **5** samples. The simulated patterns of **5**•CH_3OH and **5** were calculated based on SCXRD results of **5**•CH_3OH at 273 K and **5** at 93 K, respectively.

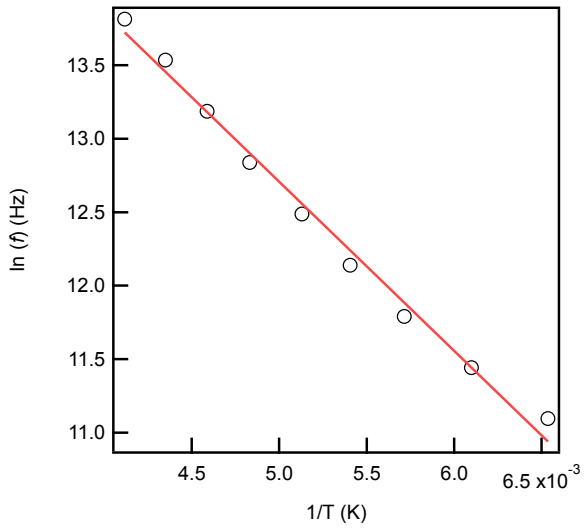

Figure 3-6. The activation energy in salt **5** was calculated based on dielectric relaxation in Figure 3-4. The activation energy for the "Merry-go-round" motion of [18]crown-6 was calculated as 41.41 kJ/mol.

3-6. Magnetic properties

Temperature dependence of molar magnetic susceptibility (χ_m) in addition to magnetization curves are shown in Figures 3-7. The crystals **5**•CH_3OH and **5** showed identical magnetic behavior within experimental errors. In both crystals, the rapid increase of $\chi_m T$ values at around 5 K was observed. The Curie constant (C) and Weiss temperature (θ) for crystal **5**•CH_3OH were 6.09 cm^3 K mol^{-1} and 10.92 K, respectively, and those for crystal **5** were 6.00 cm^3 K mol^{-1} and 10.08 K, respectively.

The ferromagnetic order of the crystal was indicated by the magnetization curve measured at 1.8 K, with the saturation at 8.5 μ_B and 8.3 μ_B, respectively, for **5**•CH_3OH and **5**. The values were in good agreement with the high spin state of Mn^{2+} (S = 5/2) and Cr^{3+} (S = 3/2).

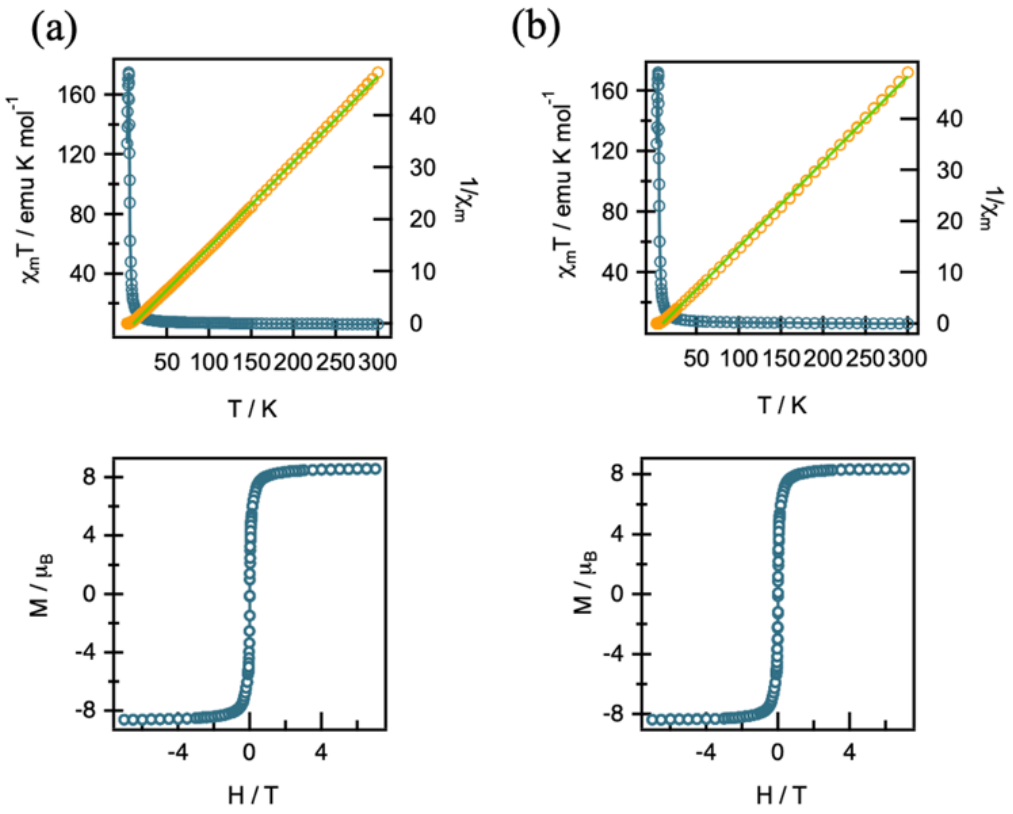

Figure 3-7. Temperature dependence of χ_m (up) and magnetization at 1.8 K (below) for **5**•CH_3OH(a), and **5** (b).

3-7. Conclusions

In conclusion, a two-dimensional hybrid crystal of $(CBA^+)([18]crown-6)][MnCr(oxalate)_3]^-(CH_3OH)$ (**5**•CH_3OH) was obtained based on supramolecular structure and bimetallic oxalate-bridged complex. The desolvation of guest CH_3OH induced a crystal-to-crystal structural transformation to a solvent-free crystal of $(CBA^+)([18]crown-6)[MnCr(oxalate)_3]^-$ (**5**). Upon desolvation, the supramolecular cation structure of $(CBA^+)([18]crown-6)\cdots CH_3OH$ reorganized to a columnar structure constructed from an alternate stack of CBA^+ and [18]crown-6 with the head-to-tail arrangement of CBA^+ in each column. The dynamic disorder of [18]crown-6 due to Merry-go-round motion in crystal **1**, induced dielectric relaxation. The activation energy was calculated to be 41.41 kJ/mol. Both **5**•CH_3OH and **5** showed ferromagnetic ordering. Although the structural change did not show a significant effect on the magnetic susceptibility and magnetization behavior, the polar structure of the crystal may affect chiral magnetic behaviors. The studies on these lines are in progress.

Reference

1. H. Okawa, A. Shigematsu, M. Sadakiyo, T. Miyagawa, K. Yoneda, M. Ohba and H. Kitagawa, *J. Am. Chem. Soc.*, 2009, **131**, 13516-13522.
2. E. Coronado, J. R. Galan-Mascaros, C. J. Gomez-Garcia and V. Laukhin, *Nature*, 2000, **408**, 447-449.
3. C. Train, R. Gheorghe, V. Krstic, L. M. Chamoreau, N. S. Ovanesyan, G. L. J. A. Rikken, M. Gruselle and M. Verdaguer, *Nat. Mater.*, 2008, **7**, 729-734.
4. M. Clemente-Leon, E. Coronado, C. Marti-Gastaldo and F. M. Romero, *Chem. Soc. Rev.*, 2011, **40**, 473-497.
5. M. Clemente-Leon, E. Coronado and M. Lopez-Jorda, *Dalton Trans.*, 2013, **42**, 5100-5110.
6. M. Clemente-Leon, E. Coronado, M. C. Gimenez-Lopez, A. Soriano-Portillo, J. C. Waerenborgh, F. S. Delgado and C. Ruiz-Perez, *Inorg. Chem.*, 2008, **47**, 9111-9120.
7. A. California, V. F. Cardoso, C. M. Costa, V. Sencadas, G. Botelho, J. L. Gomez-Ribelles and S. Lanceros-Mendez, *Eur. Polym. J.*, 2011, **47**, 2442-2450.
8. T. Endo, K. Kubo, M. Yoshitake, S. Noro, T. Akutagawa and T. Nakamura, *Chem. Lett.*, 2013, **42**, 137-139.
9. Y. X. Wang, Q. T. Xu, P. Ren, W. Shi and P. Cheng, *Dalton Trans.*, 2019, **48**, 2228-2233.
10. D. W. Fu, J. X. Gao, P. Z. Huang, R. Y. Ren, T. Shao, L. J. Han, J. Liu and J. M. Gong, *Angew. Chem. Int. Ed.*, 2021, **60**, 8198-8202.
11. T. Endo, T. Akutagawa, S. Noro and T. Nakamura, *Dalton Trans.*, 2011, **40**, 1491-1496.
12. T. Akutagawa, H. Koshinaka, D. Sato, S. Takeda, S. I. Noro, H. Takahashi, R. Kumai, Y. Tokura and T. Nakamura, *Nat. Mater.*, 2009, **8**, 342-347.
13. M. Yoshitake, K. Kubo, T. Endo, S. Noro, T. Akutagawa and T. Nakamura, *Bull. Chem. Soc. Jpn.*, 2016, **89**, 354-360.

14. K. Kubo, M. Yoshitake, N. Hoshino, S. Noro, T. Akutagawa and T. Nakamura, *Eur. J. Inorg. Chem.*, 2020, **2020**, 1670-1675.
15. S. Nishihara, T. Akutagawa, D. Sato, S. Takeda, S. I. Noro and T. Nakamura, *Chem. Asian J.*, 2007, **2**, 1083-1090.
16. T. Akutagawa, K. Shitagami, S. Nishihara, S. Takeda, T. Hasegawa, T. Nakamura, Y. Hosokoshi, K. Inoue, S. Ikeuchi, Y. Miyazaki and K. Saito, *J. Am. Chem. Soc.*, 2005, **127**, 4397-4402.
17. G. W. Buchanan, M. Gerzain and C. I. Ratcliffe, *Can. J. Chem.*, 1999, **77**, 1911-1921.

Chapter 4. Novel three-dimensional networks based on the organic supramolecular structure

4-1. Introduction

Highly symmetric structures, such as honeycomb and diamond, have attracted much research interest because they can arise unique properties on mechanical strength and particular photonic and electronic properties.[1,2] Gyroid is a type of three-dimensional period structure with an infinitely connected triply-periodic minimal surface discovered by Shoen.[3] Due to the presence of maximal symmetry and a strong isotropic property in gyroid structure, the crystals with gyroid structure can show exotic electronic properties. For example, K. Awaga group has reported a molecular gyroid formed by naphthalene diimide (NDI)-Δ, which consisted of three planar NDI moieties, connected by three cyclohexane moieties. Strong spin frustration was observed in (NDI)-Δ lattice, resulting in the unique spin liquid state at low temperature.[4]

Bimetallic oxalate-bridged networks of $[MnCr(oxalate)_3]^-$ are an interesting subject for the study of gyroid. This is because while they exhibit magnetic behaviors, they can form three-dimensional networks via the templating effect of incorporated cations. A few gyroid structures based on monometallic or bimetallic oxalate-bridge complexes have been reported,[5,6] and the metallic complex cations were used for constructing the gyroid structure in these crystals. Though their magnetic states were formed in the 3D gyroid networks of localized spin, unfortunately, the magnetic states did not show any uniqueness to the exotic gyroid structure.

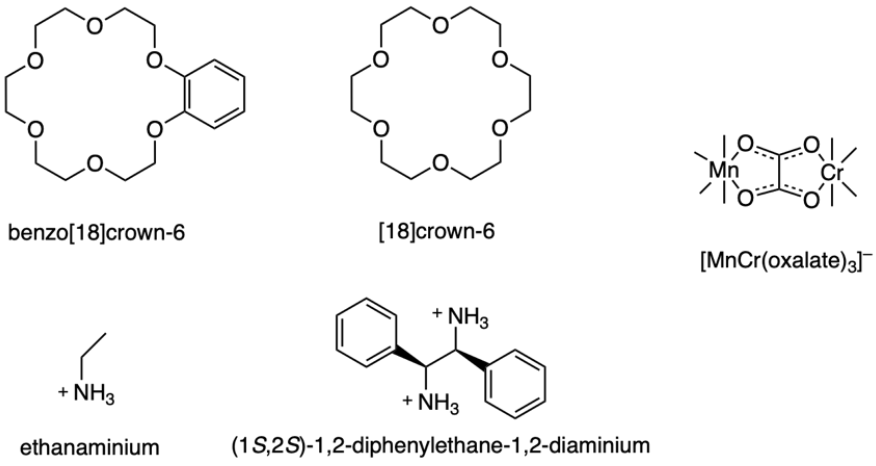

Scheme 4-1. Components of crystals in Chapter **4**.

4-2. Crystal structures

In this study, two chiral crystals with three-dimensional structures were obtained by using organic supramolecular cations and $[MnCr(oxalate)_3]^-$ anion, denoted as (ethanaminium$^+$)benzo[18]crown-6$[MnCr(oxalate)_3]^-$(1.5CH_3OH) (**6**), and [(1*S*,2*S*)-1,2-diphenylethan-1,2-diaminium^{2+}][18]crown-6$\{[MnCr(oxalate)_3]_2\}^{2-}$ (1.5CH_3OH)(0.5CH_3COCH_3) (**7**).

Table 4-1. Crystallographic data of **6** and **7**

	6	**7**
Temperature / K	100	223
Chemical formula	$C_{25.5}H_{38}CrMnO_{19.5}N$	$C_{22}H_{28.5}CrMnO_{17}N$
Formula weight	777.5	685.89
Space group	$Pna2_1$	$P2_12_12_1$
a, Å	22.0182(6)	23.1706(10)
b, Å	22.9212(5)	22.7711(10)
c, Å	13.7686(4)	12.6087(7)
β, deg	90	90
V, Å^3	6948.79	6652.6
Z	4	4
D_{calc}, g·cm^{-3}	1.535	0.350
μ, mm^{-1}	2.488	2.932
Reflections measured	47863	42538
Independent reflections	15786	12868
R_{int}	0.0308	0.1386
R_{sigma}	0.0357	0.1075
R_1 [a]	0.0581	0.1072
$R_w(F^2)$ [a]	0.1665	0.2697
GOF	1.047	0.960

[a] $R_1 = \Sigma||F_o| - |F_c|| / \Sigma|F_o|$ and $R_w = (\Sigma\omega(|F_o| - |F_c|)^2 / \Sigma\omega F_o^2)^{1/2}$.

The supramolecular structure and the bimetallic oxalate structure in crystals **6** and **7** were shown in Figure 4-1. Achiral supramolecular (ethanaminium)benzo[18]crown-6 adopt four independent metal ions Mn1, Mn19, Cr8, and Cr9 in crystal **6** with the same clockwise chirality, the same chirality, which is identical to the reported three-dimensional $[MnCr(oxalate)_3]^-$ networks. However, in crystal **7**, a rare configuration of metal ions was templated by the chiral supramolecular [(1*S*,2*S*)-1,2-diphenylethan-1,2-diaminium^{2+}]. Four independent metal ions Mn2, Cr5, Mn1, and Cr4 did not align in the same chiral configuration, instead, Mn2(Λ)-Cr5(Λ)-Mn1(Δ)-Cr4(Δ) was observed. The adjacent Mn2 and Cr2 showed anticlockwise configuration (Λ), while the adjacent Mn1 and Cr4 showed clockwise configuration(Δ), and the chirality from $[MnCr(oxalate)_3]^-$ was canceled in crystal **7**.

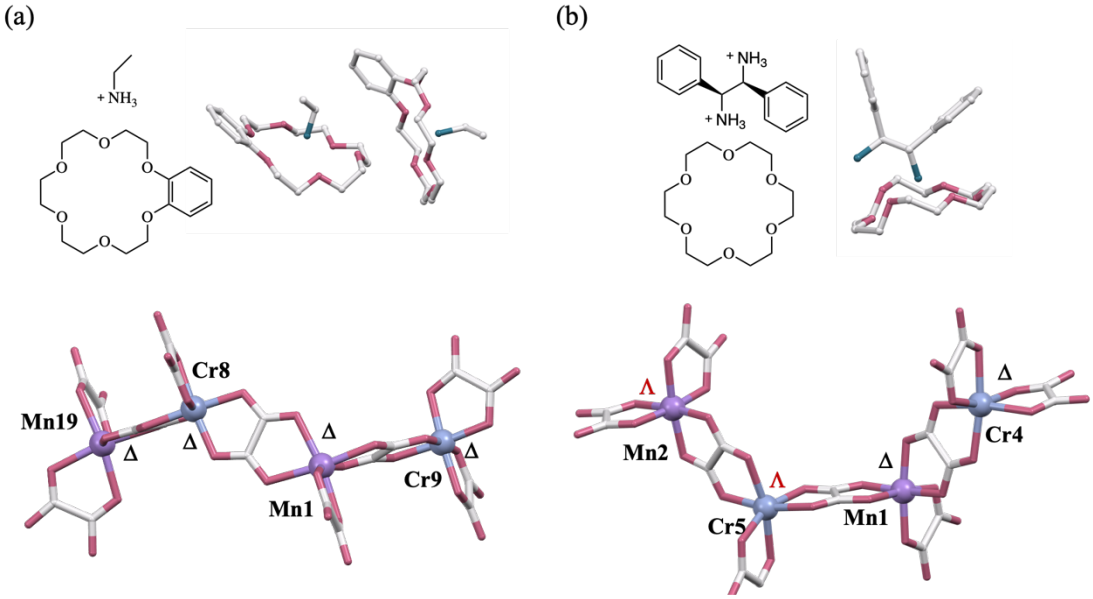

Figure 4-1. Achiral supramolecular cation and chiral supramolecular cation template different 3D structures in crystals **6** and **7**.

The networks of $[MnCr(oxalate)_3]^-$ in **6** and **7** were shown in Figure 4-2, and Figure 4-3, for clarity, the oxalate bonds, and supramolecular structures were omitted, and the metal ions with the same chirality in crystal **7** were represented by the same color. A typical chiral three-dimensional network was formed in crystal **6**. The chirality of the whole structure was attributed to the same configuration of Mn^{2+} and Cr^{3+} ions. However, due to the rotational direction, as shown in Figure 4-2 (b), being different between adjacent channels, the gyroid structure with strong isotropic features did not obtain.

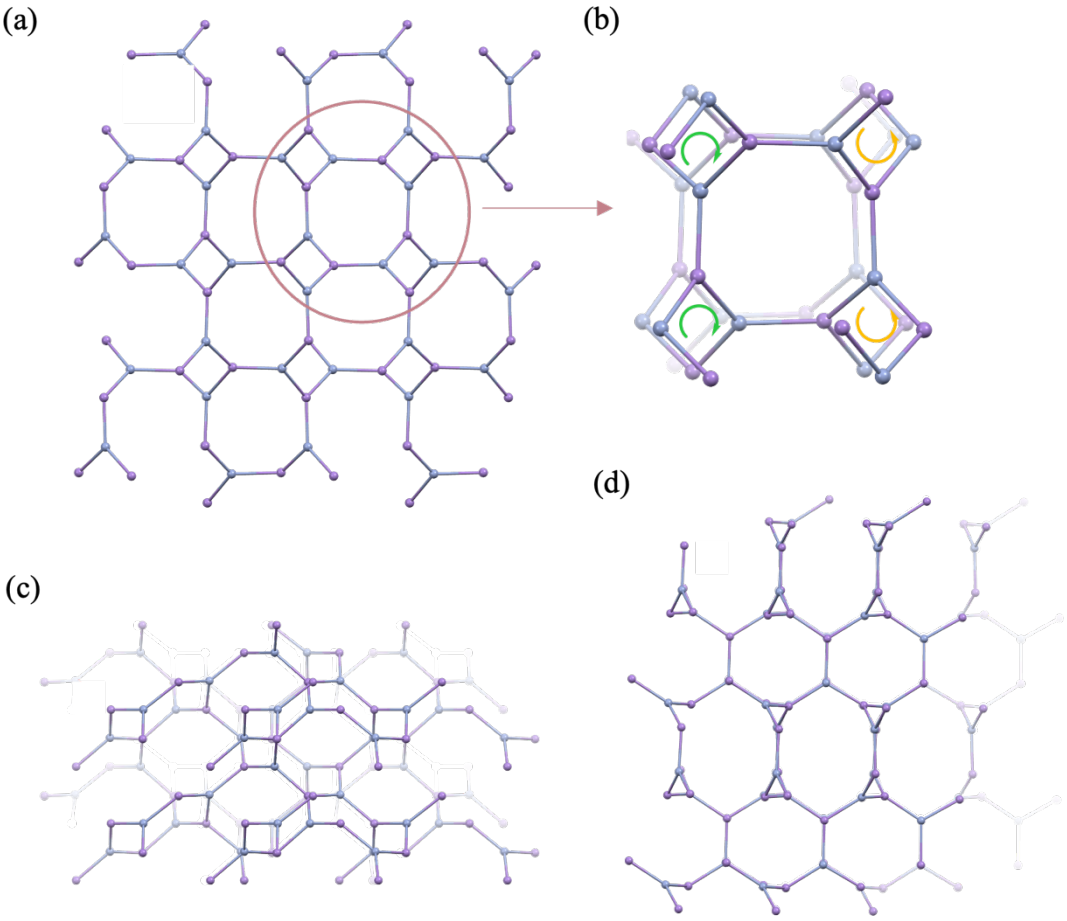

Figure 4-2. Three-dimensional networks projected in (a) *ab* plane, (c) *bc* plane and (d) *ac* plane in crystal 6. (b) Metals formed a C_4 spiral axis in each channel. The adjacent channels show opposite rotational directions.

We already reported that large flexible supramolecular cation of (H_2PPD^{2+})benzo[18]crown can induce a novel three-dimensional architecture with the combination of $[Mn(\Lambda)Cr(\Delta)(oxalate)_3]^-$ and $[Mn(\Lambda)Cr(\Lambda)(oxalate)_3]^-$ (Space group: *P*2/*c*).[7] Here, a new type of three-dimension network was formed in crystal **7**. Transition metal ions with Λ configuration were represented as the yellow color, that with Δ was represented as red color. The chirality of the whole anionic network should be net-zero due to the alternative chirality of center metals. The alignment of chiral cation of [(1*S*,2*S*)-1,2-diphenylethan-1,2-diaminium^{2+}] gave the chiral structure, crystallized in chiral space group $P2_12_12_1$. From the rotational direction in Figure 4-3 (b), we know this structure was not gyroid. However, the projection structure in plane *bc* and plane *ac* showed a similar network, indicating the possibility of supramolecular induced gyroid oxalate.

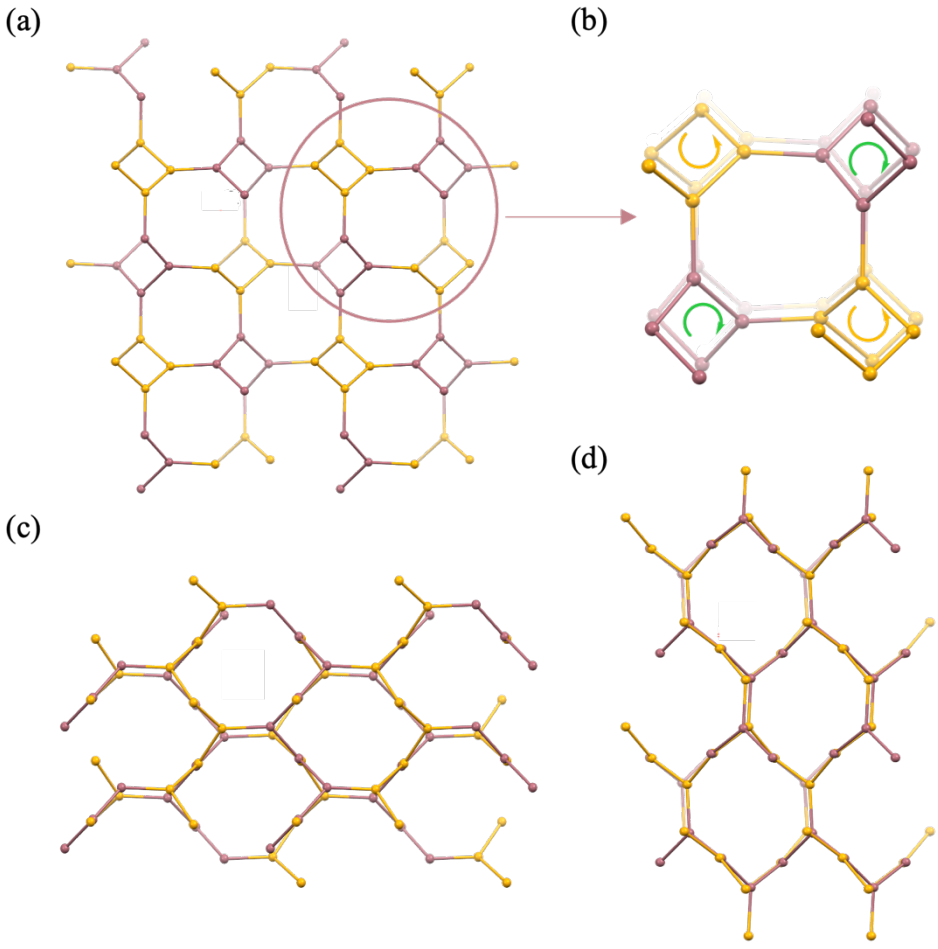

Figure 4-3. A novel three-dimensional structure in crystal **7**.

The alignment of supramolecular structure in crystals **6** and **7** are summarized in Figure 4-4 and Figure 4-5. In crystal **6**, there were two crystallographically independent supramolecular (ethanaminium)benzo[18]crown-6. There was no disorder at this temperature point.

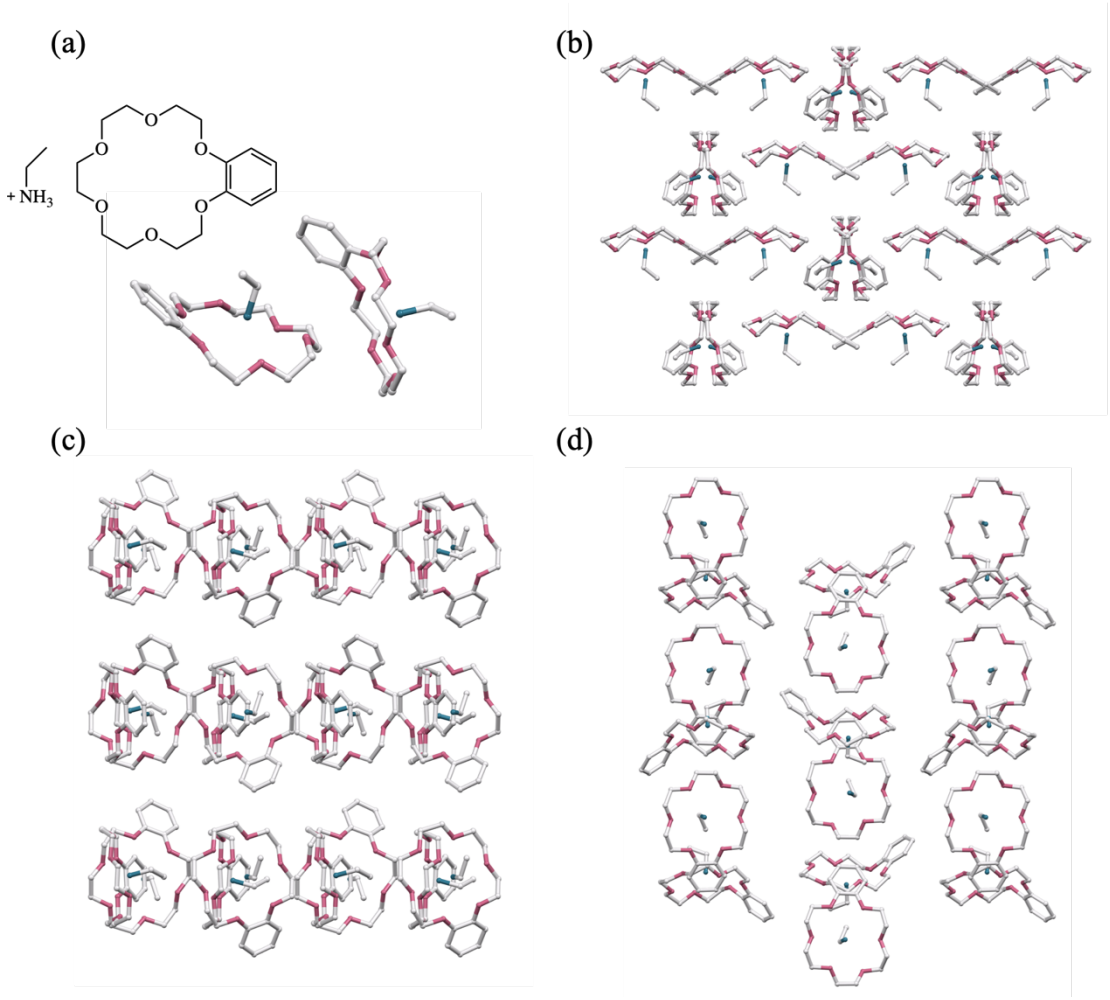

Figure 4-4. Supramolecular assembling in crystal **6**.

The origin of chirality in crystal 7 should be from [(1*S*,2*S*)-1,2-diphenylethan-1,2-diaminium]$^{2+}$ cations. However, at this stage, the insight of chirality and physical properties is not investigated yet. This work is introduced here as forward-looking research.

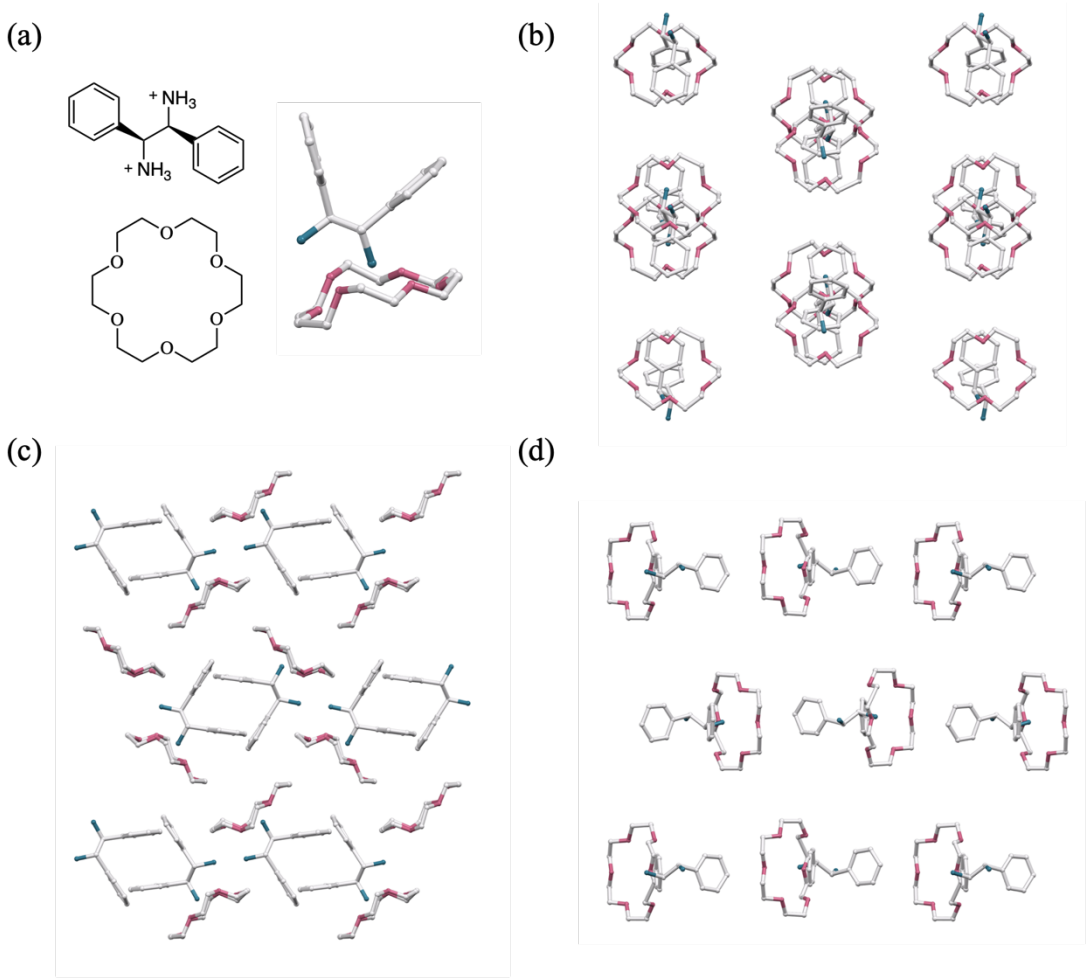

Figure 4-5. Supramolecular assembling in crystal **7**.

Reference

1. J. A. Dolan, B. D. Wilts, S. Vignolini, J. J. Baumberg, U. Steiner and T. D. Wilkinson, *Adv Opt Mater*, 2015, **3**, 12-32.
2. A. Mizuno, Y. Shuku and K. Awaga, *Bull. Chem. Soc. Jpn.*, 2019, **92**, 1068-1093.
3. A. H. Schoen, *National Aeronautics and Space Administration*, 1970, **5541**.
4. A. Mizuno, Y. Shuku, M. M. Matsushita, M. Tsuchiizu, Y. Hara, N. Wada, Y. Shimizu and K. Awaga, *Phys. Rev. Lett.*, 2017, **119**.
5. S. Decurtins, H. W. Schmalle, P. Schneuwly and H. R. Oswald, *Inorg. Chem.*, 1993, **32**, 1888-1892.
6. C. R. Li, S. L. Li and X. M. Zhang, *Cryst. Growth Des.*, 2009, **9**, 1702-1707.
7. T. Endo, K. Kubo, M. Yoshitake, S. Noro, N. Hoshino, T. Akutagawa and T. Nakamura, *Cryst. Growth Des.*, 2015, **15**, 1186-1193.

Chapter 5. Conclusions

In this thesis, organic supramolecular structures were used for designing multifunctional materials in two-dimensional or three-dimensional $[MnCr(oxalate)_3]^-$ systems.

In chapter **2**

(1) Anilinium derivatives combined with [benzo]18crown-6 adopt a series of hybrid crystals (*x*-anilinium$^+$)(benzo[18]crown-6)$[MnCr(oxalate)_3]^-$, where *x* = H, *o*-fluoro, *m*-fluoro, and *p*-fluoro, for **1**, **2**, **3**, and **4**, respectively. They crystallized in polar space groups $P2_1$, *Cc*, $P2_1$, and $Pna2_1$ with no solvents, for **1**, **2**, **3**, and **4**, respectively. The supramolecular layer is alternatively stacked with a honeycomb layer of $[MnCr(oxalate)_3]^-$.

(2) The alignment of Mn^{2+} and Cr^{3+} bridged by oxalate ligand afforded ferromagnetic ordering in **1**-**4** with Weiss temperature from 5.59 to 8.85 K. Their saturated magnetization values of 7.76, 7.92, 7.97, and 7.83 μ_B at 2 T for **1**-**4** showed good agreement with the high spin state of Mn^{2+} (S = 5/2) and Cr^{3+} (S = 3/2).

(3) The displacement of benzo[18]crown-6 and the distortion in $[MnCr(oxalate)_3]^-$ induced asymmetric structures in **1, 3,** and **4**, the space group of $P2_1$, $P2_1$, and $Pna2_1$ for crystals **1**, **3,** and **4** indicate a possibility for symmetric breaking toward ferroelectrics. The tilting motion of benzo[18]crown-6 in crystals **1, 3,** and **4** was also observed by the temperature-varied X-ray diffraction method. The motion gave rise to dielectric relaxation at around 200–250 K. The activation energies for crystals **1**, **3,** and **4** were calculated as 31.8 kJ/mol, 51.2 kJ/mol, and 36.4 kJ/mol.

(4) Compared to the improper spatial environment of (*m*-fluoroanilinium)dibenzo[18]crown-6$[MnCr(oxalate)_3]^-(CH_3CN)(CH_3OH)$, the rotation of (*m*-fluoroanilinium$^+$) cation was realized in crystal **2** via adjusting dibenzo[18]crown-6 to asymmetric benzo[18]crown-6. The disorder of fluorine substituent in (*m*-fluoroanilinium$^+$) cation with temperature dependence evidenced the flip-flop motion of (*m*-fluoroanilinium$^+$), and this molecular motion gave another dielectric relaxation at higher temperature regions 250 to 350 K. The activation energy was calculated as 34.1 kJ/mol.

(5) A ferroelectric to paraelectric phase transition at around 460 K was observed in crystal **2**, crystallized in the *Cc* space group at 223 K. Upon the phase transition, the structure transformed to the $P2_1/c$ space group. A ferroelectric response was observed upon this phase transition by pyroelectric measurement. The coexistence between ferroelectric and ferromagnetic orders was successfully constructed in crystal **2**.

(6) The magnetoelectric coupling effects of multiferroic **2** were investigated by magnetic measurement. The difference in saturated magnetization values between electric-polled and depolarized samples reached 1.5%, indicating an electric-induced magnetization correlation in this molecular multiferroic material.

In chapter **3**

(7) A polar crystal of (CBA^+)([18]crown-6)[$MnCr(oxalate)_3$](CH_3OH) (CBA^+ = 4-carboxybutan-1-aminium) (**5**•CH_3OH), crystallized in *Cc* space group, was designed in chapter **3**. The desolvation of guest CH_3OH induced a crystal-to-crystal structural transformation to the solvent-free crystal of (CBA^+)([18]crown-6)[$MnCr(oxalate)_3$] (**5**), solved in the *C*2 space group. The good crystallinity of **5** upon desolvation makes it possible to conduct relative physical property measurements.

(8) Desolvation of CH_3OH intrigued a "merry-go-round" motion of [18]crown-6 in crystal **5**. The dynamic disorder was revealed by dielectric relaxation. The activation energy was calculated to be 41.41 kJ/mol.

Although the structural change did not show a significant effect on the magnetic susceptibility and magnetization behavior, the polar structure of the crystals may affect chiral magnetic behaviors and multifunctional materials based on molecular motion.

In chapter **4**

(9) Three dimensional crystals of (ethanaminium$^+$)benzo[18]crown-6[$MnCr(oxalate)_3$]$^-$($1.5CH_3OH$) (**6**) and [(1*S*,2*S*)-1,2-diphenylethan-1,2-diaminium^{2+}][18]crown-6{[$MnCr(oxalate)_3$]}$_2^{2-}$($1.5CH_3OH$)($0.5CH_3COCH_3$) (**7**) with polar space group $Pna2_1$ and $P2_12_12_1$ were synthesized. In crystal **6**, achiral supramolecular (ethanaminium$^+$)benzo[18]crown-6 templated a homochiral structure in [Mn(Δ)Cr(Δ)$(oxalate)_3$]$^-$. This result implied that in addition to chiral cations with D_3 symmetry, the achiral, less symmetric supramolecular structure can also induce a

homochiral three-dimensional $[MnCr(oxalate)_3]^-$. The largely flexible structure of organic supramolecular structure provides a new idea for multifunctionality in three-dimensional materials.

(10) In crystal **7**, chiral supramolecular cation [(1*S*,2*S*)-1,2-diphenylethan-1,2-diaminium^{2+}] unexpectedly induced a rare combination of $[Mn(\Delta)Cr(\Delta)(oxalate)_3]^-$, $[Mn(\Lambda)Cr(\Lambda)(oxalate)_3]^-$, and $[Mn(\Delta)Cr(\Lambda)(oxalate)_3]^-$ or $[Mn(\Lambda)Cr(\Delta)(oxalate)_3]^-$, leading to the anionic network be achiral. Isotropic network in *bc* and *ac* plane provides a forward-looking example for gyroid structure with interesting magnetic behavior.

In this thesis of chapter **2**, a very rare molecular multiferroic (*o*-fluoroanilinium$^+$)(benzo[18]crown-6)$[MnCr(oxalate)_3]^-$ with magnetoelectric effect was synthesized. This result offers a whole new research subject for molecular multiferroics.

The solvent effects on molecular motion were demonstrated in chapter **3**. The crystal-to-crystal structural transformation and the desolvation-induced molecular motion provide a design strategy for multifunctional hybrid materials that can add new functions based on molecular motion.

In the preliminary work of chapter **4**, supramolecular structures templated two distinct three-dimensional networks of $[MnCr(oxalate)_3]^-$ in chiral space groups $Pna2_1$ and $P2_12_12_1$. The structure of crystal **7** is interesting as a gyroid-like structure in the aspect of magnetic properties, and this result demonstrated the usefulness of supramolecular structures to build novel networks with exotic physical properties.

Chapter 6. Experimental and Methods

Chemical reagents

All reagents and solvents were commercially available and used without further purification. $K_{0.08}Ag_{2.92}[Cr(ox)_3]\bullet 3H_2O$ complex was prepared according to previously described methods.[1, 2] The cations of $(Ani^+)(BF_4^-)$, $(o\text{-}FAni^+)(BF_4^-)$, $(m\text{-}FAni^+)(BF_4^-)$, $(p\text{-}FAni^+)(BF_4^-)$, and [(1*S*,2*S*)-1,2-diphenylethan-1,2-diaminium^{2+}]$(BF_4)_2^{2-}$ were prepared according to literature reported before.[2] Carbon, nitrogen, and hydrogen contents of **1**-**4** were determined by an organic microanalytical equipment MICRO CORDER JM10 elemental analyzer at the Instrumental Analysis Division, Equipped Management Center, Creative Research Institution, Hokkaido University.

(*x*-anilinium$^+$)(benzo[18]crown-6)[$Mn^{II}Cr^{III}(ox)_3$] (*x* = H, *o*-fluoro, *m*-fluoro, and *p*-fluoro for crystal 1, 2, 3 and 4, respectively)

1 was synthesized as follows: $K_{0.08}Ag_{2.92}[Cr(ox)_3]\cdot 3H_2O$ (1 mmol; 0.689 g) and $MnCl_2\cdot 4H_2O$ (1.5 mmol; 0.297 g) were suspended in 15 mL of methanol and stirred for 10 min. The white precipitate AgCl was removed by filtration. The dark violet-colored solution was carefully poured into one side of the H-shaped cell. Powder benzo[18]crown-6 (1 mmol; 0.313 g) and $(Ani^+)(BF_4^-)$ (1 mmol; 0.180 g) in 15 mL acetonitrile were added into the other side of H-shaped cell. Methanol was further added into the middle part of the H-shaped cell to control the rate of crystallization.[4] The product formation was observed within three days, and crystallization was maintained for a period of two weeks. The blue-black-colored single crystals were filtered and washed thoroughly with methanol and dried at room temperature. Crystals **2, 3,** and **4** were obtained from the same methods for the synthesis of crystal **1** except for using 0.5 mmol of $(o\text{-}FAni^+)(BF_4^-)$, 1.0 mmol of $(m\text{-}FAni)(BF_4^-)$, and 1.0 mmol of $(p\text{-}FAni^+)(BF_4^-)$, respectively, instead of using $(Ani^+)(BF_4^-)$. Anal. Calcd for **1**, $C_{28}H_{32}NO_{18}CrMn$ (777.48): C, 43.26%; H, 4.15%; N, 1.80%. Found: C, 42.97%; H, 3.96%; N, 1.72%. Anal. Calcd for **2**, $C_{28}H_{31}NO_{18}FCrMn$ (795.47): C, 42.28%; H, 3.93%; N, 1.76%. Found: C, 42.06%; H, 3.80%; N, 1.67%. Anal. Calcd for **3**,

$C_{28}H_{31}NO_{18}FCrMn$ (795.47): C, 42.28%; H, 3.93%; N, 1.76%. Found: C, 42.06%; H, 3.80%; N, 1.67%. Anal. Calcd for **4**, $C_{28}H_{31}NO_{18}FCrMn$ (795.47): C, 42.28%; H, 3.93%; N, 1.76%. Found: C, 42.08%; H, 3.79%; N, 1.67%. All the compounds did not contain any solvents in the crystal determined by thermogravimetric analysis and single-crystal X-ray analysis.

(CBA^+)[18]crown-6[$MnCr(oxalate)_3$]$^-$(CH_3OH) (5•CH_3OH)

Single crystals of (CBA^+)([18]crown-6)[$MnCr(oxalate)_3$]•CH_3OH were obtained by the diffusion method in a methanolic solvent in a 5 mL test tube. The top layer in the diffusion tube was a supramolecular cation layer containing 5-aminovaleric acid hydrochloride (0.05 mmol) and [18]crown-6 (0.05 mmol) in 1 mL CH_3OH**.** The middle layer was 2 mL **CH_3OH**, and the bottom layer was the anionic layer (1 mL) filtered from the mixture of $K_{0.08}Ag_{2.92}Cr(oxalate)_3$•$3H_2O$ (0.05 mmol) and $MnCl_2$•$4H_2O$ (0.08 mmol) in 1 mL **CH_3OH**. After two weeks, block-shaped, dark-purple single crystals were produced (yield: 8.10 mg, 20.62%).

Desolvation of crystal 5•CH_3OH

To obtain a solvent-free crystal of (CBA^+)([18]crown-6)[$MnCr(oxalate)_3$], **5**, a single crystal of **5**•CH_3OH was heated at 380 K for 30 min under nitrogen. The heating rate was set at 1 K/min from 298 to 380 K to prevent crystal cracking.

Thermalgravimetric and differential scanning calorimetry analysis

Thermogravimetric (TGA) measurements of the compounds were conducted using a Rigaku Thermo Plus TG8120 thermal analysis station with an Al_2O_3 reference from 298 to 773 K at a heating rate of 10 K min^{-1} under flowing nitrogen gas. Differential scanning calorimetry (DSC) measurement was carried out using a Q2000 differential scanning calorimeter (TA Instruments) in the temperature range 193-500 K with 5 K min^{-1} heating/cooling rates.

X-ray powder diffraction

X-ray powder diffraction data were collected in the 2θ regions of 5 to 50° at 293 K using a Rigaku RINT-Ultima III diffractometer employing Cu Kα radiation.

Crystal structure determination

Crystal structure analysis of the single crystals was performed using a Rigaku XtaLAB synergy diffractometer with a single microfocus Mo Kα X-ray radiation source (Proton Jet-S) equipped with a hybrid pixel (HyPix) array detector (HyPix-6000HE). Multiscan absorption corrections were applied to the reflection data. Single crystals were mounted with Paratone® 8277 on a CryoLoop (Hampton Research). Data collection, cell refinement, and data reduction were performed using CrysalisPRO (Rigaku Oxford Diffraction, 2017). The initial structures were solved using SHELXT, [3] and structure refinement was performed using full-matrix least-squares techniques on F^2 using the OLEX2 package.[4] All parameters were refined using anisotropic temperature factors, except for hydrogen atoms, which were refined using the riding model, with a fixed C–H bond distance.

Impedance measurement

The temperature- and frequency-dependent dielectric constants (real part ε_1 and imaginary part ε_2) were collected using an impedance analyzer 4294A (Agilent) with the four-probe AC impedance method in the frequency range of 10^3 to 10^6 Hz with 20 points. The pellet sample was compacted using polycrystals after powdering. Gold paste ((No. 8556, Tokuriki Chemical Research Co., Ltd.) and 10 μm ϕ gold wires (Nilaco Corp.) were used for electrical contact between the sample and the electrical wire from the device. The temperature was controlled using a cryostat with a temperature controller (Model 331; Lake Shore Cryotronics, Inc.).

Magnetic measurements

The temperature-dependent molar magnetic susceptibility (χ_m) was measured in the temperature range of 2–300 K under a constant magnetic field of 500 Oe using an MPMS 3 SQUID magnetometer (Quantum Design). The magnetic field-dependent magnetic susceptibility was collected at 1.8 K in the range of -7 to 7 T or -5 to 5 T using an MPMS 3 SQUID magnetometer (Quantum Design). All compounds were wrapped in plastic wrap. The diamagnetic component of the sample holder was ignored owing to the strong magnetic susceptibility of the samples.

Second Harmonic Generation

Optical second harmonic generation (SHG) measurements of powdered compounds of **1**-**4** were conducted with a laser beam at a wavelength of 1030 nm at 293 K, SHG light was detected by a photomultiplier tube. The compounds were mounted on a motor-controlled rotating stage and the angle of incidence of the laser beam relative to the compounds varied from 0º to 150º.

Pyroelectric current measurement

Compound **2** was compressed as a plate with 0.1096 cm thickness and 0.0360 cm^2 superficial area, within Au electrodes. The plate was treated by an electric field at 466 K as poling procedure. After cooling to room temperature in the vacuumed sample chamber, the pyroelectric current was monitored (by using Agilent 6517B).

Reference

1. H. Tamaki, Z. J. Zhong, N. Matsumoto, S. Kida, M. Koikawa, N. Achiwa, Y. Hashimoto and H. Okawa, *J. Am. Chem. Soc.*, 1992, **114**, 6974-6979.

2. T. Endo, T. Akutagawa, S. Noro and T. Nakamura, *Dalton Trans.*, 2011, **40**, 1491-1496.

3. G. M. Sheldrick, *Acta Crystallogr., Sect. A: Found. Crystallogr.*, 2015, **71**, 3-8.

4. O. V. Dolomanov, L. J. Bourhis, R. J. Gildea, J. A. K. Howard and H. Puschmann, *J. Appl. Crystallogr.*, 2009, **42**, 339-341.